

Compressive Sensing with Low-Power Transfer and Accurate Reconstruction of EEG Signals

Manika Rani Dey

A thesis submitted in partial fulfilment of the requirements of the University of East London for the degree of Doctor of Philosophy



School of Architecture, Computing and Engineering

September 2019

Abstract

Tele-monitoring of EEG in WBAN is essential as EEG is the most powerful physiological parameters to diagnose any neurological disorder. Generally, EEG signal needs to record for longer periods which results in a large volume of data leading to huge storage and communication bandwidth requirements in WBAN. Moreover, WBAN sensor nodes are battery operated which consumes lots of energy. The aim of this research is, therefore, low power transmission of EEG signal over WBAN and its accurate reconstruction at the receiver to enable continuous online-monitoring of EEG and real time feedback to the patients from the medical experts. To reduce data rate and consequently reduce power consumption, compressive sensing (CS) may be employed prior to transmission. Nonetheless, for EEG signals, the accuracy of reconstruction of the signal with CS depends on a suitable dictionary in which the signal is sparse. As the EEG signal is not sparse in either time or frequency domain, identifying an appropriate dictionary is paramount. There are a plethora of choices for the dictionary to be used. Wavelet bases are of interest due to the availability of associated systems and methods. However, the attributes of wavelet bases that can lead to good quality of reconstruction are not well understood. For the first time in this study, it is demonstrated that in selecting wavelet dictionaries, the incoherence with the sensing matrix and the number of vanishing moments of the dictionary should be considered at the same time.

In this research, a framework is proposed for the selection of an appropriate wavelet dictionary for EEG signal which is used in tandem with sparse binary matrix (SBM) as the sensing matrix and ST-SBL method as the reconstruction algorithm. Beylkin (highly incoherent with SBM and relatively high number of vanishing moments) is identified as the best dictionary to be used amongst the dictionaries are evaluated in this thesis. The power requirements for the proposed framework are also quantified using a power model. The outcomes will assist to realize the computational complexity and online implementation requirements of CS for transmitting EEG in WBAN. The proposed approach facilitates the energy savings budget well into the microwatts range, ensuring a significant savings of battery life and overall system's power.

The study is intended to create a strong base for the use of EEG in the high-accuracy and low-power based biomedical applications in WBAN.

Table of Content

Table of Content	ii
List of Figure	v
List of Table	vii
Abbreviations and Symbol	viii
Aknowledgement	xi
Chapter 1: Introduction	1
1.1 Overview and Motivation of the Thesis.....	1
1.2 Research Questions	2
1.3 Aim of the Thesis	2
1.4 Objective of the Thesis.....	3
1.5 Research Knowledge Gap	3
1.6 Contributions of the Thesis	3
1.7 List of Workshop, Conference and Submitted Publication.....	4
1.9 Outline of the Thesis	4
Chapter 2: Literature Review	6
Chapter 3: Overview of EEG Transmission over Wireless Body Area Network	9
3.1 Introduction	9
3.2 Background information about EEG.....	9
3.2.1 Electroencephalogram Signals (EEG).....	9
3.2.2 Generation of EEG	10
3.2.3 EEG Recording System	10
3.2.4 EEG signal Natures or Rhythms	12
3.2.5 Applications of EEG Signals	14
3.3 WBAN-oriented EEG transmission	14
3.3.1 Advantages of WBAN-oriented System	17
3.3.2 Challenges in WBAN-based EEG transmission system.....	17
3.3.3 Methodology to resolve challenges in WBAN	18
3.4 Summary	19
Chapter 4: Research Methodology	20

Chapter 5: Wavelet Bases for Compressive Sensing of EEG Signals with Accurate Reconstruction	22
5.1 Introduction	20
5.2 Overview of Compressive Sensing and its Background Knowledge.....	23
5.2.1 Challenges in CS-based EEG transmission	25
5.2.3 Sensing Basis	25
5.2.4 Sparsifying Dictionary	26
5.2.4.1 Discrete Wavelet Dictionary (DWT).....	30
5.2.5 Incoherence between Sensing Basis and Sparsifying Dictionary	30
5.2.6 Selection of Wavelet (DWT) dictionary	31
5.2.7 Vanishing Moment of Wavelet Dictionary	33
5.3 Methods and Materials	34
5.3.1 Incoherence of SBM with DWT Dictionaries.....	34
5.3.2 Reconstruction by exploiting block sparsity in the DWT coefficients	35
5.3.3 Performances Indicators.....	37
5.3.4 Comparison of DWT, DCT and no dictionary	38
5.3.5 Classification error	38
5.4 Summary	38
Chapter 6: Results and Discussion	40
6.1 Introduction	40
6.2 Experimental Datasets.....	40
6.2.1 Visual attention tasks EEG dataset	40
6.2.2 Car driving tasks EEG dataset.....	41
6.2.3 Epileptic and non-epileptic dataset	41
6.3 Results	42
6.3.1 Incoherence of SBM with DWT dictionaries.....	42
6.3.2 Reconstruction using DWT dictionary.....	45
6.3.2.1 Reconstruction results for the visual attention tasks EEG dataset.....	45
6.3.2.2 Reconstruction results for the car driving tasks EEG dataset.....	47
6.3.2.3 Reconstruction results for the epileptic and non-epileptic dataset.....	48
6.3.3 Result analysis with coherence and vanishing moments	49
6.3.4 Comparison of Beylkin, DCT and No dictionary for different CRs	53
6.3.4.1 Comparison for the visual attention task dataset	53
6.3.4.2 Comparison for the car driving task dataset	54
6.3.4.3 Comparison for the epileptic and non-epileptic dataset.....	55
6.3.5 Classification Error	57
6.4 Discussion	57

6.5 Summary	58
Chapter 7: Power Consumption Analysis.....	60
7.1 Introduction	60
7.2 The Necessity of Energy Efficient Sensing System.....	60
7.3 Types of Wireless Sensor nodes	62
7.4 Multiple hops WBAN system	63
7.5 Design of WBAN Sensor Node	63
7.6 Power consumption analysis of a sensor node	64
7.7 Power Consumption at different CR.....	71
7.8 Further Power Savings in WBAN.....	72
7.9 Summary	72
Chapter 8: Conclusion and Future Research Scopes	74
8.1 Conclusion.....	74
8.2 Future Research Scopes	76
References and Bibliography	77
Appendix: MATLAB Code	87

List of Figure

Figure 3.1. Typical EEG system (Waltz, 2017).....	11
Figure 3.2. The international 10-20 electrode placement system (Sazgar and Young, 2019)	12
Figure 3.3. Typical EEG rhythms (Crystal Blue Enterprises, 2015)	13
Figure 3.4. EEG-Based WBAN architecture	16
Figure 5.1. Block diagram of CS-based EEG Transmitter-Receiver.....	24
Figure 5.2 Example of EEG signal and its DWT coefficients	27
Figure 5.3. 3-level decomposition of DWT coefficients of a signal with 32 samples...	28
Figure 5.4. Reconstruction of approximation and details of the single-level signal.....	29
Figure 5.5. Block diagram of reconstruction of 3-level decomposed signal	29
Figure 5.6. Mother wavelets of different DWTs.....	30
Figure 6.1. Frequency spectra of aggregate EEG signal for all subjects	42
Figure 6.2. Coherence with varying number of non-zero elements.....	43
Figure 6.3. Variation of reconstruction error with no of non-zero elements, where red marks represent mean and error bar shows variance	43
Figure 6.4. Coherence between Φ and Ψ	44
Figure 6.5. NMSE of the visual attention task EEG signal.....	45
Figure 6.6. SSIM of the visual attention task EEG signal	46
Figure 6.7. Example of the visual attention task EEG signal (channel 1 and channel 22) of the original and reconstructed with Beylkin DWT	46
Figure 6.8. NMSE of the car driving task EEG signal reconstruction.....	47
Figure 6.9. SSIM for the car driving task EEG signal reconstruction.	47
Figure 6.10. Example of the car driving task EEG signal (channel 5 and channel 25) of the original and reconstructed with Beylkin DWT.	48
Figure 6.11. NMSE of epileptic and non-epileptic EEG signal reconstruction, where bar indicates mean and errorbar gives standard deviation.	49
Figure 6.12. SSIM of epileptic and non-epileptic EEG signal reconstruction, where bar indicates mean and errorbar gives standard deviation.	49
Figure 6.13. Demonstrating the relationship between coherence and vanishing moments for the 15 DWT dictionaries. Also, the correlations between vanishing moment and coherence with reconstruction performance for all the dictionaries are shown.....	50

Figure 6.14. Coiflet CDF plot for $d_e(a, b)$ for $n=3,4,5$.	51
Figure 6.15. Variation of $d_e(a, b)$	51
Figure 6.16. NMSE for different CRs associated with Beylkin, DCT and when no dictionary is used in visual attention task EEG dataset.	53
Figure 6.17. SSIM for different CRs associated with Beylkin, DCT and when no dictionary is used in visual attention task EEG dataset.	53
Figure 6.18. NMSE for different CRs associated with Beylkin, DCT and when no dictionary is used in car driving task EEG dataset.	54
Figure 6.19. SSIM for different CRs associated with Beylkin, DCT and when no dictionary is used in car driving task EEG dataset.	54
Figure 6.20. Examples of normalised aggregate EEG signal (addition of all 23 channels at a given time) of the original and reconstructed for different values of CR for Beylkin, discrete cosine and the case of using no dictionary. Blue traces show the original while the red traces are the reconstructed	55
Figure 6.21. The box plot of NMSE and SSIM for different CRs associated with Beylkin and discrete cosine and when no dictionary was used	56
Figure 6.22. The raster plot of misclassification using the classification algorithm is used in this paper in the original training data and the reconstructed test data (Dey et al., 2019).	57
Figure 7.1. Bandwidth and energy constraints for the transmission of EEG signals. Nyquist sampling shows rigid constraints, requiring information to be reduced to a great extent that can possibly be accomplished through effective signal compression techniques like CS. (ECoG: electrocorticogram, LFP: local field potential) (Shoaib, 2013).	61
Figure 7.2. Multi-hop EEG based WBAN system	63
Figure 7.3. Block diagram of a WBAN sensor node.	64
Figure 7.4. The architecture of EEG WBAN sensor/server node	65
Figure 7.5. Total power consumption Vs ADC Resolution	68
Figure 7.6. The circuitry of a sensor node	69
Figure 7.7. Power consumption Vs EEG Nyquist rate	70
Figure 7.8. Power consumption at different CR, while ADC sampling rate is 250 Hz.	71

List of Table

Table 3.1 EEG rhythms types, frequency band and associated mental states.....	13
Table 6.1 Statistical values of results	52
Table 7.1. Power consumption at different sampling rates of ADC	67
Table 7.2. Power consumption at different resolution of ADC	67
Table 7.3. Summary of the parameters used in power consumption analysis	71

Abbreviations and Symbol

$ac(n)$	Approximation Coefficients
ADC	Analog to Digital Converter
b	Number of Blocks
BSBL	Block Sparse Bayesian Learning
C	Number of Channel
CCU	Central Control Unit
CDF	Cumulative Density Function
Coef	Coefficients
Coif	Coiflet
CR	Compression Ratio
CS	Compressive Sensing
CW	Continuous Wavelet
d	Number of non-zero entries in SBM
Db	Daubechies
$dc(n)$	Detail Coefficient
DCT	Discrete Cosine Transform
d_e	Euclidean Distance
d_i	Block size
DFT	Discrete Fourier Transfer
DSP	Digital signal Processor
DWT	Discrete Wavelet Transform
ECG	Electrocardiography
ECoG	Electrocorticographic
EEG	Electroencephalography
EKG	Electrocardiogram
EMG	Electromyography
ENOB	Effective Number of Bits
fJ	Femto Joule
FOM	Figure-of-Merit
f_s	Sampling Frequency

G	Low-Pass Filter
GT	Gabor Transform
H	High-Pass Filter
IDWT	Inverse Discrete Wavelet Transform
IoT	Internet of Things
ISM	The Industrial, Scientific and Medical
j	Per Bit Transmission Power
J	Number of Segments
K	Nonzero elements in DWT coefficients
kS/s	Kilo Samples per Second
L	Number of Columns
LFP	Local Field Potential
m	Mean
M	Number of samples in the reconstructed signal
mW	Milliwatt
MICS	Medical Implant Communication Service
MS	Medical Server
n	Order
n_c	Filter Coefficients
N	Length of the signal/ Number of samples / Number of rows
nJ/b	Neno Joule per Bit
NMSE	Normalised Means Square Error
p	Vanishing Moment
PC	Personal Computer
PS	Personal Server
P_{ADC}	ADC Power
P_{amp}	Amplifier Power
P_{micro}	Microcontroller Power
P_{proc}	Processing Power
P_{sense}	Sensing Power
P_{sen_CS}	CS-Based sensor node's power
P_{RNG}	RNG Power
QMF	Quadrature Mirror Filter

R	ADC Resolution
RIP	Restricted Isometry Property
RNG	Random Number Generator
SBL	Sparse Bayesian Learning
SBM	Sparse Binary Matrix
SSIM	Structural Similarity index
ST-SBL	Spatiotemporal Block Sparse Bayesian Learning
TUH	Temple University Hospital
UWB	Ultra Wide Band
\mathbf{V}	Noise Signal
WBAN	Wireless Body Area Network
Wi-fi	Wireless Fidelity
WT	Wavelet Transform
x	EEG signal vector
\mathbf{X}	Multichannel EEG signals
$\hat{\mathbf{X}}$	Estimated Signal
y	Measured signal vector
\mathbf{Y}	Multichannel Measured signals
z	DWT coefficients vector
\mathbf{Z}	DWT coefficients Matrix
Φ	Sensing Basis/ Sparse Binary Matrix
Ψ	Dictionary/ DWT Dictionary
Θ	$\Phi\Psi$
μ	Coherence
μ_x	Mean of Original Signal
$\mu_{\hat{x}}$	Mean of measured Signal
φ	Continuous Wavelet
σ^2	Variance
σ_x^2	Variance of the original signal
$\sigma_{\hat{x}}^2$	Variance of the estimated signal
$\sigma_{x\hat{x}}$	Cross-Variance
μW	Microwatt

Acknowledgement

First of all, I would like to thank the Almighty Creator for everything. Then I would like to show my gratitude to my supervisor Dr. Jaswinder Lota for his conscientious guidance, supervision and encouragement to accomplish this thesis. This dissertation would have been impossible without his experienced guideline.

I am very thankful to my second supervisor Prof. Hassan Abdalla for his support.

I would like to thank and pay my gratitude to the AMR panel for their valuable comments and feedbacks; Dr. Julie Wall and Dr. Saeed Sharif.

I also had the opportunity to collaborate with excellent research teams whom I am always grateful. I should thank Dr. Arsam Shiraz and Prof Andreas Demosthenous from University College of London.

I would like to thank the University of East London for giving me this golden opportunity to conduct my PhD with such valuable resources and facilities.

I would like to show my gratitude towards my parents and other members of my family. Without their support, it would have not been possible.

At last, I am very thankful to all my friends who always encouraged me to accomplish my work properly.

Chapter 1

Introduction

1.1 Overview and Motivation of the Thesis

Electroencephalography (EEG) is one of the most vital physiological signals which presents brain's electrical activity. Therefore its interpretation plays an important role in the research of brain and diagnosis of neurological disorders. Especially in the diagnosis of epilepsy, the examination of EEG is essential. However, in the typical wired EEG monitoring system, patients need to stay very close to the monitoring device and medical specialist in the hospital. This significantly interrupts daily lives of patients and also restricts EEG studies.

Recently, tele-monitoring of EEG via wireless body area network (WBAN) has become an evolving trend in home-based e-health. Tele-monitoring EEG is a way of recording patient EEG signals constantly in the ambulatory environment by using a portable device that the patient can carry without interrupting their daily activities.

On the other hand, the high volume of data and power consumptions are main constraints in the transmission of EEG signal through WBAN, due to the short life of battery and processing capability of wireless sensor nodes. It is stated that the most energy hungry part in WBAN is its transmitter. Hence, sensing and processing methodologies are required to apply to the signal before transmission. In this thesis, compressive sensing (CS) being an energy efficient data compression technique is employed prior to the transmission.

However, a requirement of CS is that the signal has to be sparse in the domain where it is compressed. The problem is EEG signal is not sparse in time or the frequency domains. Thus the main challenge of employing CS for EEG signal is to identify the domain known as the dictionary in which the EEG signal is sufficiently sparse. Wavelet bases are widely used as a dictionary in CS; however, its features have not been analyzed fully, except the existing widely adopted approach of its high incoherency with the sensing matrix. In most other applications, a key feature employed in the selection of a wavelet basis is the number of vanishing moments, which determines its ability to represent complex signals efficiently or more sparsely.

This study demonstrates that during the selection of the wavelet dictionaries, the incoherence with the sensing matrix and the number of vanishing moments of the dictionary should be considered simultaneously. There are dictionaries with high incoherence that lead to poor reconstruction and there are those with high number of vanishing moments that lead to a similarly poor outcome. However, dictionaries having both a high incoherence with the sensing matrix and relatively large number of vanishing moments tend to lead to less error in reconstruction.

In this work, Beylkin is identified as the best dictionary to be used amongst the dictionaries are used. This has a similar performance to discrete cosine dictionary while demonstrating a moderately better performance at higher compression levels. Furthermore, Beylkin leads to substantially better performance at higher compression ratios compared to reconstruction without using sparsifying dictionaries.

1.2 Research Questions

EEG signals need a prolong periods of recording, resulting in large volume of data which lead to huge storage and communication bandwidth requirements in WBAN. Moreover, battery-operated WBAN sensor nodes consume lots of energy. Therefore, an energy efficient EEG transmission and reconstruction is required. CS may be employed prior to transmission to reduce data rate and thereby to reduce power consumptions, but a CS prerequisite is that in the domain where it is compressed the signal must be sparse. Moreover, EEG signal is neither sparse in time domain nor in frequency domain. The main challenge of using CS for EEG signal is therefore to determine the domain referred to as the dictionary in which EEG signal is sparse enough. Wavelet bases are commonly used in CS as a dictionary; however, their features are not thoroughly studied. Therefore, the research question is which features of wavelet bases need to be considered for the selections of appropriate wavelet dictionary of EEG signal.

1.3 Aim of the Thesis

The aim of this research is energy efficient transmission of EEG signal over WBAN and its accurate reconstruction at the receiver with the aim of ensuring continuous EEG monitoring and real time feedback from the physicians to the patients.

1.4 Objectives of the Thesis

The objective of this study is to identify a suitable wavelet dictionary by investigating incoherence and vanishing moment with an aim to improving accuracy of reconstruction of the EEG signals. Although state-of-the-art approaches show accurate reconstruction of EEG, however the specific features that make these dictionaries appropriate, have not investigated yet. In this thesis, these features are investigated fully. Another objective of this work is to analyse the power requirements for the proposed framework-based EEG sensor node.

1.5 Research Knowledge Gap

The properties of dictionary that make them appropriate selections for EEG signals have not analyzed fully in the state-of-the-art studies. While incoherence has been investigated and is understood well for CS, vanishing moment, on the other hand, is understood in terms of wider Discrete Wavelet Transform (DWT) applications to represent complex signals efficiently and sparsely. These two important properties are considered in isolation and to the best of my knowledge have not been analyzed together for CS in EEG signals. The investigation of this research indicates that both features should be looked at the same time in the selection of the dictionary; this is something that is often overlooked.

1.6 Contributions of the Thesis

Based on the addressed problems and the purpose of the work, the contribution of this research can be divided into the following two parts:

- A. In this dissertation, a framework is proposed for the selection of an appropriate wavelet dictionary for EEG signal which is used in tandem with sparse binary matrix (SBM) as the sensing matrix and Spatiotemporal Block Sparse Bayesian Learning (ST-SBL) method as the reconstruction algorithm. The results would assist users in identifying an appropriate dictionary to be employed for CS of EEG signals.

This research is primarily aimed at investigating incoherence of dictionary with SBM, together with vanishing moments of wavelet dictionaries for effective implementation of compressive sensing for EEG signal acquisition. In this work,

clear evidence is provided that Beylkin having high incoherence with SBM and relatively high number of vanishing moments leads to the best performance and subsequently assess the effects on possible clinical outcome in detecting epilepsy.

- B.** The power requirements of transmitting EEG signal in WBAN are investigated by exploring the effectiveness of proposed approach. The studies are carried out by numerical experiments following a power model. The outcomes will assist to realize the computational complexity and online implementation requirements of CS for EEG transmission in WBAN. The proposed framework enables the energy savings budget well into the μW range which contributes substantially to the savings of battery life and overall energy of the system.

1.7 List of Workshop, Conference and Submitted Publication

Dey, M.R., (2018) ‘Compressive Sensing of EEG signal with Discrete Wavelet Transform (DWTs)’, Presented at Workshop on Sensors, Circuits and Systems: University College of London, 25 June.

Dey, M.R., Shiraz, A., Lota, J. and Demosthenous, A. (2019) ‘Compressive Sensing of EEG Signals over Wireless Body Area Network with Incoherent DWT Dictionary’, *UEL Research and Knowledge Exchange Conference*, 27 June. London.

1.8 Outline of the Thesis

The thesis is structured as follows.

Chapter 2 depicts literature review of the research.

Chapter 3 provides the concept of EEG signal transmission over WBAN with the background knowledge of EEG signal, generation, recording system and application of EEG signals. The chapter also presents the overview of WBAN based EEG system, its advantages, challenges and also gives a brief discussion of the methodologies are used to overcome the challenges. The chapter concludes by introducing CS as energy efficient method.

Chapter 4 provides research methodology which includes research problem, research literature survey, properties of DWT, proposed approach, data Selection and Simulations and Validation of the Proposed Approach.

Chapter 5 proposes the framework of identifying an appropriate wavelet dictionary. The details of CS method are given in this chapter as well as the generation of DWT dictionary and the key features of selecting the suitable dictionary also described elaborately. Method and materials are also provided in this chapter.

Chapter 6 presents all the experimental results of the proposed approach that are discussed in chapter 5. The chapter starts with providing the datasets which are used for the experiments. The outcomes of incoherence, reconstruction using DWT dictionaries to identify an appropriate dictionary also provides this chapter. A comparison of DWT, DCT and the case of using no dictionary for different compression ratios (CRs) are also given, classification error of clinical data is also shown. The chapter ends with a brief discussion of the results.

Chapter 7 has analyzed the feasibility of the proposed framework to enable online data reduction, from the power point of view. The power requirements for the proposed framework based EEG sensor node are quantified in this chapter using a power model. The chapter also presents the approach of further reduction of power consumption.

Finally, Chapter 8 concludes this dissertation by summarizing the research contributions and ended with suggesting the potential extension of the research.

Chapter 2

Literature Review

The dynamic nature of physiological signals such as electroencephalographic (EEG) or electrocorticographic (ECoG) signals in individuals results in a broad range of normal and pathological characteristics. In order to predict pathological events the use of manually extracted features with a large volume of data is not practical even for a small number of electrodes because it causes processing delays (Hosseini *et al.*, 2017). For real time and clinically useful implementation in such applications, thus automated feature extraction and signal processing are required. The real-time processing can be facilitated using cloud computing, Internet of Things (IoT) and deep learning, to effectively monitor and predict seizures using EEG signal (Hosseini *et al.*, 2017), which requires high data volume transmission of the acquired bio-signals. In addition, remote online monitoring and diagnosis of EEG signals can reduce patient's frequency of visits to hospitals (Ivanov *et al.*, 2012; Lim, Baumann and Li, 2011; Seyedi *et al.*, 2013; Zhang *et al.*, 2013a).

Due to the limited battery life and processing capacity of sensor nodes, energy consumption and high volume of data are major constraints in EEG signal transmission. Recent efforts aimed at increasing battery life focus on reducing the transmission power and data rate with compressed sensing (CS) (Liu, Vosand and Huffel, 2015; Candes and Wakin, 2008). CS provides a significant computational savings during on-chip implementation, therefore, it is considered as most feasible technique for the transmission of large volumes of data and high data rate signals (Balouchestani, Raahemifar and Krishnan, 2012a; Balouchestani, Raahemifar and Krishnan, 2012b; Zhang *et al.*, 2013a; Casson and Rodriguez-Villegas, 2014; Lalos *et al.*, 2014; Majumdar and Ward, 2016; Kaliannan and Pasupureddi, 2016; Djelouat *et al.*, 2017; Gogna, Majumdar and Ward, 2017; Hanafy, Ali and Shaalan, 2017;). In CS data is projected into a compressed format non-adaptively upon acquisition using a sensing matrix, which differs from conventional compression techniques where data is acquired then compressed and indices are stored (Majumdar, Gogna and Ward, 2014).

One main requirement of CS is that the signal must be sparse (Candes and Wakin, 2008). EEG signal is not sparse, however, in time or the frequency domains (Zhang *et al.*, 2013a). A challenge, therefore, in employing CS for the EEG signal is to identify the domain known as the dictionary in which the EEG signal is sufficiently sparse. This

leads to another important requirement for CS which is the incoherence between the dictionary and the sensing matrix (Singh *et al.*, 2014; Zhang, Rao and Jung, 2013; Majumdar, Gogna, and Ward, 2014). Incoherence defines the level of dissimilarity between the two (Candes and Wakin, 2008). In order to achieve accurate reconstruction of the original signal, the dictionary and sensing matrix has to be highly incoherent (Majumdar, Gogna and Ward, 2014). For EEG signals, the accuracy of reconstruction of the signal with CS depends on a suitable dictionary that is maximally incoherent with the sensing basis (Majumdar, Gogna, and Ward, 2014). Different dictionaries have been developed and investigated to make EEG signal sparse, for example, Gabor transforms (GT), discrete wavelet transforms (DWT), spline and discrete cosine transforms (DCT) (Zhang, *et.al* 2013a; Aviyente, 2007; Abdulghani, Casson, and Rodriguez-Villegas, 2010; Mahrous and Ward, 2016a; Gangopadhyay *et al.*, 2011; Kamal *et al.*, 2013). Kronecker Fourier basis is used as a dictionary in (Shukla, Majumdar and Ward, 2015). DCT is used as dictionary in (Zhang (2013a); Majumdar, Gogna and Ward, 2014). It is stated in (Higgins, Ginley, *et al.*, 2010; Hilton, Jawerth and Sengupta, 1994) at lower compression ratio it shows better performance but at higher compression ratio its performances deteriorates quickly while DWT degrades much more gradually. Aviyente (2007) uses GT for sparse representation of EEG signal.

The findings of these techniques suggest correct reconstructions with less error; however, there has been no explanation or clarification of the particular features that make these dictionaries appropriate. It is challenging to select a particular DWT for a given application to ensure that the compressed signal is accurately reconstructed. A key feature used in selecting a DWT in most applications is the number of vanishing moments, which defines its ability to effectively or sparsely represent complex signals. Unser (1996) states that the approximation order of a DWT increases with the number of vanishing moments up to the smoothness index (Hlder regularity) of the approximated signal according to the Strang-Fix condition (as a special case). An equal number of vanishing moments for the DWT can also be seen as all doing same amount of works (Selesnick, 2004).

Besides the dictionary the Block Sparse Bayesian Learning (BSBL) is used to achieve the block sparsity of EEG/ECG (Electrocardiography) signals. EEG signals have a correlation structure. Reconstruction efficiency of the algorithms deteriorates if the correlation structure is ignored. This function has been ignored by most state-of - the-art

algorithms. Sparse Bayesian Learning (SBL) methods stated in (Zhang and Rao, 2011; Zhang, Rao and Jung, 2013) take advantage of signal correlation structure to make significant improvements in reconstruction efficiency. It is reported Zhang *et al.*, 2013a; Zhang *et al.*, 2013b, Zhang *et al.*, 2014) that the exploitation of the correlation structure with the sparsity of the non-sparse physiological signals may significantly increase the efficiency of reconstruction. It is demonstrated in (Zhang *et al.* 2013a; Zhang *et al.*, 2013b) SBL algorithms obtain the high performance to reconstruct sparse signals. A spatio-temporal sparse Bayesian learning (ST-SBL) approach is proposed in (Zhang, Rao and Jung 2013; Zhang *et al.*, 2014) to exploit both the intra-channel and inter-channel correlation of the signals. ST-SBL simultaneously reconstructs the multichannel EEG signals. This exploits temporal correlation in each channel signal and also the spatial correlation between different channel signals (Zhang, Rao and Jung 2013).

A novel method is proposed in (Zhang *et al.*, 2013a) to use BSBL algorithm to compress and reconstruct raw FECG signals. Findings demonstrated that the in comparison of other BSBL and CS DWT based methods the algorithm can reconstruct the signals with greater quality. A matrix completion based method is used in (Majumdar, Gogna. and Ward, 2014) for signal reconstruction from under-sampled measurements. In order to develop an optimal dictionary and its suitability for hardware implementation a comparison of various dictionaries is made in (Craven *et al.*, 2015). The authors, however, do not reflect dictionary properties such as incoherence and vanishing moments when choosing the dictionaries in prior study. In (Mahrous and Ward 2016b) a novel BSBL approach is presented and as a dictionary DCT is used for both ECG and EEG signals, but does not contribute to the option of DCT selection (Mahrous and Ward 2016b). An explanation of incoherence is provided by (Majumdar and Ward 2015) for choosing the dictionary on the basis of a pre-selected class of dictionaries followed by an optimization algorithm. The research in (Singh *et al.*, 2017) specific on hardware implementation, there is no discussion on the novel properties of the dictionaries. The research carried out in (Zhang *et al.*, 2014) provides a novel computational improvement over the BSBL methods, which is referred to as a ST-SBL method, and is not intended to highlight DWT attributes for optimal dictionary selection. An approach is given in (Mishra *et al.*, 2012) for comparing the reconstruction accuracy with different dictionaries, but in terms of the properties of incoherence and vanishing moments, it does not address the choice or selection of wavelets.

Chapter 3

Overview of EEG Transmission over Wireless Body Area Network

3.1 Introduction

The aim of this dissertation is the transmission of Electroencephalogram (EEG) signals over wireless body area network (WBAN) in an energy-efficient way. In order to have a clear idea about the transmission of EEG signals over WBAN, this chapter mainly presents the overview of EEG transmission through the wireless sensor network including its concept, architectures, limitations and solutions.

Before providing the detail of EEG transmission over WBAN, this chapter introduces the background information about EEG in section 3.2 which includes the generation, frequency bands, recoding process, rhythms and applications of EEG. Section 3.3 depicts the concept of EEG transmission over WBAN, this section is divided into some subsections which provide challenges and shortcomings of WBAN and also the methodologies to use to overcome the limitations of EEG transmission over WBAN. The summary of the chapter is presented in section 3.4.

3.2 Background information about EEG

This section provides the background information about EEG. Before the brief discussion on EEG signal transmission, it is necessary to know what EEG is, how it generates, what the frequency bands are, how it records and what its applications are. The following subsections will provide all the information to introduce some terminologies and associated information of this research.

3.2.1 Electroencephalogram Signals (EEG)

The human brain comprises millions of neurons that play a key role in regulating the human body's conduct in relation to internal/external motor/sensory stimulation. These neurons act as carriers of information between the human body and the brain. Cognitive brain behaviours can be understood through the analysis of either signals or brain images (Kumar and Bhuvanewari, 2012). Electroencephalogram (EEG) is a powerful

physiological parameter which measures brain's electrical activity. It has been considered as the gold standard for neurology and neurophysiology research over the years (Meng *et al.*, 2014; Gil Y *et al.*, 2011). The EEG is commonly used to study brain functions and to diagnose neurological disorders by doctors and researchers.

An English physicist Richard Caton found the presence of electrical currents in the brain in 1875 (Teplan, 2002). Caton noted the EEG from the rabbit and monkey's exposed brains. In 1924, a German neurologist Hans Berger first introduced the electrical activity of human brain. Using a regular radio device, he amplified the brain signal which captured from the human scalp without exposing the skull. He showed a graphical representation of brain signal. He also noticed that the brain signal changed with the functional status of the human, such as anesthesia, sleep, absence of oxygen, epilepsy (Teplan, 2002).

3.2.2 Generation of EEG

Local current flows are generated during the stimulations of brain cells (neurons). EEG mainly measures the currents which flow in the cerebral cortex during synaptic excitations of the dendrites of brain cells (Teplan, 2002). A great amount of activated neurons can produce sufficient electrical activity to provide a recordable signal. It is necessary to amplify and process the recorded EEG signal (Taywade and Raut, 2012). EEG can record both the regular or critical signals of brain, therefore it is considered as a strong tool in the field of medical science.

3.2.3 EEG Recording System

EEG recording system comprised of a variety of electrodes, amplifiers, filters and a monitor or computer. Electrodes acquire the electrical signal from the brain. Generally, one pair of electrodes are connected to the amplifier. Since EEG is a microvolt range signals (typically 1 to 100 μ V of amplitude); it needs to amplify before digitization (Nuwer *et al.*, 1998). Finally, the recorded EEG displays a continuous graphical representation of the electrical activity of the brain on the computer screen. Figure 3.1 shows a typical EEG system. EEG can be recorded in two different ways based on the location from where the signal is recorded in the head. The first way is known as scalp EEG or non-invasive EEG; electrodes are placed on the scalp with good mechanical and electrical contact. The other one is known as intracranial EEG or electrocorticogram (ECoG) where electrodes are directly implanted in the cerebral cortex of brain by

surgery (Adeli *et al.*, 2003). This kind of EEG recording also called invasive EEG (Mansor *et al.*, 2011). There are various kinds of electrodes available, such as disposable conductive gel (Ag-Cl), reusable disc electrodes (with gold, silver, tin compositions), headband and cap electrode and needle electrode.

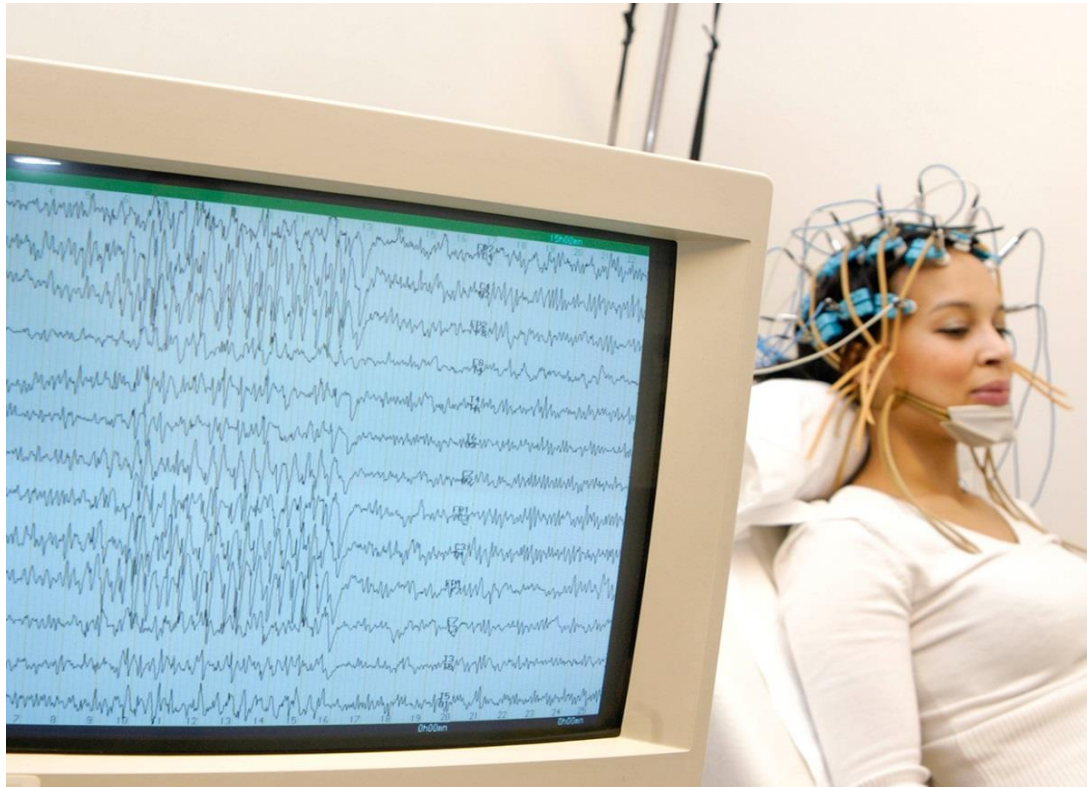


Figure 3.1. Typical EEG system (Waltz, 2017).

EEG system can have up to 128 or 256 electrodes on the basis of use (Teplan, 2002). This is known as multichannel EEG system. Usually, each pair of electrodes indicates a single channel that presents a signal in the EEG system. Usually, electrodes placement for the non-invasive EEG recording follows the internationally standardized 10-20 system (Jasper, 1958). The numbers "10" and "20" indicate the matter that the real distances between two neighbouring electrodes are either 10% or 20% of the skull's complete front-back or right-left range. It can be seen in Figure 3.2, one measurement is drawn from the starting reference point nasion, over the top of the head to the other reference point inion. Similarly other measurement is taken from the right ear across the top of the head to the left ear (Klem *et al.*, 1999). The electrodes are marked with letters indicating the position of the brains' lobe, for example, F-frontal, T –Temporal, C-Central, P-Parietal, O-Occipital. The electrode that is positioned in the midline is marked by 'z'. Besides, numbers are used to define the

position of electrodes on the hemisphere, such as odd numbers refer left hemisphere and even numbers show the position of the right hemisphere (Kumar and Bhuvaneshwari, 2012). For example, F8 is placed on right frontal lobe of the brain.

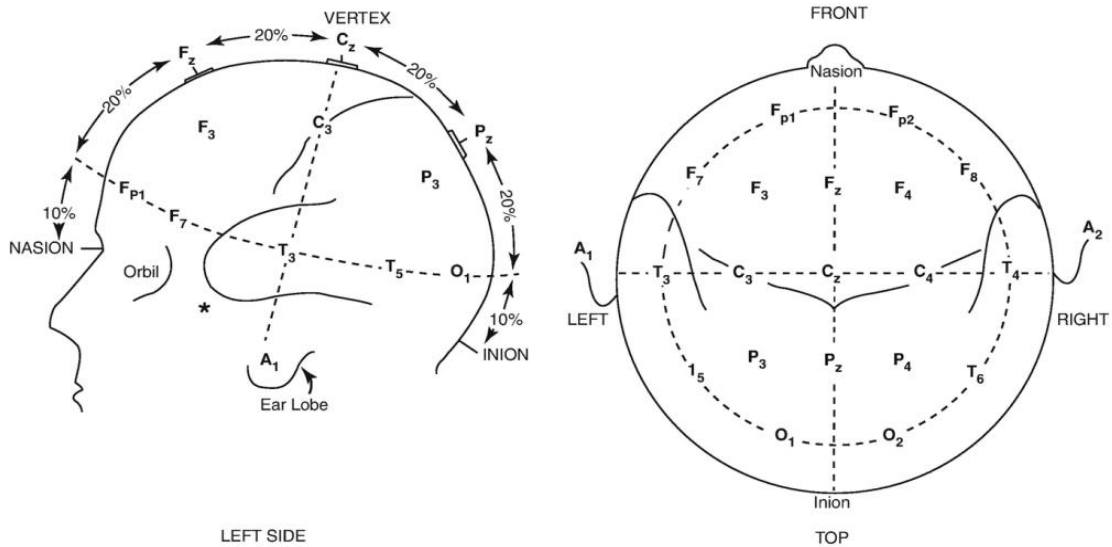


Figure 3.2. The international 10-20 electrode placement system (Sazgar and Young, 2019).

3.2.4 EEG signal Natures or Rhythms

The frequency of brain signal is one of the most significant factors that help to detect any neurological disorder. The frequency of EEG signal differs according to the states of human, such as, sleeping or awakens state or physical condition. Depending on the frequency band and mental states EEG rhythms generally classified in particular groups, such as delta (0.1-4 Hz), theta (4-8 Hz), alpha (8-13 Hz) beta (13-30 Hz) and gamma (>30 Hz) (Kumar and Bhuvaneshwari, 2012). Figure 3.3 displays the waveforms of these five types of EEG rhythms and the frequency bands and the associated mental states of human are presented in Table 3.1.

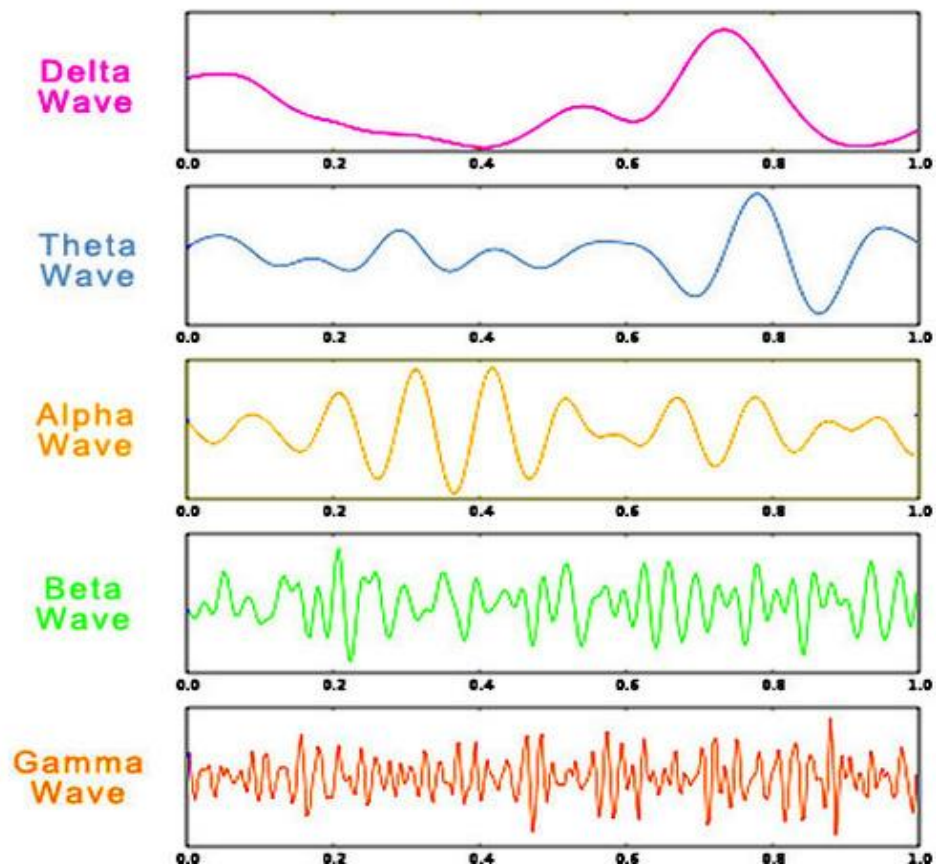


Figure 3.3. Typical EEG rhythms (Crystal Blue Enterprises, 2015).

Table 3.1 EEG rhythms types, their frequency band and associated mental states.

EEG Rhythm Types	Frequency Band	Mental States.
Delta (δ)	0.1 Hz-4 Hz	Profound sleep, severe brain disorder and awake conditions.
Theta (θ)	4 Hz -8 Hz	Creative thought, profound meditation, drowsiness, unconscious content, frustration or disappointment.
Alpha (α)	8 Hz -13 Hz	Relaxation, closed eyes, subconscious.
Beta (β)	13 Hz -30 Hz	Conscious, concentration, problem-solving, active thinking.
Gamma (γ)	30 Hz -100 Hz	Hyper alertness, certain cognitive and motor functions.

3.2.5 Applications of EEG Signals

EEG signal can be used to identify any neurological disorders, brain diseases, physical abnormalities and also can use for research purposes. The applications of EEG are stated below.

Clinical Application:

- Detection of epilepsy and locating the region of seizure.
- Sleeping disorder and drowsiness investigation
- The depth of anaesthesia monitoring
- Monitoring consciousness, coma and brain death.
- Locating harm regions after brain injury, stroke, tumour, etc.

Research Application:

EEG signals have enormous applications in the field of neuroscience, cognitive science and psychophysiological research.

It is very evident from the above list of applications that it has a huge scope for EEG signal analysis, processing and transmission with advanced technique and technology so that EEG interpretation becomes easier and clears to the clinicians. The following section describes the tele-monitoring of EEG signals in the application of WBAN.

3.3 WBAN-oriented EEG transmission

In the typical wired EEG system, patients need to remain very close to the monitoring device and medical expert in the hospital (Figure 3.1). This significantly interrupts patients' daily life and also constricts the research on EEG applications (Gil *et al.*, 2011). For example, for real-time epileptic seizure detection, patient's EEG needs to be monitoring continuously for a long period of time which is a lengthy and expensive effort. This also consumes both the resources of hospitals and the time of the physicians. In addition, the patient is separated from their regular environment and therefore any related variables may affect their epilepsy (Higgins *et al.*, 2010).

Recently, tele-monitoring of EEG through wireless body area network (WBAN) has become an emerging trend in home-based e-health (Zhang *et al.*, 2013a; Higgins *et al.*, 2010). Tele-monitoring of EEG is a way of capturing EEG signals of patient continuously in an outpatient environment using a portable device which is carried by the patient even without interrupting their regular activities (Higgins *et al.*, 2010; Búsze

et al., 2010). WBAN- based EEG system consists of a number of EEG sensor nodes. These sensor nodes are either place on the scalp to get non-invasive EEG signal or directly implanted inside the brain to acquire ECoG signal. The sensor nodes also compress the EEG signal (Negra, Jemili and Belghith, 2016). The compressed EEG is sent to a neighbouring computer or smartphone via Bluetooth and then transferred over the internet to the receiver or medical server where the original EEG can be reconstructed using a computer (Zhang *et al.*, 2013a). Thus the system enables patients to keep track of their medical status without visiting hospitals frequently (Balouchestani *et al.*, 2012a). Therefore, the development of wireless sensor networks has enhanced healthcare applications and real-time patient monitoring systems (Hussein *et al.*, 2015).

The rapid development of wireless communication technology paves the way to support medical and healthcare system in order to enhance the quality of treatment and reduced associate expenses. WBAN is an emerging technology which offers remote monitoring of the patient's health using some embodied sensors that collect health information of the patient (Al-Janabi *et al.*, 2016). Figure 3.4 shows the general architecture of WBAN.

WBAN incorporates several sensors which are positioned either directly on the surface of the user's body or implanted inside the body. The sensor nodes collect vital information from the human body. There are various types of sensor nodes depending on the requirement of the users such as EEG sensor is used to study user's brain activity, similarly to gather information about user's heart activity, ECG sensor nodes are incorporated. Some other sensor nodes are used to measure blood pressure, body temperature, etc. (Al-Janabi *et al.*, 2016). Since the focus of this research is EEG signal transmission, only EEG sensor node is considered in the WBAN architecture (Figure 3.4). The EEG sensor node is placed on the user's head which collects EEG signal from the human brain and as EEG signal has high volume of data it needs to be compressed before transmission. WBAN used different compression techniques to compress physiological signals in energy efficient way. The compressed EEG is sent to a nearby personal server (PS) through ultralow-power short-haul radios (for example, Bluetooth, Zigbee, Medical Implant Communication Service (MICS), Ultra Wide Band (UWB), Wireless fidelity (Wifi), etc.) (Khan *et al.*, 2010). Mobile phone or computer can be used as personal server which also controls WBAN and transmits the user's physiological information to the remote terminal via the internet.

The remote terminal can be considered as medical server (MS) as the ultimate goal of transmitting signals is to monitor user's physical status. In the medical server, the original signal is retrieved using computer. Medical databases store the health information of each registered patient and offer them different services according to the demands. For example if the patient needs immediate attention they send emergency service. The patients need not visit hospitals frequently because of portable monitoring devices. This wireless network also ensures location independent healthcare services, for instance, the user can be at home or at work continuing with their regular activities, and still their health can be monitored flawlessly and continuously.

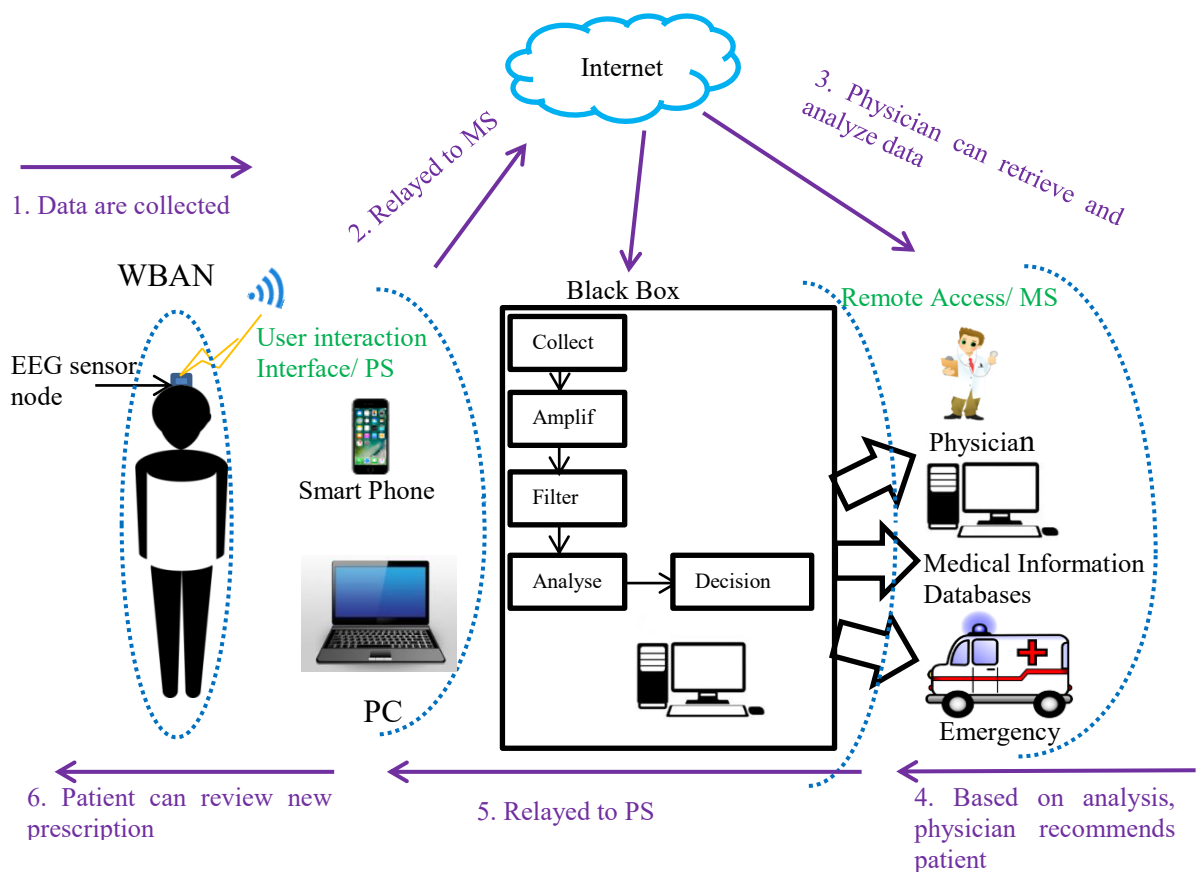


Figure 3.4. EEG-Based WBAN architecture.

The physiological data acquired from this wireless network can also be used for research purposes. The black box in Figure 3.4 indicates the research database where the collected data are going through further analysis with filter out the noise and then send the related decision to the medical server.

3.3.1 Advantages of WBAN-oriented System

WBAN offers a number of advantages over the existing wired system that is discussed below:

- WBAN provides real time data acquisition, processing, transmitting and monitoring remotely.
- The main constraint of the existing wired systems is they are made of location-specific sensors which are clumsy in nature. Whereas, WBAN facilities location independent services (Khan *et al.*, 2010).
- WBAN also ensures mobility of users because of wearing portable devices. Users can continue their daily activities carrying the portable device of WBAN which will continuously collect and transfer their health information to the healthcare centre to monitor it ubiquitously.

3.3.2 Challenges in WBAN-based EEG transmission system

Despite the numerous advantages of WBAN, there are some limitations that need to be considered during designing the network. Energy consumption is the essential one (Zhang *et al.*, 2013a; Singh *et al.*, 2014). WBAN sensor nodes are battery-driven which is confined in longevity. Therefore, it is important to save power as much as possible which will consequently increase battery life as well as the efficiency of the overall system (Liu *et al.*, 2015).

The second challenge of WBAN based EEG system is high volume of data of the EEG signal which needs to be compressed to a great extent before transmission. The reason for high level of compression is that the transmission link (for example, Bluetooth) that used to transmit data has limited transmission capacity. In addition, usually mobile phone is used as the personal server which initially stores the data. Therefore it is essential to ensure that data volume does not overwhelm the mobile phone's capacity by interrupting its main tasks like calling, texting and browsing (Zhang *et al.*, 2013a).

Hardware expenses are another limitation. Minimum equipment expenses will make the portable online-monitoring device economically feasible and acceptable to the users. Furthermore, economically reasonable equipment also indicates the fact that its data processing and reconstruction technique is also less complex.

3.3.3 Methodology to resolve challenges in WBAN

The constraints in WBAN introduce three major requirements: i) lower energy consumption at the sensor node, ii) higher data compression rate and iii) minimum equipment cost. In order to address all these requirements, an energy efficient signal processing methodology is required to ensure that EEG signal is compressed, transmitted and reconstructed energy efficiently (Lalos *et al.*, 2015).

There exists a variety of EEG signal processing methods. Some of these methods, EEG is compressed directly in time domain, for example, Antoniol and Tonella (1997) used Huffman coding technique to compress EEG signal in time domain, a near-lossless compression technique is used in (Memon *et al.*, 1999, Sriraam and Eswaran, 2008). According to (Mahajan and Bansal, 2014) these methods are able to compress signal at high level but they are not computationally effective.

There are some researches that used wavelet transform (WT) to compress EEG (Sornmo and Laguna, 2005; Fira and Goras, 2010; Dehkordi *et al.*, 2011; Sriraam, 2012; Kamat *et al.*, 2013; Chitra *et al.*, 2015; Panessai and Abdulbaqi, 2019). Zhang (2013a) stated that wavelet compression is not able to address all the WBAN constraints together. Moreover, WT is also a computationally complex technique.

Most of the methodologies that are mentioned above fail to recover the clinical features in EEG because of poor reconstruction quality. Therefore, automated feature extraction and signal processing methods are necessary for real time and clinically useful implementation in such applications.

Recent efforts aiming to increase battery life focus on reducing the power of transmission and data rate with compressive sensing (CS) (Zhang *et al.*, 2013a; Sing *et al.*, 2014; Liu *et al.*, 2015; Candes and Wakin, 2008) As CS can lead to significant computational savings for on-chip implementation with relatively low sampling rates, recently, it has been viewed with considerable interest as a viable technique for the transmission of large data volumes and high data rate signals over WBAN (Zhang *et al.*, 2013a; Balouchestani *et al.*, 2012b; Djelouat *et al.*, 2017; Imtiaz *et al.*, 2014; Gogna *et al.*, 2017; Hanafy *et al.*, 2017; Majumdar and Ward, 2016; Kaliannan and Pasupureddi, 2016; Lalos *et al.*, 2014; Balouchestani *et al.*, 2012a). In CS data is projected into a compressed format non-adaptively upon acquisition using a sensing matrix, which differs from conventional compression techniques where data is acquired then compressed and indices are stored. In this study, CS is employed for transmission of EEG signal over WBAN. The detail of CS is discussed in the next chapter.

3.4 Summary

This chapter provides the concept of EEG signal transmission over WBAN. Tele-monitoring of EEG in WBAN is very important since EEG is the most powerful physiological parameters for diagnosing any brain diseases. EEG signal usually needs to be recorded for a longer period of time which results in a large volume of data leading to huge storage and communication bandwidth requirements in WBAN. Besides, WBAN sensor nodes are functioned by the battery which consumes lots of energy. The aim is, therefore, to transmit EEG signal in an energy and computationally efficient way. This chapter also provides information about the existing methodologies that are used for EEG signal processing. From the literature review it can be concluded that compressive sensing method is the best approach compared to others as it compresses EEG signal at a low sampling rate and also enables to reconstruct the signal from much lower number of samples while retaining the significant clinical information.

The detail discussion on CS and the proposed framework is presented in chapter 5.

Chapter 4

Research Methodology

4.1 Research Problem

For a successful transmission and reconstruction of EEG signals using CS relies on the selection of the dictionary which make the signal sparse. Wavelet bases are widely used as dictionaries in CS; however, their properties are not studied in depth. The research problem is, therefore, which properties of wavelet bases need to be considered for selecting the suitable wavelet dictionary of EEG signal.

4.2 Literature Survey

The authors in (Craven *et al.*, 2015) make a comparison of several dictionaries for CS in EEG and ECG signals for developing an optimal dictionary and its suitability for implementing in embedded hardware. However, there is no reflection in prior analysis of dictionary properties such as incoherence and vanishing moments for the choice of the dictionaries. A novel BSBL method is described in (Mahrous and Ward 2016b) and the DCT is used to increase sparsity with the results shown for both ECG and EEG signals, but is not linked to the option of choosing DCT (Mahrous and Ward 2016b). An explanation in terms of incoherence is given in (Majumdar and Ward, 2015) for dictionary choice followed by an optimization algorithm that leads to optimal dictionary selection, based on a pre-selected dictionary class. The research discussed in (Singh *et al.*, 2017) is on hardware implementation, there is no discussion of novel dictionary properties. The research in (Zhang *et al.*, 2014) provides a novel computational improvement over the BSBL methods known as the ST-SBL method, and is not intended to highlight DWT attributes for optimal dictionary selection. The methodology in (Mishra *et al.*, 2012) contrasts the accuracy of the reconstruction for specific dictionaries. In terms of the properties of incoherence and vanishing moments, it does not address the choice or selection of wavelets.

4.3 Properties of DWT

In the state-of-the-art research, the dictionary properties that make them ideal choices for EEG signals have not been thoroughly studied. Although incoherence has been studied and is well understood for CS, the vanishing moment, on the other hand, is understood to represent complex signals efficiently and sparsely in terms of Discrete Wavelet Transform (DWT) applications. These two essential properties are considered in isolation and have not been jointly investigated for CS in EEG signals. The study of this research shows that both features should be explored simultaneously in the dictionary selection; this is often ignored.

4.4 Proposed Approach

This research propose an approach for the selection of an appropriate wavelet dictionary by investigating incoherence of dictionary with SBM, together with vanishing moments of wavelet dictionaries for effective implementation of compressive sensing for EEG signal transmission and reconstruction. Spatiotemporal Block Sparse Bayesian Learning (ST-SBL) method is used as the reconstruction algorithm.

4.5 Data Selection and Simulations

The research is based on transmission and reconstruction of EEG signal. There are various EEG datasets are available. In this research, three types of EEG datasets are used for validating proposed approach; they are driving task, visual task and epileptic and non-epileptic datasets. The details of datasets selections are given in chapter 6.

All the simulations involve in this study are accomplished in MATLAB.

4.5 Validation of the Proposed Approach

Clinical data are used for validation. The proposed approach is validated to determine the clinical effects of CS using the appropriate DWT using a classification algorithm based on feedforward neural network which classify epileptic from nonepileptic EEG signal.

Chapter 5

Wavelet Bases for Compressive Sensing of EEG Signals with Accurate Reconstruction

5.1 Introduction

Tele-monitoring of electroencephalogram (EEG) signals over wireless body area networks (WBAN) is challenging due to high volume of data and power requirements. To reduce data rate and consequently reduce power consumption, compressive sensing (CS) is employed prior to transmission. Generally, there are three main components in compressive sensing; a sensing matrix, a sparsifying dictionary/basis and a reconstruction algorithm.

Sparse binary matrix is of interest for the sensing matrix in the target application due to its ease of implementation and reduced power footprint.

A requirement of CS is that the signal has to be sparse in the domain where it is compressed. A challenge, therefore, in employing CS for the EEG signal is to identify the domain known as the dictionary in which the EEG signal is sufficiently sparse. There are a plethora of choices for the dictionary to be used. Wavelet base is widely used as a dictionary in CS; however, its features have not been analyzed fully. Two key criteria for an appropriate selection of the dictionary are the number of vanishing moments, indicating to what extent it can represent complex signals sparsely; and with respect to CS, incoherence of the dictionary with the sensing basis, denoting how accurately the original signal may then be reconstructed.

Spatiotemporal block sparse Bayesian learning method (ST-SBL) is a suitable choice for the reconstruction algorithm since it is designed for multichannel acquisition by exploiting inter-channel correlation. While such an algorithm only requires block sparsity, in the absence of temporal correlation transferring the signal onto a domain in which the signal is sparse may compensate for it. Current motivations in employing CS include low hardware complexity with optimization algorithms, and novel ST-SBL approaches to reduce latency.

In this chapter, the background knowledge of CS and the framework associated with selecting a suitable wavelet dictionary for accurate reconstruction of EEG signal are presented.

A brief introduction of the background and the theory of CS are given in section 5.2 followed by the subsections of sensing basis, sparsifying dictionary, incoherence, selection of the wavelet dictionary and vanishing moment. Section 5.3 provides method and materials and section 5.4 presents the summary of the chapter.

5.2 Overview of Compressive Sensing and its Background Knowledge

The traditional approach of signal processing follows the well-known Shannon theorem for sampling signal which states that it is possible to represent and reconstruct a signal successfully by sampling it at a rate twice of its maximum frequency (known as Nyquist rate). However, there exist many signals which have such a high bandwidth that it is impractical to process them especially, in wireless sensor systems. Moreover, signals with lower bandwidth such as EEG signals (0.1-100 Hz bandwidth) (Kumar and Bhuvaneshwari, 2012) sampling at Nyquist rate generate a large volume of data that are expensive for wireless transmission and also significantly restricts WBAN's battery lifetime (Mamaghanian *et al.*, 2011). Therefore, to transmit EEG signal energy efficiently over WBAN, it is required to lessen the number of EEG samples before transmission. Compressive sensing (CS) is possibly a very appropriate approach for this purpose which asserts that it is possible to reconstruct some signals from a far lesser number of samples than the conventional approach (Candes and Wakin, 2008; Donoho, 2006). In order to achieve this, CS is based on two criteria; the sparsity of the signals of concern and incoherence of the sensing mode (Candes and Wakin, 2008).

CS Theory: CS relies on the assumption that a signal of length N , denoted by $x \in \mathbb{R}^{N \times 1}$, is compressed by a random matrix denoted by $\Phi \in \mathbb{R}^{M \times N}$, to yield, which is the measured signal is given by:

$$y = \Phi x \quad (5.1)$$

here M is the number of samples in the compressed signal and $M \ll N$; which means the signal is sampled at a comparatively much lower rate. Φ is the sensing matrix and should be known at the receiver for reconstruction of the original signal x . The success

of reconstructing the original signal relies on the assumption that the signal x is sparse i.e., it has only a few non-zero entries and the rest of the entries are all zero. If x is not sparse in time, it is necessary to represent it in a suitable domain in which it exhibits sparsity. This domain represented by a dictionary matrix, denoted by $\Psi \in \mathbb{R}^{N \times N}$. Thus, x can be represented as:

$$x = \Psi z \quad (5.2)$$

where z contains the coefficients of x in Ψ domain. Assume x is K -sparse in this domain (i.e., z has only $K < N$ non-zero elements; in practice, z may contain K relatively large elements whilst the rest may be ignored, in which case the signal is compressible in this domain). Using (5.1) and (5.2):

$$y = \Phi \Psi z = \Theta z \quad (5.3)$$

Therefore, for reconstructing the original signal, CS algorithms need to reconstruct z first using y and Θ , and subsequently, the original signal x can be reconstructed by using (5.2). At the receiver end, a recovery algorithm is applied to reconstruct the original signal. It is not necessary to have knowledge of Ψ in the compression stage but receiver side users must have the prior knowledge of Ψ to reconstruct signal from its sparse representation (Imtiaz, Casson and Rodriguez-Villegas, 2014). Figure 5.1 shows the block diagram of CS in EEG transmitter and receiver.

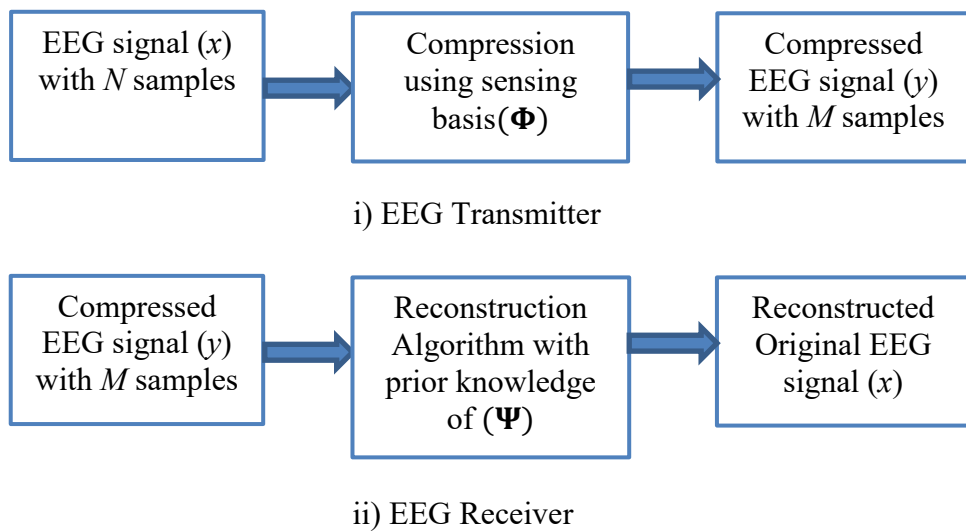


Figure 5.1. Block diagram of CS-based EEG Transmitter-Receiver.

In summary, CS consists of two stages; i) compression stage: which randomly samples input signal. This stage consumes energy of the sensor node but it is computationally less complex since it is run on-chip/online. ii) reconstruction stage: which computational complexity is bit higher but it operates off-line with much relaxed energy limitations on remote computer (Casson and Rodriguez-Villegas, 2012).

During designing a low-power and efficient CS-based system two important factors are considered in this research:

- Reconstruction accuracy and energy efficiency: the system maintains a high level of compression with excellent quality of reconstruction which satisfies the low power requirements of WBAN.
- Computational simplicity: an optimal system must sustain an easy on-line compression and efficient algorithms for off-line reconstruction. Nevertheless, there always has some trade-off between system complexity and efficiency.

5.2.1 Challenges in CS-based EEG transmission

A requirement of CS is that the signal has to be sparse in the domain where it is compressed (Candes and Wakin, 2008). EEG signal, however, is not sparse in time or the frequency domains (Zhang *et al.*, 2013a). A challenge, therefore, in employing CS for the EEG signal is to identify the domain known as the dictionary in which the EEG signal is sufficiently sparse. This leads to another significant requirement for CS which is the incoherence between the dictionary and the sensing basis matrix termed as sensing matrix henceforth (Singh *et al.*, 2014; Zhang, Rao and Jung, 2013; Majumdar, Gogna, and Ward, 2014) i.e., the level of dissimilarity between the two. For an accurate reconstruction of the original signal, the dictionary and sensing matrix must be highly incoherent. Therefore two main challenges of CS-based EEG transmission are i) selection of sparsifying dictionary and ii) incoherence between sensing basis and sparsifying dictionary. Before describing these two challenges it is necessary to have knowledge about sparsifying dictionary and sensing basis. The following sections present these two bases.

5.2.3 Sensing Basis

Sensing basis (Φ) is responsible for the compression of signal in CS. The choice of Φ is mostly directed towards minimal power usage and low complexity in the hardware of

WBAN-based EEG transmission system. One of the main requirements of CS is sensing basis needs to be highly incoherent with sparsifying dictionary and random sensing basis are found maximally incoherent with any sparsifying dictionary (Candes & Wakin, 2008). Usually, Gaussian and Sparse Binary basis are most frequently used as random sensing basis.

Gaussian Basis: the entries of this basis are selected from normal distribution with zero mean and $1/N$ variance (Shukla, 2014). This is a dense basis which means each entry of the matrix has some value (Majumdar, Gogna, and Ward, 2014). Though this is mostly used basis it is not efficient to use in embedded platforms like WBAN sensor node because it requires huge storage and needs to perform large computation for matrix multiplication of compression process (Tiwari, Bansod and Kumar, 2015; Mamaghanian *et al.*, 2011). In contrast to this, sparse binary basis enables the matrix multiplication in CS very quickly and efficiently.

Sparse Binary Basis (SBM): a sparse binary matrix is often used as it consumes very low power (Mamaghanian *et al.*, 2011; Zhang, *et al.*, 2013b; Pei and Wang, 2017). This is because sparse binary matrix (SBM) has very few of its entries as ones and most the entries are zeros (Zhang, *et.al* 2013a). This reduces less storage, complexity and power requirements as it simplifies the hardware implementation, which is crucial to design of low-power and efficient transmitters in WBANs.

5.2.4 Sparsifying Dictionary

Sparse representation of the desired signal is another fundamental requirement of CS. Some biomedical signals, such as EEG is not sparse in nature. Therefore, it requires a dictionary to represent it sparsely. For CS of EEG signals various dictionaries have been developed and investigated to enable sparse representation. These include discrete cosine transform (DCT), Gabor transforms (GT) and wavelet bases, i.e., discrete wavelet transforms (DWT) (Zhang, *et.al* 2013a; Aviyente, 2007; Abdulghani, Casson, and Rodriguez-Villegas, 2010; Mahrous & Ward, 2016a; Gangopadhyay *et al.*, 2011; Kamal *et al.*, 2013). Other methods include using Kronecker Fourier basis as a dictionary (Shukla, Majumdar and Ward, 2015). DCT is used in (Zhang, *et.al* 2013a; Majumdar, Gogna and Ward, 2014) as sparsifying domain. It shows good performance at lower compression ratio but investigation shows that at higher compression ratio its performances degrade quickly while DWT deteriorates much more gradually (Higgins,

Ginley, *et al.*, 2010; Hilton, Jawerth and Sengupta, 1994). GT is used in (Aviyente, 2007) for sparse representation of EEG signal which is supposed to consist of short sinusoidal waves. EEG signals have varying spike structures that are more complicated than short-term sinusoidal waves. In addition, EEG are designed as windowed, piece-wise smooth polynomials and it is well established that a piece-wise polynomial can be represented sparsely in DWT (Mallat, 2008). Therefore, the performance of sparsification of EEG signals in DWT is significantly better than GT (Gangopadhyay *et al.*, 2011). Thus, the focus of this research is DWT as sparsifying dictionary.

5.2.4.1 Discrete Wavelet Transforms (DWT) Dictionary

EEG signal has a concise representation while presenting in a proper sparsifying domain. For example, Figure 5.2 depicts an EEG epoch and its DWT wavelet coefficients.

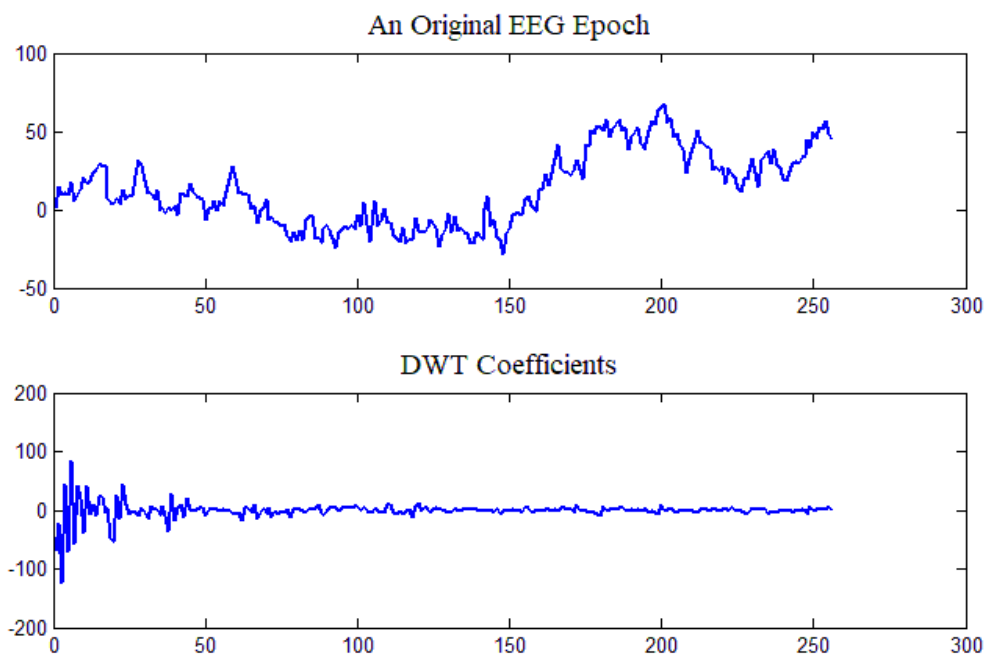


Figure 5.2. Example of EEG signal and its DWT coefficients.

It can be seen that the EEG epoch has most of the non-zero values but the DWT coefficients providing a concise presentation where most of the coefficients are zero and comparatively a few non-zero coefficients which capturing the most of the signal information.

Mathematically, suppose x is the EEG signal and the wavelet dictionary is Ψ . The sparse representation of x is then as follows:

$$x(t) = \sum_{i=1}^N z_i \Psi_i(t) \quad (5.4)$$

where, z is the coefficients of x , $z_i = \langle x, \Psi_i \rangle$. For convenient x is presented as (5.2). Since the dictionary is fixed, all the information are captured by the coefficients (Hilton, Jawerth and Sengupta, 1994). The impact of sparsity is apparent now: once a signal has its sparse presentation, the small coefficients can be discarded without any significant loss (Candes and Wakin, 2008). In this work, z_i are the DWT coefficients and Ψ is the inverse DWT matrix which is known as mother wavelet.

Generation of the DWT coefficients: The DWTs use a multi-level decomposition to generate the coefficients using Quadrature Mirror Filter (QMF) bank. The filter bank is composed of a number of high-pass (h) and low-pass filters (g) correspond to the type of the wavelet used (Yger, and Rakotomamonjy, 2011). The high-pass filter generates a detail coefficient (coef), $dc(n)$ while low-pass filter generates an approximation coefficient, $ac(n)$ (Figure 5.3). After filtering, the DWT coefficients are downsampled by a factor of 2. The process is repetitively implemented in the low-pass sequence until the required level of decomposition is achieved (Higgins, Ginley, *et al.*, 2010). The level of decomposition depends on the signal's sampling frequency, for instance, a signal with 256 sampling frequency needs to go through a 5-levels of decompositions (Mahmoodin *et al.*, 2015). Owing to the decomposition process, signal should have the samples which are multiple of 2^n , where n indicates the number of decomposition levels.

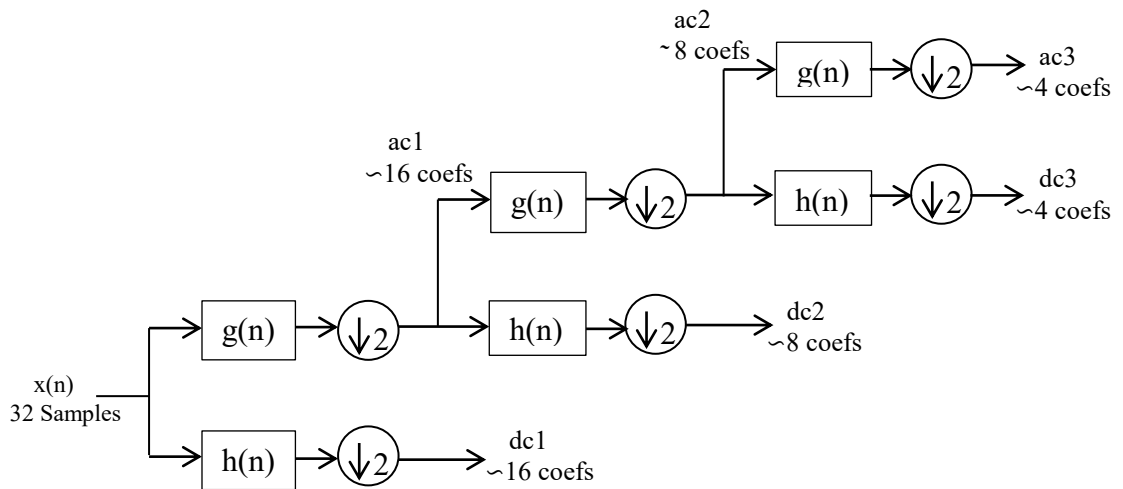


Figure 5.3. 3-level decomposition of DWT coefficients of a signal with 32 samples.

Figure 5.3 shows 3 levels decomposition of DWT coefficients of a signal which have 32 samples.

Reconstruction of the signal from the DWT coefficients: The inverse DWT (IDWT) is used to reconstruct the signal from its DWT coefficients of details and approximation. This is the opposite process of the decomposition where upsampling is performed by inserting zeroes between samples. Since the coefficient vectors were generated by downsampling, they contain only half the length of the original. For that reason, it is not possible to add them directly to reconstruct the signal. The approximation and details need to be reproduced before merging them; they are the real components of the original signal. Figure 5.4 indicates the process of reconstruction (Misiti *et al.*, 2004).

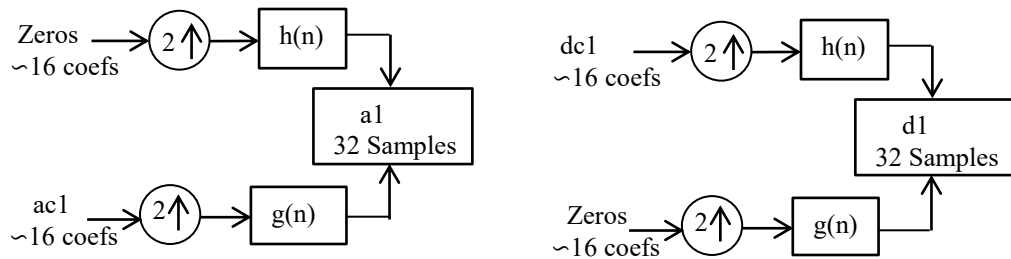


Figure 5.4. Reconstruction of approximation and details of the single level signal.

Thus the original signal can be obtained by adding the reconstructed approximation and details:

$$a1 + d1 = x$$

Accordingly, the 3-level decomposed signal can be reconstructed as Figure 5.5.

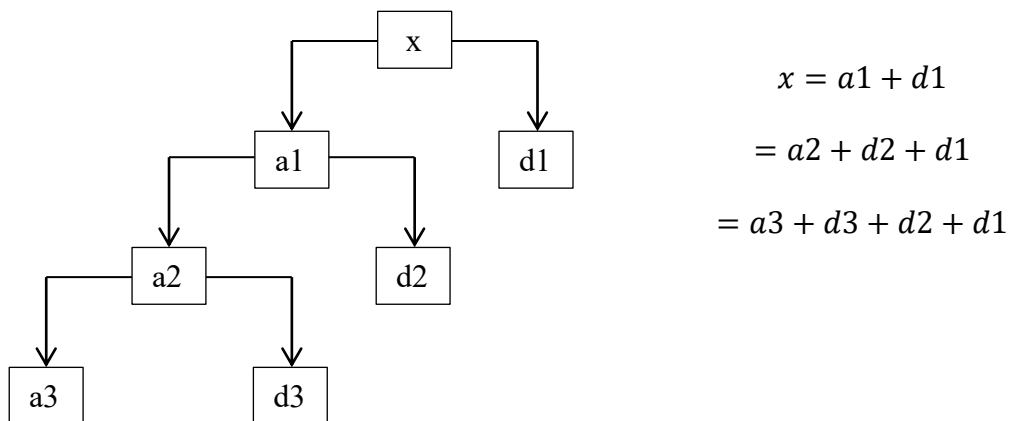


Figure 5.5. Block diagram of reconstruction of 3-level decomposed signal.

In this research, 15-different DWTs are used from wavelet families to reconstruct the EEG signal, they are: 4-DWTs from Daubechies wavelet family (db3, db4, db8, and db10), 2 from Battle family (Battle-1, Battle-3), 5 from Coiflet family (coif1, coif2, coif3, coif4 and coif5), Haar, Vaidianathan, Symelt-10, and Beylkin. Figure 5.6 shows the mother wavelet of these 15-DWTs.

All the simulations of this work are done in MATLAB but the problem is MATLAB does not have any function for generating wavelet dictionary. The wavelab toolbox (Buckheit and Donoho, 1995; Stanford University, 2005) is, therefore, used to generate wavelet dictionary in MATLAB.

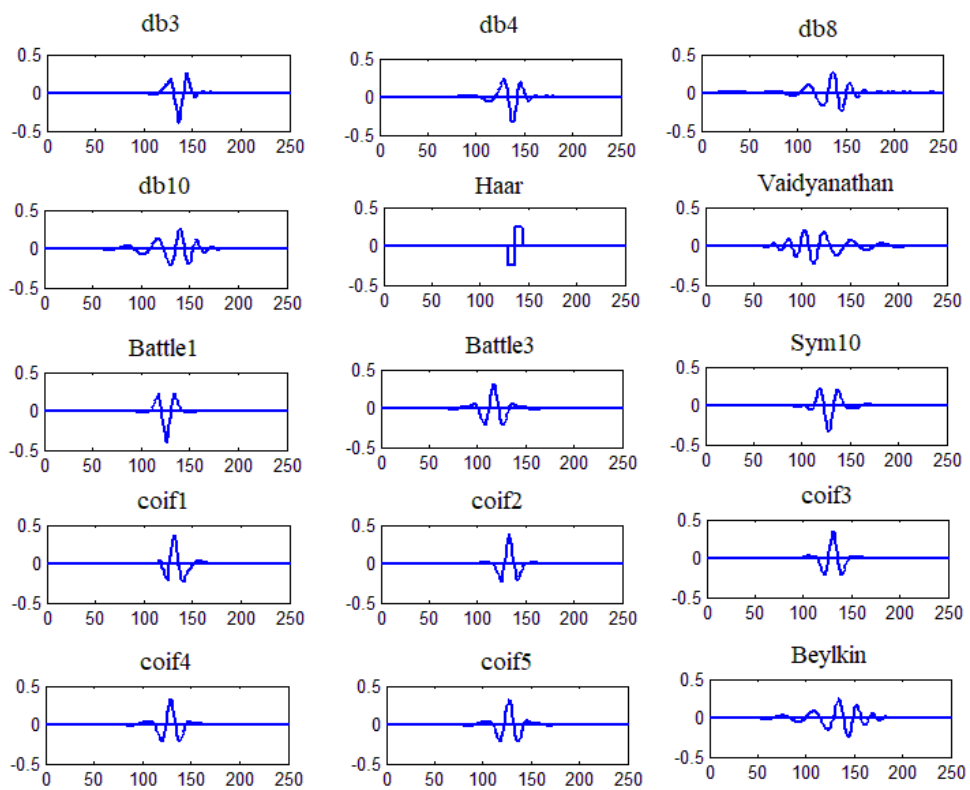


Figure 5.6. Mother wavelets of different DWTs.

5.2.5 Incoherence between sensing basis and Sparsifying dictionary

The accuracy of reconstruction of the EEG signal with CS depends on a suitable dictionary that is maximally incoherent with the sensing basis (Singh *et al.*, 2014; Zhang, Rao and Jung, 2013; Majumdar, Gogna, and Ward, 2014). The reconstruction performance of CS depends on the level of incoherence between Φ and Ψ (Majumdar, Gogna, and Ward, 2014). For successful reconstruction, Θ should follow a condition referred to as restricted isometry property (RIP). RIP may be achieved with high

probability if sensing matrix is random (Candes and Wakin, 2008). A condition related to RIP is the incoherence that denotes rows of Φ , $\{\phi_k\}$, and columns of Ψ , $\{\psi_j\}$ should not be correlated. It is noted that M should be sufficiently large. Coherence (μ) is quantified as shown in (5.5) (Candes and Wakin, 2008).

$$\mu(\Phi, \Psi) = \sqrt{N} \max_{1 \leq k, j \leq N} |\langle \Phi_k, \Psi_j \rangle| \quad (5.5)$$

where N indicates the total number of samples of the signal. A smaller μ indicates a lower level of similarity between the elements of the two bases, i.e., Φ and Ψ are highly incoherent. The value of μ is between 1 and N (Candes and Wakin, 2008).

As EEG is not sparse in either time or frequency domain (Majumdar, Gogna and Ward, 2014) it is essential to find a suitable Ψ for sparsity, and ensuring that it is maximally incoherent with Φ (Pereira *et al.*, 2014). Thus the main concern of CS in EEG is to find a high incoherent pair for accurate reconstruction of EEG. In (Candes and Wakin, 2008) some examples are given of such pairs: the coherence between noiseltes (Φ) and wavelet basis (Haar, db4 and db8 are 1.4, 2.2 and 2.9, respectively. Nevertheless, the investigation results of this study show that the coherence between SBM (and these 3 wavelet dictionaries are 1.6, 1.4 and 1.5, respectively and the lowest coherence is found with Beylkin DWT which is 1.3. Consequently, the reconstruction of EEG is supposed to be more accurate with Beylkin (Ψ) and SBM (Φ) incoherent pair. Details are given in the results chapter.

5.2.6 Selection of wavelet (DWT) dictionary

The different incoherent sparsifying dictionaries that are used in the state-of-the-art CS-based techniques are mentioned in section 5.2.4. Results of those techniques indicate accurate reconstructions with less error; however, the specific features that make these appropriate or suitable dictionaries have not been investigated or explained. Selecting a specific DWT for a given application to ensure an accurate reconstruction of the compressed signal is challenging. In most applications, a key feature employed in selection of a DWT is the number of vanishing moments, which determines its ability to represent complex signals efficiently or more sparsely. According to the Strang-Fix condition (as a special case) the approximation order of a DWT increases with the number of vanishing moments up to the smoothness index (Hlder regularity) of the approximated signal (Unser, 1996). That is, the sparseness of the wavelet-transformed signal is, in general, higher for longer wavelets. An equal number of vanishing moments

for the DWT can also be viewed as all doing ‘similar amounts of work’ (Selesnick, 2004).

In addition to the dictionary the Block Sparse Bayesian Learning (BSBL) may employ to exploit the block sparsity of EEG/ECG (Electrocardiography) signals. The authors in (Zhang *et al.*, 2013a) propose a novel method to use the BSBL framework to compress/reconstruct non-sparse raw FECG recordings. Experimental results show that the framework can reconstruct the raw recordings with higher quality as compared to other BSBL and CS DWT based methods. The authors in (Majumdar, Gogna. and Ward, 2014) depart from previous CS-based approaches and formulate signal recovery from under-sampled measurements as a matrix completion problem. In (Craven *et al.*, 2015) the authors compare and detail performance of various dictionaries for CS in EEG and ECG signals in order to come up with an optimal dictionary and its suitability for deployment in embedded hardware. However, the authors do not reflect in prior analysis of dictionary properties such as incoherence and vanishing moments for the choice of the dictionaries. A novel BSBL approach is given in (Mahrous and Ward 2016b) and the DCT is employed for increasing sparsity with the results presented for both ECG and EEG signals, but does not relate to choice of selecting the DCT (Mahrous and Ward 2016b). In (Majumdar and Ward, 2015) an explanation in terms incoherence is given for choice of dictionary followed by an optimization algorithm that leads the optimal selection of the dictionary, based on a pre-selected class of dictionaries. The work detailed in (Singh *et al.*, 2017) is on hardware implementation, no novel properties of the dictionaries are discussed. The work in (Zhang *et al.*, 2014) offers a novel computational improvement over the BSBL methods known as ST-SBL method and is not aimed at highlighting the attributes of DWTs for an optimal dictionary choice. The approach in (Mishra *et al.*, 2012) compares the accuracy of reconstruction for various dictionaries. It does not mention of the choice or selection of wavelet in terms of the properties of incoherency and vanishing moments.

This thesis is not aimed at comparisons of any BSBL approaches which is done in, or offering an improved BSBL approach, or comparison of DWT CS methods with any BSBL methods. The state-of-the-art studies (Zhang *et al.*, 2013a; Mahrous and Ward 2016b) compares BSBL approaches and offers an improved BSBL approach but there is no proper explanation regarding the choice of dictionaries. This study mainly aims to investigate the incoherence of the dictionary with the sparse binary matrix (SBM), along with the vanishing moment of DWT dictionaries for the effective implementation of

compressive sensing for the reconstruction of EEG signals. While incoherence has been explored and is well known for CS, on the other hand, vanishing moments are understood to represent complex signals effectively and sparsely in terms of wider DWT applications. These two significant properties are considered in isolation and there has been no joint analysis for CS in EEG signals to the best of my knowledge.

The incoherence is already discussed in section 5.2.5 and the details of the vanishing moment for DWT are described in the following section.

5.2.7 Vanishing Moment of Wavelet Dictionary

The number of vanishing moments is related to the order, decay rate and smoothness of wavelets. A continuous wavelet (CW) φ has p vanishing moments when:

$$\int t^k \varphi(t) dt = 0, \quad \text{for } 0 \leq k \leq p \quad (5.6)$$

and for the DWT with filter coefficients h

$$\sum_k k^n h(k) = 0, \quad \text{for } n = 0, 1, \dots, p-1 \quad (5.7)$$

The number of vanishing moments is the differentiability or a measure of the smoothness of functions. The DWT has p vanishing moments if and only if the wavelet scaling function can generate polynomials up to degree $p-1$. The "vanishing" part means that the wavelet coefficients are zero for polynomials of degree at most $p-1$. A higher value of p implies that the wavelet filter is able to filter out high frequency components of the signal accurately from any of the low-frequency or long-term data variations. This accordingly leads to an accurate reconstruction of the signal. CWs and DWTs with a higher value of p can represent more complex functions.

A higher p also increases sparsity of a large class of signals being represented by the DWTs. The p indicates the number of zeros at $z = -1$ i.e. at half the sampling frequency for the low-pass Discrete Fourier Transfer (DFT) filter or the scaling filter ; which is the same as number of zeros at $z = 1$ i.e. at DC for the high-pass DFT filter or the wavelet filter. In most cases the DWT name is suffixed by its order n . The Daubechies- n and Symlet- n DWTs both have $p = n$ vanishing moments and accordingly has p number of zeros at $z = 1$ and -1 for the scaling and the wavelet filters respectively. The number of filter coefficients n_c for the DWTs is $2p$. Their difference lies wherein Symlet filters are as symmetrical as possible as compared to the Daubechies filters which are highly asymmetrical. The Coiflet- n DWT has $p = 2n$ vanishing moments with $n_c = 6n$. The

Battle-Lemarie also known as Battle- n DWT generates spline orthogonal wavelet filters, where n is the degree of spline. The Battle- n DWTs have $p = n + 1$. The Battle- n have infinite support but with an exponential decay, and filter coefficients below 10^{-4} are neglected in this work, giving $n_c = 12$ and 21 for Battle-1 and Battle-3 respectively. The Beylkin is optimised for placement of additional zeros close to half the sampling frequency for obtaining higher attenuation of high-frequency components for the scaling filter and close to DC for attenuation of the low-frequency components. It has fixed number of filter coefficients $n_c = 18$ and although it has three zeros at $z = -1$ and 1 , it has $p \sim 9$. The Vaidyanathan DWT is optimised for speech coding with $n_c = 24$ with additional zeros close to high frequency and DC for the scaling and wavelet filters. It offers accurate reconstruction of the decomposed signal just as in case of other DWTs including Beylkin but does not satisfy any moment condition. The Haar DWT is least complex to implement as it has $n_c = 2$, has one zero at $z = -1$ and 1 for the scaling and wavelet function indicating $p = 1$.

5.3 Methods and Materials

This section provides the method and materials of the proposed framework. Subsection 5.3.1 gives the method and material of measuring incoherence of SBM with DWT dictionary. The algorithm is used to reconstruct the EEG signal is described in section 5.3.2. The performances matrices use to measure the quality of the reconstruction signal are presented in section 5.3.3. The comparison of DWT, DCT and the case using no dictionary is given in section 5.3.4. The method uses to measure classification error of clinical EEG signal is presented in section 5.3.5.

5.3.1 Incoherence of SBM with DWT dictionaries

At first, the number of non-zero entries (d) in each column of the sparse binary matrix (SBM) that would lead to a moderate incoherence for all the DWT dictionaries to be used is identified by measuring the coherence of randomly generated SBM with each dictionary for a varying number of non-zero entries. It is also verified if d has any impact on the reconstruction algorithm by investigating error in terms of variation of d . After identifying the specific value of d that gives a moderate incoherence between SBM and DWT, the coherence between them for that value of d is also measured. The identified d value with moderate coherence is used across the work.

5.3.2 Reconstruction by exploiting block sparsity in the DWT coefficients

Physiological signals like EEG signals have correlation structure. The reconstruction performance of the algorithms degrades if the correlation structure is disregarded. Most of the state-of-the-art algorithms have overlooked this feature. Sparse Bayesian Learning (SBL) (Zhang and Rao, 2011; Zhang, Rao and Jung, 2013) methods exploit correlation structure in the signal and consequently ensure significant improvement in the performance of reconstruction. It is stated that the exploitation of correlation feature with the sparsity of the non-sparse physiological signals can significantly enhance the reconstruction efficiency (Zhang *et al.*, 2013a; Zhang *et al.*, 2013b, Zhang *et al.*, 2014). SBL algorithms achieve top performance to reconstruct sparse signal (Zhang *et al.*, 2013a; Zhang *et al.*, 2013b).

In this thesis, EEG is reconstructed by exploiting the block sparsity of the signal. Exploiting such a block sparsity of a non-sparse signal can further improve the reconstruction performance of the CS algorithms for energy-efficient wireless tele-monitoring (Pei & Wang, 2017). A block structured signal \mathbf{x} may be represented as in (5.8) where b blocks are shown.

$$\mathbf{X} = [X_1, \dots, X_{d_1}, \dots, X_{d_{b-1}+1}, \dots, X_{d_b}]^J \quad (5.8)$$

where $d_i(\forall i)$ is the block size and J indicates the number of segments. For a block sparse signal, only $K \ll b$ blocks are non-zero. The Block size can be chosen arbitrarily and it is not necessary that the block partition of the signal has a clear block structure (Zhang *et al.*, 2013a; Zhang and Rao, 2013). Different block sizes are usually employed indicating that block size does not affect the algorithm performance in SBL, as is also indicated in (Zhang *et al.*, 2013b). This is because the block size is kind of regularization in SBL algorithm to estimate the covariance matrix of \mathbf{X} , which enhances the estimation of \mathbf{X} .

For exploiting both the intra-channel and inter-channel correlation of the signals a spatio-temporal sparse Bayesian learning (ST-SBL) method has been proposed in (Zhang, Rao and Jung 2013; Zhang *et al.*, 2014). ST-SBL reconstructs multichannel EEG signals simultaneously. This exploits temporal correlation in each channel signal and additionally the spatial correlation among signals of different channels (Zhang, Rao and Jung 2013). Thereby its computational complexity does not increase with the number of channels (Zhang *et al.*, 2014). The ST-SBL model is expressed as (5.9).

$$\mathbf{Y} = \mathbf{\Phi}\mathbf{X} + \mathbf{V} \quad (5.9)$$

where $\mathbf{Y} \in \mathbb{R}^{M \times L}$ represents the measured signal, $\mathbf{\Phi} \in \mathbb{R}^{M \times N}$ is the SBM matrix, $\mathbf{V} \in \mathbb{R}^{M \times L}$ are the noise and $\mathbf{X} \in \mathbb{R}^{N \times L}$ are the multichannel EEG signal which have N rows and L columns. Each channel signal is represented by a column of \mathbf{X} . In this case the block structure of \mathbf{X} can be stated as (5.10).

$$\mathbf{X} = \begin{bmatrix} \mathbf{X}_1 \\ \mathbf{X}_2 \\ \vdots \\ \mathbf{X}_b \end{bmatrix} \quad (5.10)$$

where $\mathbf{X}_i \in \mathbb{R}^{d_i \times L}$ is the i -th block of \mathbf{X} , and $\sum_{i=1}^b d_i = N$, is the block size. Most of the blocks of b blocks are zero and a few of them are nonzero. The main concept of ST-SBL is that elements in the same column of each block are correlated (temporal correlation) and also the elements of the same row of each block are correlated (spatial correlation).

It is not useful to exploit temporal correlation if the components of each channel signal do not possess any robust temporal correlation. In that case, exploiting sparsity of each channel signal in a sparsifying domain is beneficial (Zhang *et al.*, 2014). Therefore, the model of (5.9) now can be expressed as:

$$\mathbf{Y} = \mathbf{\Theta}\mathbf{Z} + \mathbf{V} \quad (5.11)$$

where $\mathbf{\Theta} = \mathbf{\Phi}\mathbf{\Psi}$, and \mathbf{Z} is the sparse representation of \mathbf{X} in the sparsifying domain $\mathbf{\Psi}$.

As EEG signal neither have any block structure in the time domain and nor have temporal correlation in each channel, ST-SBL is employed on the signal's DWT coefficients (\mathbf{Z}). The DWT dictionary matrix generates DWT coefficient vectors to present EEG signals in the transformed domain (details see in section 5.2.4.1). The DWT coefficients (\mathbf{Z}) are concatenation of a number of blocks, only a few of them are non-zero and the rest of them are all zeros. Thus, ST-SBL algorithm exploits the block sparsity (assuming the signal is block sparse) in the DWT coefficient of the signal. It is already stated that the size of block can be chosen arbitrarily. It is demonstrated in (Zhang *et al.*, 2014) that ST-SBL shows stable performance for a variety range (15-60) of block size. In this research the block size is chosen 16 for all the experiments in order to keep all the blocks of same size.

5.3.3 Performances Indicators

The reconstruction quality of EEG signals using different DWT dictionary are compared using the following three performance indicators.

- I. **Normalised Means Square Error (NMSE):** this is mostly used performance index to measure error, defined as (5.12).

$$\|\hat{\mathbf{X}} - \mathbf{X}\|_2^2 / \|\mathbf{X}\|_2^2 \quad (5.12)$$

where $\hat{\mathbf{X}}$ is the estimate of the original signal \mathbf{X} .

- II. **Structural Similarity Index (SSIM):** this metric measures the similarity between the reconstructed signal and the original signal. It is mathematically expressed as (5.13) (Wang *et al.*, 2004).

$$\text{SSIM} = \frac{2\mu_{\mathbf{X}}\mu_{\hat{\mathbf{X}}}}{\mu_{\hat{\mathbf{X}}}^2 + \mu_{\mathbf{X}}^2} \frac{2\sigma_{\mathbf{X}\hat{\mathbf{X}}}}{\sigma_{\hat{\mathbf{X}}}^2 + \sigma_{\mathbf{X}}^2} \quad (5.13)$$

where $\mu_{\mathbf{X}}$, $\mu_{\hat{\mathbf{X}}}$, $\sigma_{\mathbf{X}}^2$, $\sigma_{\hat{\mathbf{X}}}^2$ and $\sigma_{\mathbf{X}\hat{\mathbf{X}}}$ are the mean, variance and cross-covariance of original signal and the estimated signal. For higher value of SSIM indicates the better reconstruction. When the reconstructed signal and the original signal are same, SSIM = 1.

- III. **Compression Ratio (CR):** the performance matric indicates how much data of the original signal is compressed and is defined as:

$$\text{CR} = \frac{N - M}{N} 100\% \quad (5.14)$$

where N and M are the length of the original signal and reconstructed signal.

To compare the performance of the DWT dictionaries in the first instance a 50% compression ratio is considered. CR in the CS-based system strongly related to reconstruction quality and power consumption. By adjusting CR in the application of CS in WBAN system, one can achieve desired reconstruction quality with reasonable power consumption.

5.3.4 Comparison of DWT, DCT and no dictionary

As will be demonstrated in chapter 6 the best performance may be associated to Beylkin dictionary. Therefore, for comparison the performance is compared with discrete cosine dictionary as well as the case of using no sparsifying dictionary for different CR values ranging from 50% - 80%. The same block size is used across. The comparison is done for both the clinical and non-clinical EEG signals.

5.3.5 Classification error

To assess the clinical implication of CS using the suitable DWT, a classification algorithm based on feedforward neural network is used to classify epileptic from non-epileptic EEG signal. The developed artificial neural network is used 1387 iterations during the training stage on the original data. The weight and the bias values are updated according to Levenberg-Marquardt optimization approach. The algorithm is subsequently tested on the reconstructed data (Men *et al.*, 2007).

It is noted that specific errors of the classification algorithm are not of interest here. The process should primarily show that, using a conventional classification method, how much the result is different for the original and the reconstructed. This gives an indication of the level of information distortion seen by the algorithm which implies the actual distortion as a result of CS.

5.4 Summary

In recent years, CS has gained considerable attention as a key enabler for transfer of large data rate and volume signals over WBAN, primarily driven by emerging technologies such as the IoT. Even using ST-SBL algorithms, finding an appropriate sparsifying dictionary may improve reconstruction by forming block structure. As EEG signals are not sparse in time and frequency domain, CS requires a suitable dictionary in which EEG is sparse. Although many of the existing approaches indicate accurate reconstruction results but there is no rationale with regards to the choice of a suitable DWT dictionary. The choice of the DWT is normally based on its ability to represent complex signals given by the number of vanishing moments. A higher number of vanishing moments increases sparsity of a large class of signals being represented by the DWTs. However, incoherence with the sensing matrix also needs to be considered that can affect the quality of reconstructed signal. In this chapter a framework is

proposed for the selection of DWT dictionary used in tandem with SBM as the sensing matrix and ST-SBL method as the reconstruction algorithm. The following chapter presents the investigation results.

Chapter 6

Results and Discussion

6.1 Introduction

In the previous chapter, it is explained that a suitable dictionary is required for the accurate reconstruction of the EEG signal. During selection of the dictionary its incoherence with the sensing matrix as well as its number of vanishing moments should be considered at the same time. A high level of incoherence with the sensing matrix is required for accurate reconstruction of the EEG signal with minimal error, whereas a higher number of vanishing moments increases sparsity of a large class of signals being represented by the DWTs.

This chapter presents all the experimental results for selecting a suitable dictionary. Section 6.2 provides the datasets that are used for the experiments. Section 6.3 gives the results followed by the subsections associated with the results of incoherence, reconstruction results using DWT dictionaries, result analysis with coherence and vanishing moments, comparisons of DWT, DCT and no dictionary for different CRs, classification error. Section 6.4 presents discussion and summary of the chapter is given in section 6.5.

6.2 Experimental Datasets

In this research, both clinical and non-clinical EEG datasets are used in order to verify the performance of the proposed frameworks. Information about these datasets including subjects, number of channels, sampling rate and data points are provided in the following subsections.

6.2.1 Visual attention tasks EEG dataset

This is the most used EEG dataset that is collected from EEGLab (Delorme and Makeig, 2004). The dataset is recorded using 10-20 system from one subject during visual attention task. The dataset consists of one epoch, 154 events and 32 channels. Each channel contains 30464 data points. The sampling rate is 128 Hz and it is about a 4 minutes of dataset.

6.2.2 Car driving tasks EEG dataset

This is the dataset that is used in (Lin *et al.*, 2005; Zhang *et al.*, 2014) for estimating driver's drowsiness. The dataset consists of raw EEG signals recorded from a subject during car driving with a certain degree of drowsiness. The task was done in a virtual-reality driving simulator, the details can be found in (Lin *et al.*, 2005). The dataset consists of 29 channels and each channel has 12288 data points. The sampling rate is 250 Hz.

6.2.3 Epileptic and non-epileptic dataset

This is a dataset of 15 subjects involving 10 epileptic and 5 non-epileptic datasets from the Temple University Hospital (TUH) EEG data corpus. The TUH EEG corpus is the biggest online accessible database in the world (Harati *et al.*, 2014; Veloso *et al.*, 2017). It comprises of different EEG databases. The datasets for this research are taken from TUH EEG Epilepsy Corpus database which has 237 patients data among them 133 are epileptic and 104 are non-epileptic patients. For the experiment, 10 patients with epilepsy and 5 without epilepsy of ages 19 to 82 (male/female) are chosen among all the patients by studying their clinical history. EEG were recorded during different periods of time from 2002 to 2013 using standard 10-20 electrode placement system. The datasets are comprised of channels that vary among 30, 33 and 36. Some of the channels consist of Electrocardiogram (EKG) and Electromyography (EMG) signals which are ignored in this study and 23 channels containing relevant clinical information are taken which sampled at 250 samples per second. Frequency ranges between 1 Hz - 100 Hz as shown in the fast Fourier spectra of normalised aggregate signal shown in Figure 6.1. In order to form the spectra shown in Figure 6.1, data points (29952) of all 23 channels at a given time are summed up to demonstrate the spectra of all channels at the same time.

EEG features related to epilepsy were spike and sharp waves. 10 epileptic patients were diagnosed with different phases of epilepsy involving localization-related epilepsy, idiopathic generalized epilepsy, epilepsy with seizures. Among the 5 non-epileptic patients one had bike accident with multiple facial fractures, one had electric shocks in the head, someone had stroke, other one had anxiety and the last one had critical mental status (The Institute for Signal and Information Processing, 1994). Their EEG were recorded with the consideration of having epilepsy. But none of them had epilepsy; most of them were diagnosed with cerebral dysfunction.

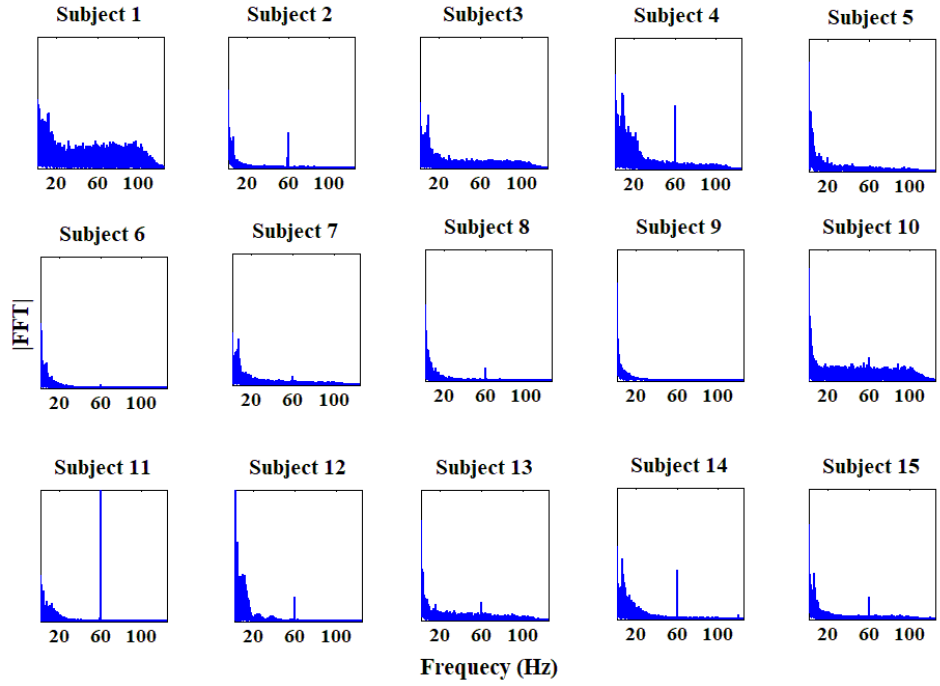


Figure 6.1. Frequency spectra of aggregate EEG signal for all subjects.

6.3 Results

In this section, the experimental results are provided for selecting a suitable dictionary for reconstruction of EEG signal of the datasets stated above. The following subsection 6.3.1 contains the incoherence results of SBM with DWT dictionary to identify the DWT which is mostly incoherent with SBM. Subsection 6.3.2 gives the results of the reconstruction with the DWT dictionaries which demonstrates the best DWT with less error and maximum similarity. Results are further analysed in subsection 6.3.3 with coherence and vanishing moments. The identified best DWT is then compared with other dictionary (DCT) and with the case of using no dictionary in subsection 6.3.4. The classification error for epileptic and non-epileptic data is presented in subsection 6.3.5.

6.3.1 Incoherence of SBM with DWT dictionaries

As the first step, the number of non-zero entries (d) of the sparse binary matrix (SBM) that would lead to a moderate incoherence for all the DWT dictionaries to be used are identified by calculating the coherence of randomly generated SBM with each dictionary for a varying number of non-zero entries. The fifteen DWT basis considered are Daubechies-3, Daubechies-4, Daubechies-8, Daubechies-10, Symmlet-10, Vaidyanathan, Coiflet-1, Coiflet-2, Coiflet-3, Coiflet-4, Coiflet-5, Harr, Battle-1, Battle-

3 and Beylkin of size 256×256 as the Ψ matrix. The outcome is shown in Figure 6.2. Subsequently, the number of nonzero entries (d) selected is 30.

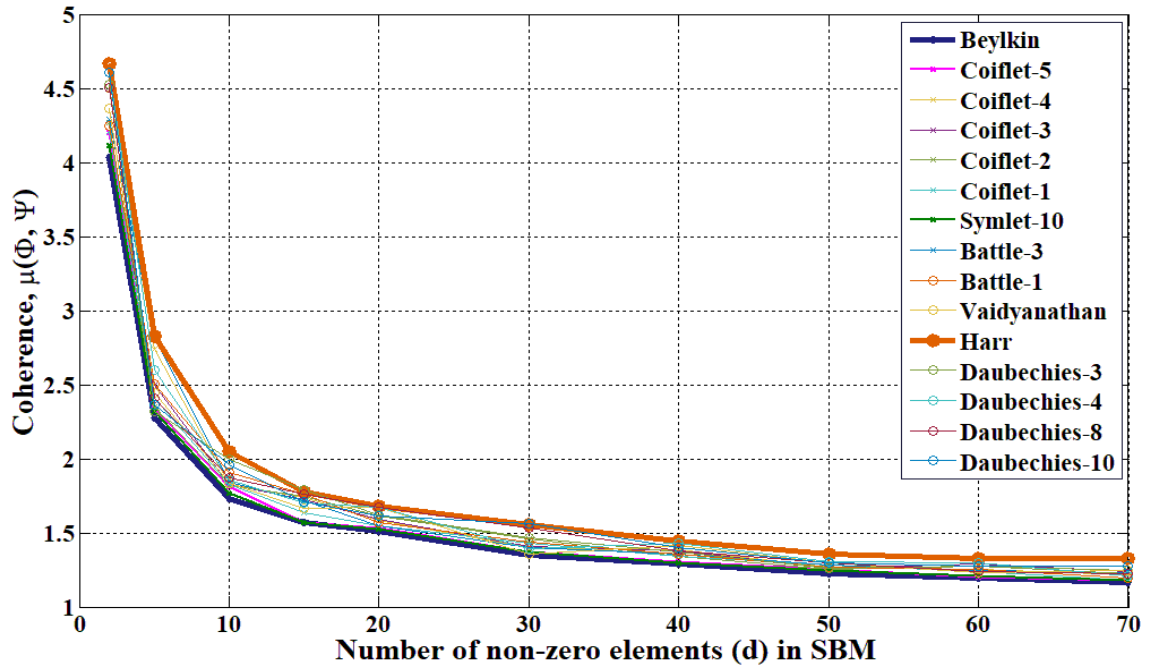


Figure 6.2. Coherence with varying number of non-zero elements. Beylkin shows least coherence (blue line) and Haar indicates the highest coherence (orange line) with SBM.

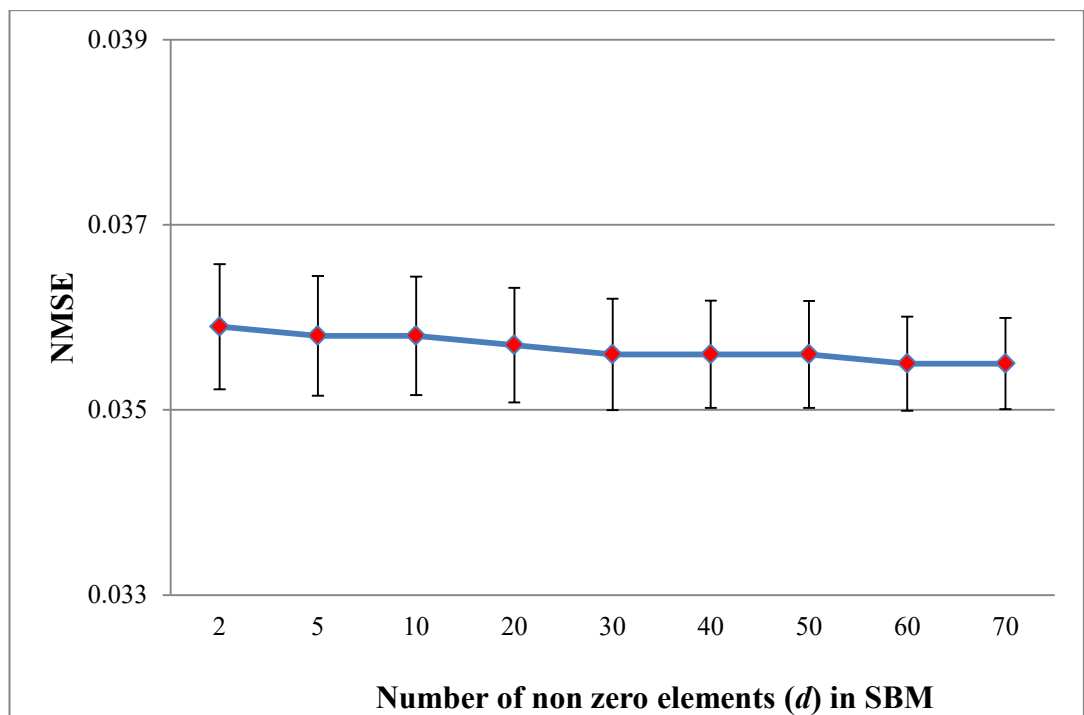


Figure 6.3. Variation of reconstruction error with no of non-zero elements, where red marks represent mean and error bar shows variance.

In order to know the impacts of the number of nonzero elements to the performance of reconstruction, a similar investigation of (Zhang *et al.*, 13b) is done here. The size of SBM (Φ) is chosen 128×256 , which has d nonzero elements of value 1 in each column. The value of d is ranged from 2 to 70 similar to experiment performed in Figure 6.2. For each range of d the experiment is performed several times on the epilepsy datasets. Figure 6.3 presents the experimental results where NMSE shows the reconstruction error of the epileptic signal and it is clear from the investigation that d does not have any impact on the reconstruction quality of the signal. The change of error is marginal for different values of d . This is another advantage of ST-SBL algorithm that it is not sensitive to d which also helps to reduce power consumption (Zhang *et al.*, 2013b). By adjusting the number of nonzero entry one can control execution time (Mamaghanian *et al.*, 2011).

In this research, $d = 30$ is used for all the experiments as it gives moderate incoherence between SBM (Φ) and DWT (Ψ) which is demonstrated in Figure 6.2. For a clear view of incoherence between the two bases Figure 6.4 presents the coherence between Φ and Ψ which is determined using (5.5), where d in Φ is chosen 30. It is shown in Figure 6.4 that the Beylkin DWT has the least coherence of 1.35. Similar lower coherencies are indicated by the Symmlet-10 and Coiflet-5 with values of 1.36 and 1.37 respectively. While the Daubechies-20 and Haar DWTs have highest coherencies of 1.562 and 1.56 in comparison.

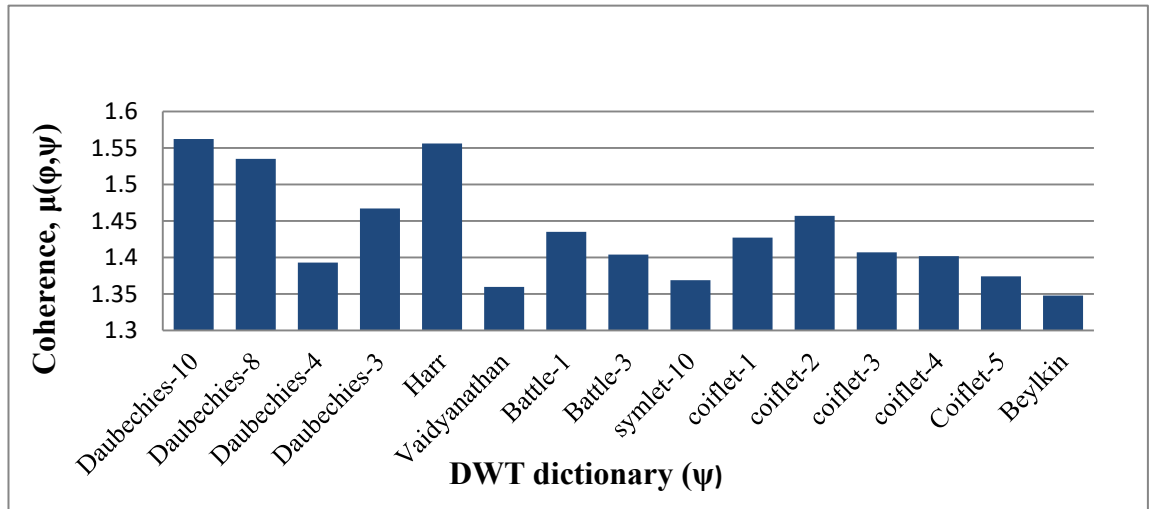


Figure 6.4. Coherence between Φ and Ψ .

6.3.2 Reconstruction using DWT dictionary

The dictionary that is maximally incoherent with SBM is already identified in the previous subsection. This subsection demonstrates that this maximally incoherent dictionary (Beylkin) gives the best reconstruction result. To measure the quality of the reconstruction two performance indexes NMSE and SSIM are used, the details of the indexes can be found in chapter 5. The dictionary with the least NMSE and highest SSIM value is selected as the best one.

6.3.2.1 Reconstruction results for the visual attention tasks EEG data

The signal has 30464 data points in each channel (32) which is partitioned into $J=238$ segments of length N , here N is set 128 since the sampling rate is 128 Hz. Each segment is compressed by 50 % (CR=50%) which means, $N/2 = M = 64$. The block size is chosen 16. The total numbers of nonzero blocks are 8 which starting locations are (1, 17, 33, 49, 65, 81, 97, and 113). The SBM (Φ) is of size 128×64 and DWT (Ψ) is of size 128×128 . ST-SBL is applied to the DWT coefficients to reconstruct the signal with all the segments together. The results are shown in Figure 6.5 and 6.6. The reconstruction quality is measured by NMSE and SSIM which is obtained using (5.12) and (5.13).

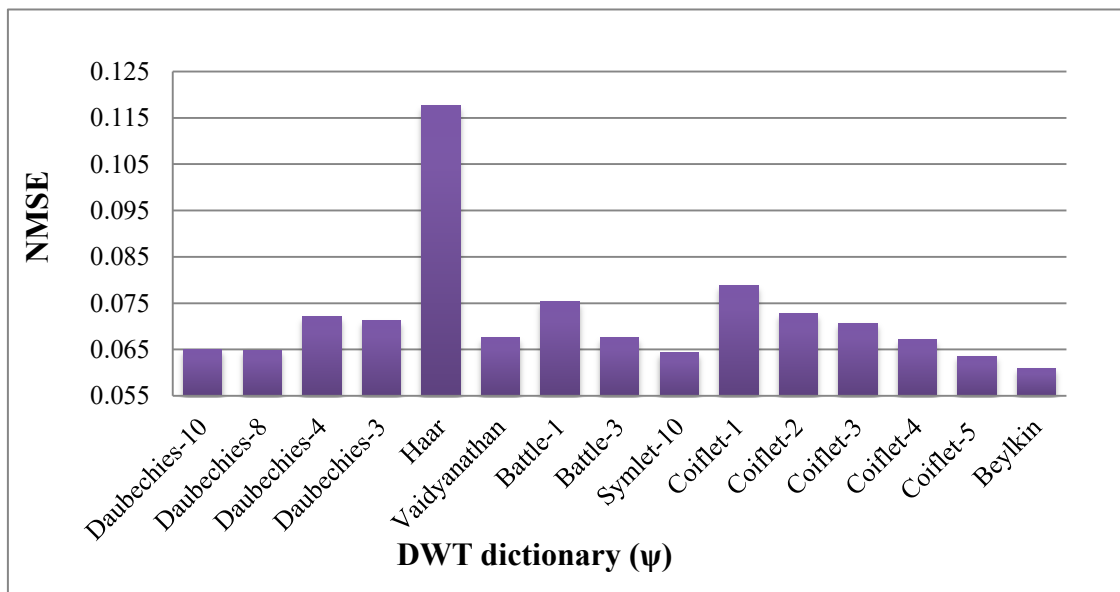


Figure 6.5 NMSE of the visual attention task EEG signal

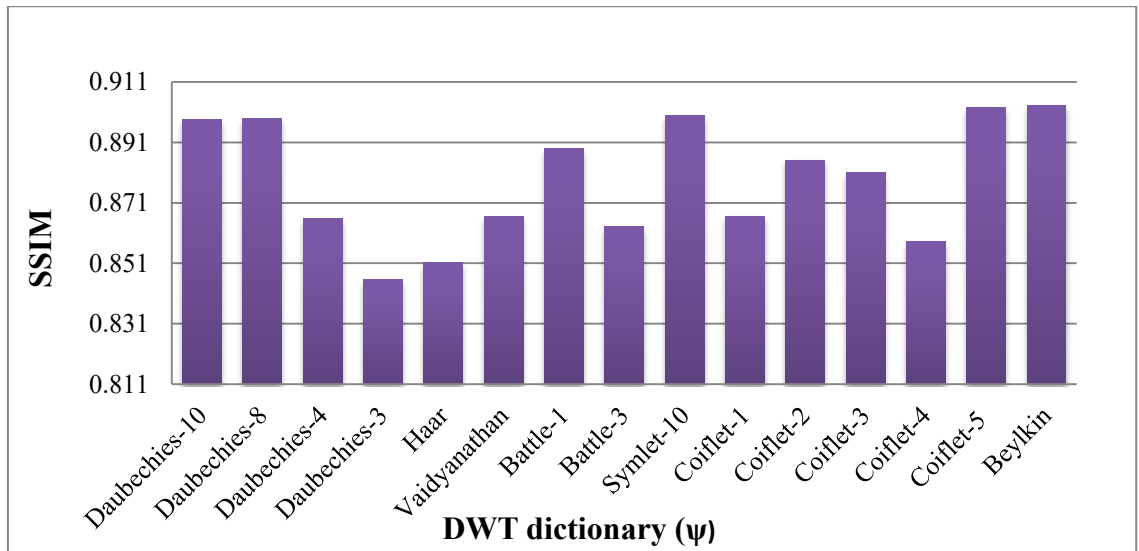


Figure 6.6. SSIM of the visual attention task EEG signal.

The Outcomes demonstrated that Beylkin reconstructed signal more accurately with the least error and highest SSIM. Similar better performances are given by Symmet-10 and Coiflet-5.

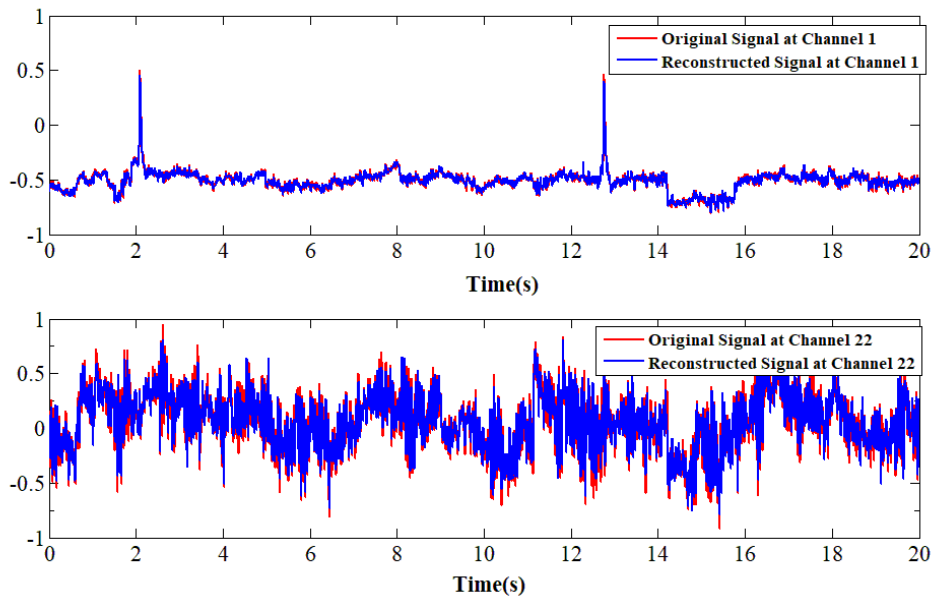


Figure 6.7. Example of the visual attention task EEG signal (channel 1 and channel 22) of the original and reconstructed with Beylkin DWT.

Reconstruction of EEG for channel 1 and channel 22 of the multichannel (32) visual attention task EEG signal using Beylkin DWT are plotted in Figure 6.7 for a given time duration. The plot indicates that the reconstructed signal is able to accurately capture the amplitude variations of the original signal for both channels 1 and 22.

6.3.2.2 Reconstruction results for the car driving tasks EEG data

Each channel has 12288 data points in this dataset which is divided 48 segments of length 256, where the sampling rate is 250 Hz. Data is compressed by 50 % (CR=50%) which gives $M = 128$. The block size is same as the previous experiment, 16. The total numbers of nonzero blocks are 16 which starting locations are (1, 17, 33, 49.....241). The starting location of each block is increasing by 16. In this case the size of SBM (Φ) and DWT (Ψ) is 256×128 and 256×256 , respectively.

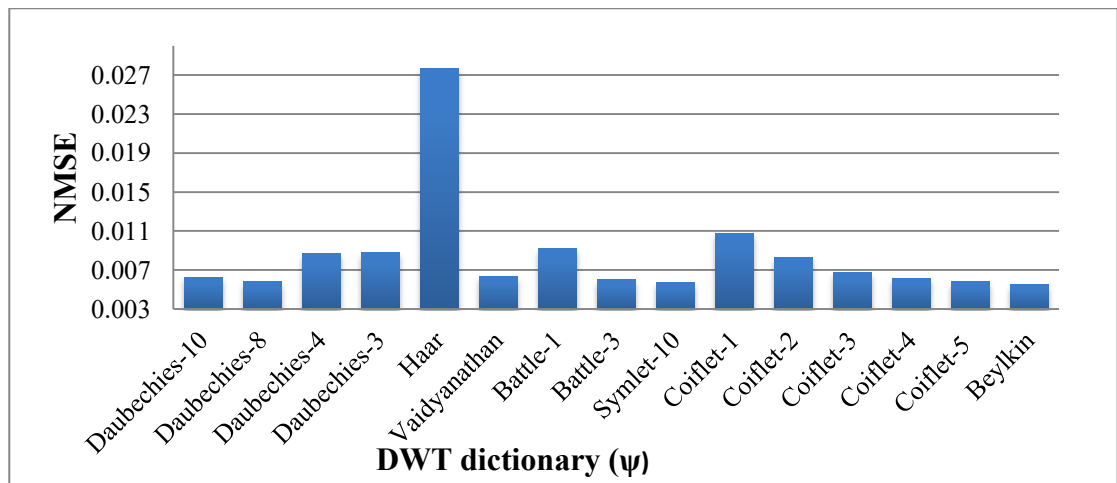


Figure 6.8. NMSE of the car driving task EEG signal reconstruction.

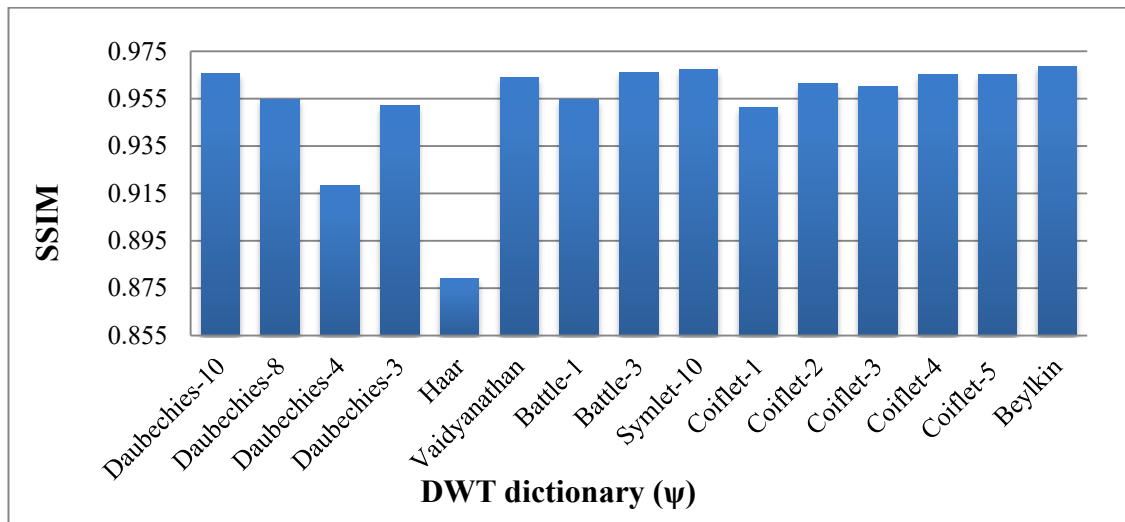


Figure 6.9. SSIM for the car driving task EEG signal reconstruction.

The NMSE and SSIM results of reconstruction are shown in Figure 6.8 and 6.9, respectively. The experimental results also indicate that Beylkin, Symmlet-10 and Coiflet-5 show better performance for reconstructing the driving task EEG signals compare to the other DWTs.

An example of reconstruction for channel 5 and channel 25 of the multichannel (29) car driving task EEG signal using Beylkin DWT are plotted in Figure 6.10 for a given time duration. The plot indicates the accurate reconstructions of the signal for both the channels.

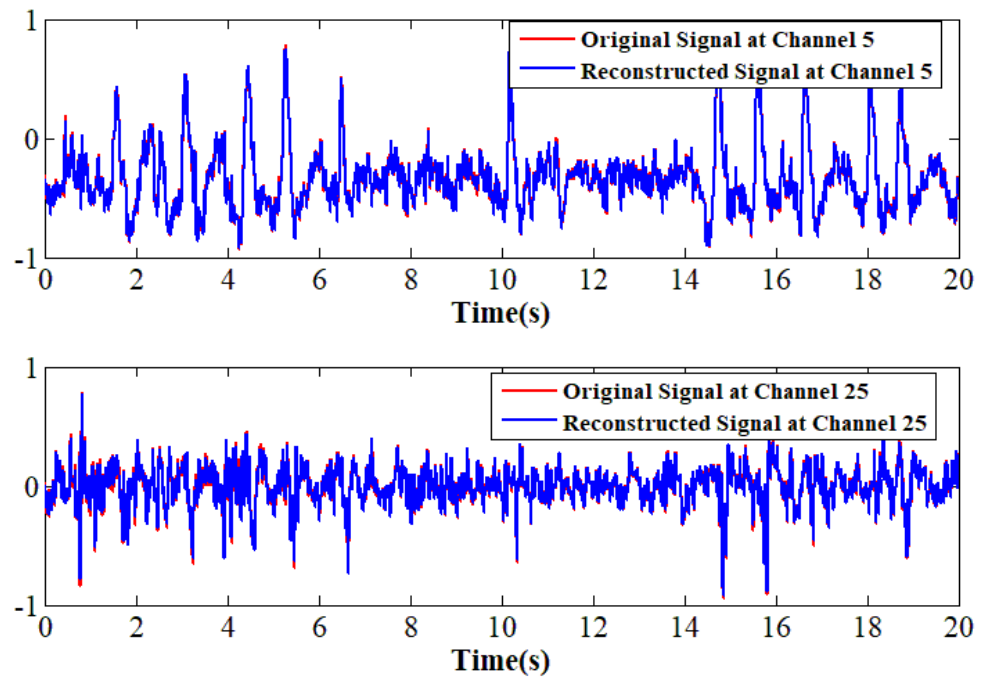


Figure 6.10. Example of the car driving task EEG signal (channel 5 and channel 25) of the original and reconstructed with Beylkin DWT.

6.3.2.3 Reconstruction results for the epileptic and non-epileptic data

The dataset which contain 29952 datapoints is partitioned into 117 segments of length 256. The sampling rate is same as the driving task data set, 250 Hz. Block size and number of nonzero blocks are same as previous experiment. The size of SBM (Φ) and DWT (Ψ) are also same as previous experiment. The median of NMSE and SSIM for all the segments associated with a subject is calculated as the measure of center due to the skewed distribution of values across the 117 segments. The mean and standard deviation of the center are subsequently calculated across the 15 subjects. Figure 6.11 and 6.12 show NMSE and SSIM (bar indicating the mean and errorbar showing the

standard deviation) of the reconstructed signal (CR=50%) for all the subjects and for all the 15 DWT dictionaries. Both figures of merit indicate a superior performance by Beylkin.

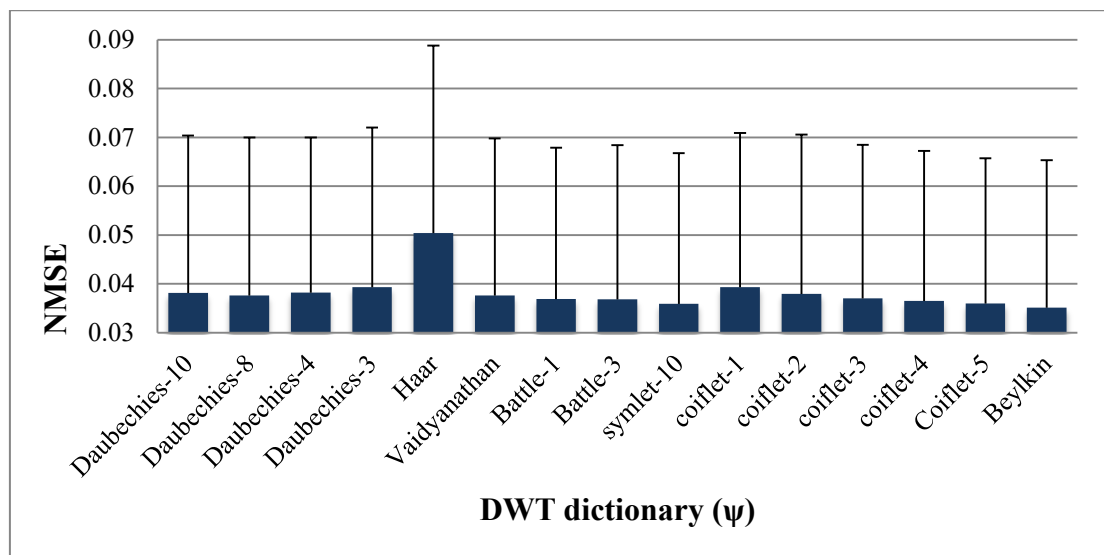


Figure 4.11. NMSE of epileptic and non-epileptic EEG signal reconstruction, where bar indicates mean and errorbar gives standard deviation.

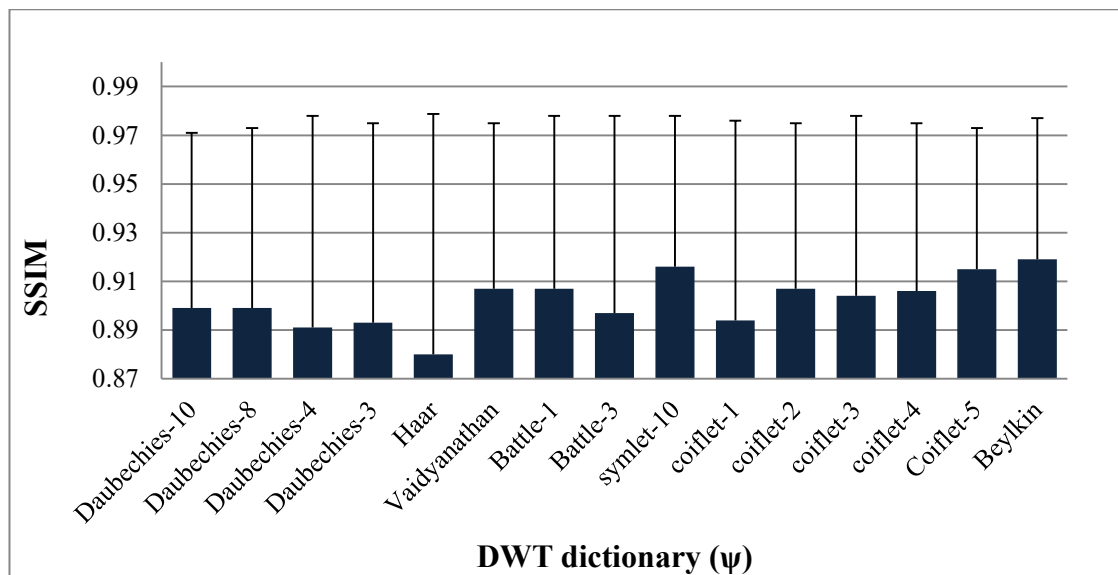


Figure 6.12. SSIM of epileptic and non-epileptic EEG signal reconstruction, where bar indicates mean and errorbar gives standard deviation.

6.3.3 Result analysis with coherence and vanishing moments

Figure 6.13 shows the scatter plot of coherence versus vanishing moments for all the dictionaries and indicates the correlation these features have (μ and p) with the

reconstruction performance (mean of NMSE). The results indicate that while those dictionaries that tend to have both high incoherence and vanishing moments tend to perform better. These show that presumably the effect of coherence is more significant when comparing Beylkin with Symlet or Coiflet. That is, Beylkin has higher incoherence with SBM but slightly lower number of vanishing moments compared to these two but the overall performance associated with Beylkin is better.

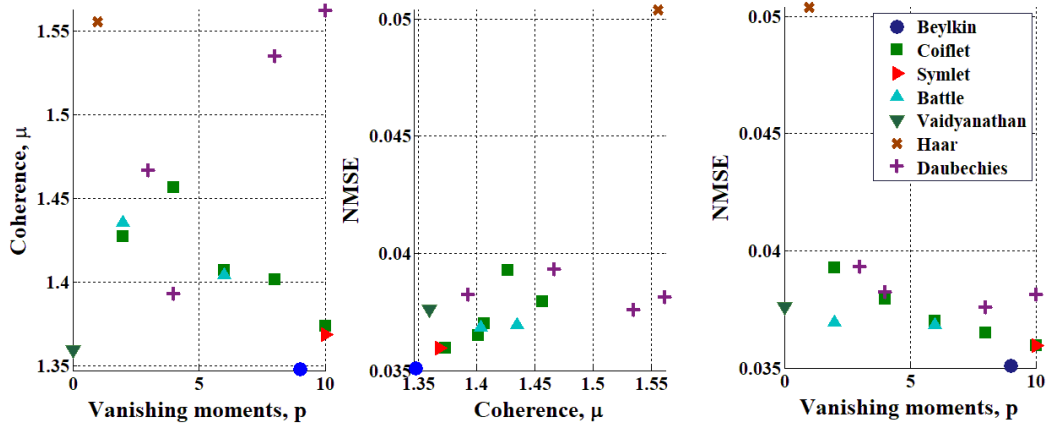


Figure 6.13. Demonstrating the relationship between coherence and vanishing moments for the 15 DWT dictionaries. Also, the correlations between vanishing moment and coherence with reconstruction performance for all the dictionaries are shown.

The increasing or decreasing trend of μ with p can be explained in terms of similarity of the DWT with the SBM. Signals with higher similarity tend to be highly coherent. The similarity between two signals a , b of length n can be defined in terms of the Euclidean Distance given by:

$$d_e(a, b) = \sum_{i=1}^n |a_i - b_i|^2 \quad (6.1)$$

More is the value of $d_e(a, b)$ means further are the signals apart in terms of the Euclidean Distance and lesser is the signal similarity. The probability cumulative density function (CDF) of $d_e(a, b)$ for various DWTs with SBM having a prior probability of 0.5 is obtained. The CDF plot for Coiflet-3, -4 and -5 is given in Figure 6.14. The $d_e(a, b)$ for 50% values i.e. $F[d(a, b)] = 0.5$ are 2.93, 3.40 and 3.82 respectively indicating that similarity is decreasing since $d_e(a, b)$ increases with increase in n .

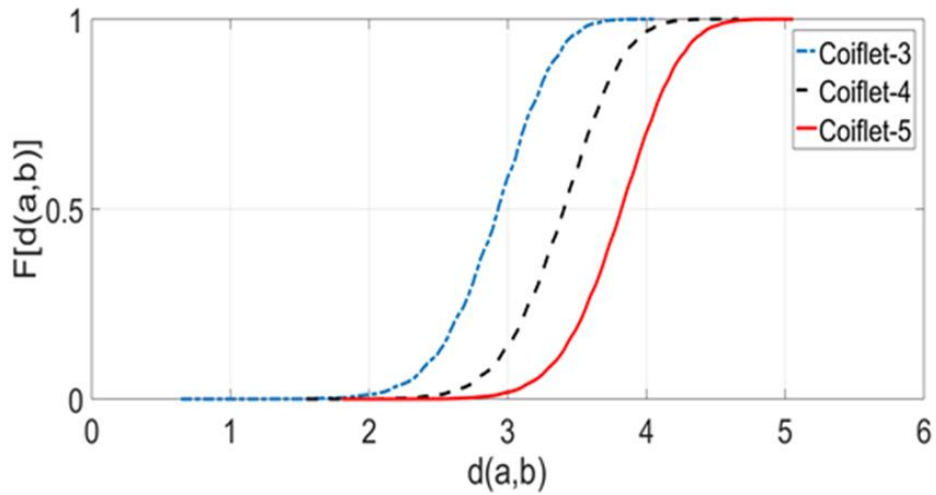


Figure 6.14. Coiflet CDF plot for $d_e(a,b)$ for $n=3,4,5$.

The $d_e(a,b)$ for $F[d(a,b)] = 0.5$ for Daubechies, Coiflet, Battle and Symlet DWTs for various filter lengths are given in Figure 6.15. As $d(a,b)$ increases the similarity of Coiflet and Symlet decreases with respect to the SBM, so does the coherency. However, the similarity of Battle and Daubechies increases since the value of $d_e(a,b)$ decreases with the filter length.

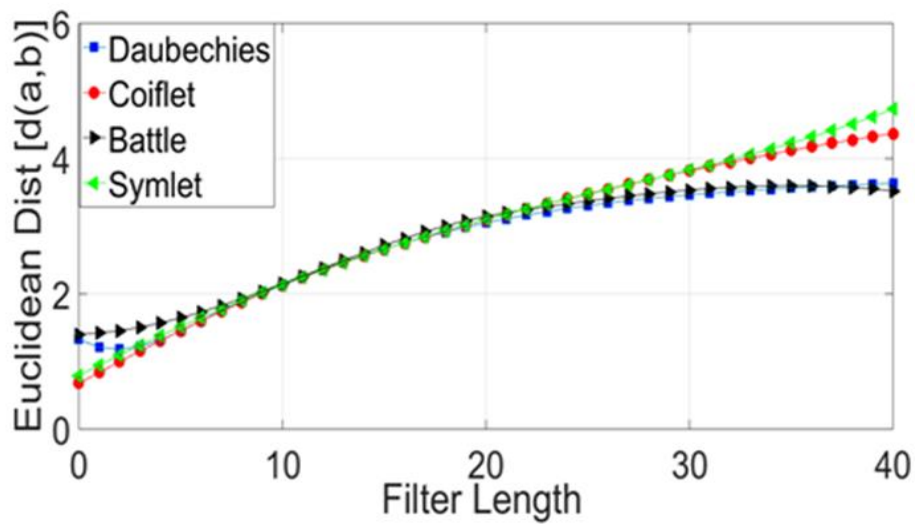


Figure 6.15. Variation of $d_e(a,b)$.

Table 6.1 Statistical values of results.

Visual attention task dataset	n	n_c	p	NMSE		SSIM	
				m	σ^2	m	σ^2
DWT							
Beylkin-	18	18	9	0.0642	0.00073	0.7731	0.1182
Symlet-10	10	20	10	0.0721	0.00098	0.6741	0.1672
Coiflet-5	5	30	10	0.0656	0.00078	0.7386	0.1353
Car driving task dataset							
Beylkin	18	18	9	0.0084	0.000047	0.9264	0.0080
Symlet-10	10	20	10	0.0091	0.000051	0.9262	0.0089
Coiflet-5	5	30	10	0.0093	0.000055	0.9221	0.0123
Epilepsy and no- epilepsy dataset							
Beylkin	18	18	9	0.0351	0.00091	0.919	0.0034
Symlet-10	10	20	10	0.0359	0.00096	0.916	0.0038
Coiflet-5	5	30	10	0.0360	0.00095	0.915	0.0036

The statistical values of results (for all the datasets) are detailed in Table 6.1. The mean (m) and variance (σ^2) values obtained in respect of Beylkin, Symlet-10 and Coiflet-5 DWTs indicate Beylkin shows a slightly better performance in terms of the reconstruction quality of the original signal than other two. However, these DWTs also differ in terms of their complexities. Table 6.1 indicates that Coiflet-5 has a higher number of filter coefficients, requiring more computational resources, as compared to Symlet-10 although they have same values of p and therefore have similar results for quality of the reconstructed signal. Since Beylkin has least n_c with a slightly smaller p value to that of Coiflet-5 and Symlet-10, it would imply as the least complexity in terms of implementation.

6.3.4 Comparison of Beylkin, DCT and No dictionary for different CRs

As demonstrated in the previous section the best performance is associated with Beylkin DWT. Therefore, in this section the performance of Beylkin is compared with DCT as well as the case of using no sparsifying dictionary for a varied range (50%-80 %) of CR.

6.3.4.1 Comparison for the visual attention task dataset

Figure 6.16 and 6.17 show NMSE and SSIM results associated with using Beylkin, DCT as the dictionary and using no dictionary at all for CR ranges from (50%-70%),

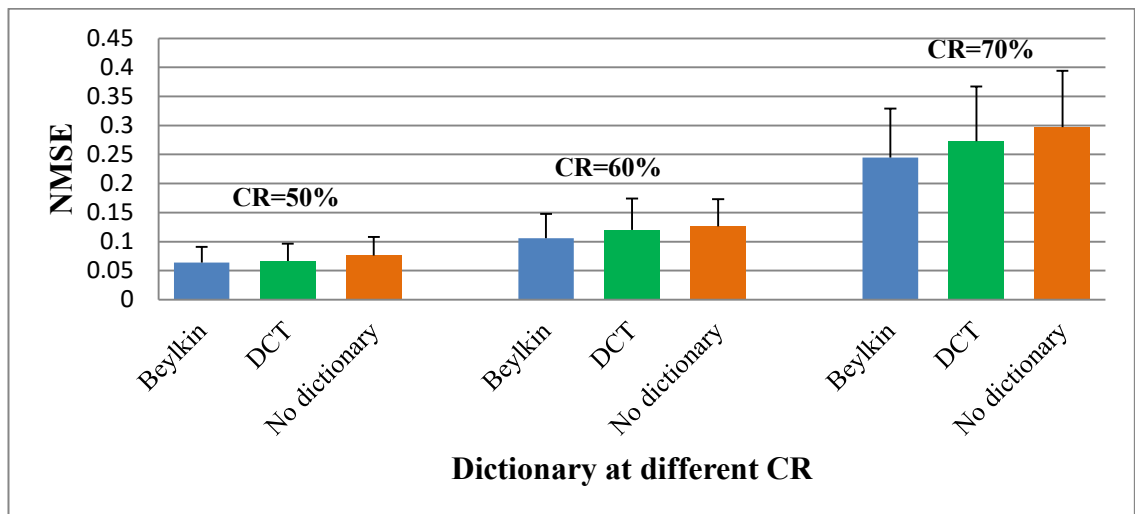


Figure 6.16. NMSE for different CRs associated with Beylkin, DCT and when no dictionary is used in the visual attention task EEG dataset.

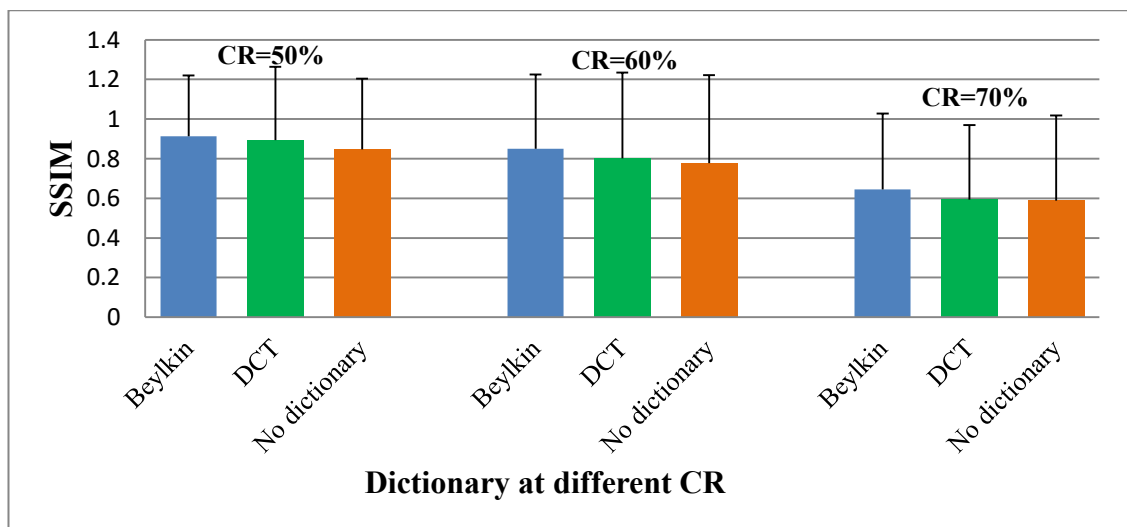


Figure 6.17. SSIM for different CRs associated with Beylkin, DCT and when no dictionary is used in the visual attention task EEG dataset.

where bar and error bar indicate mean and standard deviation, respectively. In order to keep the consistency of the work 80% compression is ignored for this experiment. As the numbers of non-zero entries are set 30 for all the study, therefore 80 % compression is not meeting the requirements of SBM. Both the outcomes (Figure 6.16 and Figure 6.17) indicate that Beylkin outperforms DCT and no dictionary for all CRs.

6.3.4.2 Comparison for the car driving task dataset

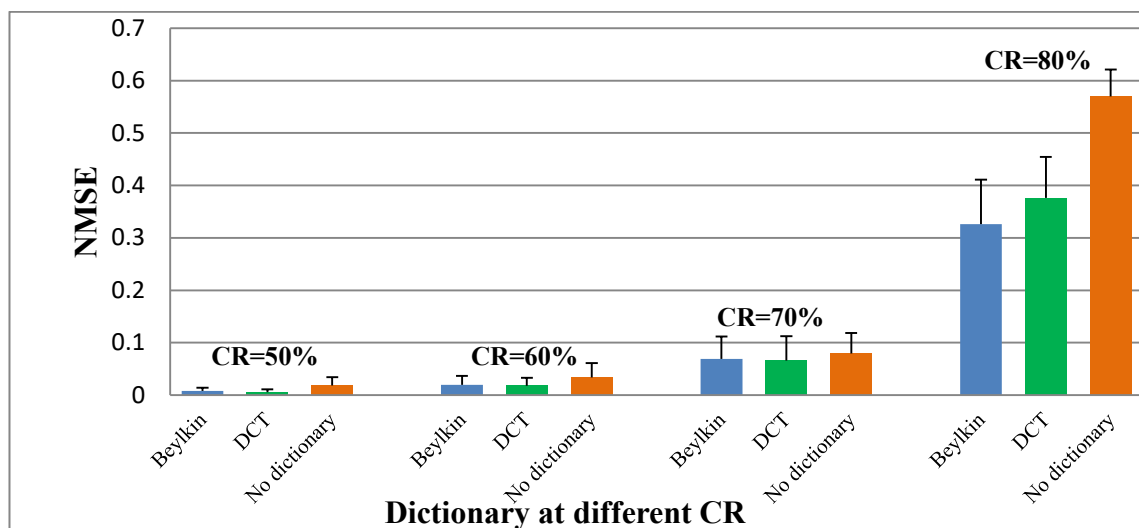


Figure 6.18. NMSE for different CRs associated with Beylkin, DCT and when no dictionary is used in the car driving task EEG dataset.

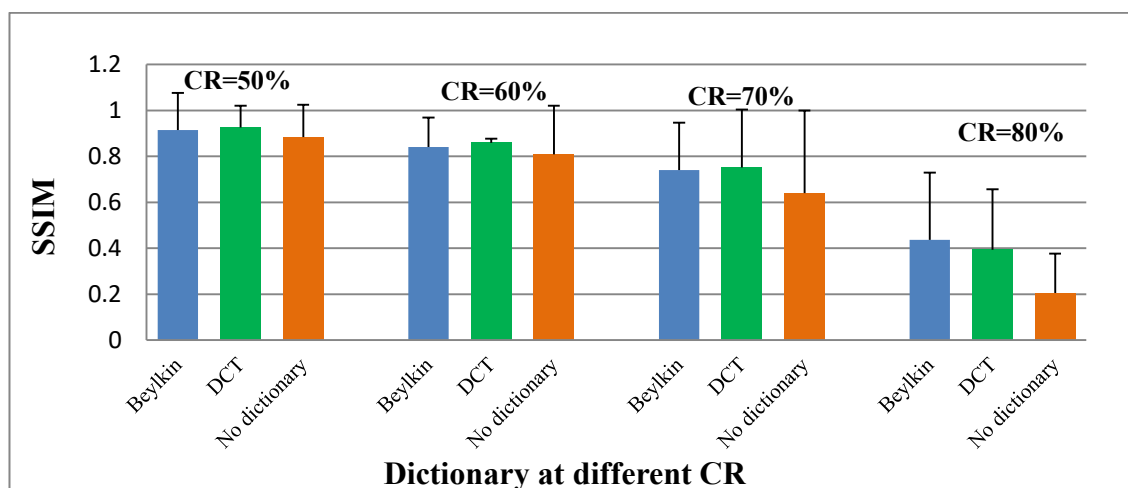


Figure 6.19. SSIM for different CRs associated with Beylkin, DCT and when no dictionary is used in the car driving task EEG dataset.

Figure 6.18 and Figure 6.19 provide the NMSE and SSIM results of comparison of the aforementioned three cases in the car driving task dataset, where bar and error bar provides mean and standard deviation, respectively. Beylkin and DCT perform almost similar up to 60% CR. At higher CRs (70%-80%) Beylkin performs better than the other two cases.

6.3.4.3 Comparison for the epileptic and non-epileptic dataset

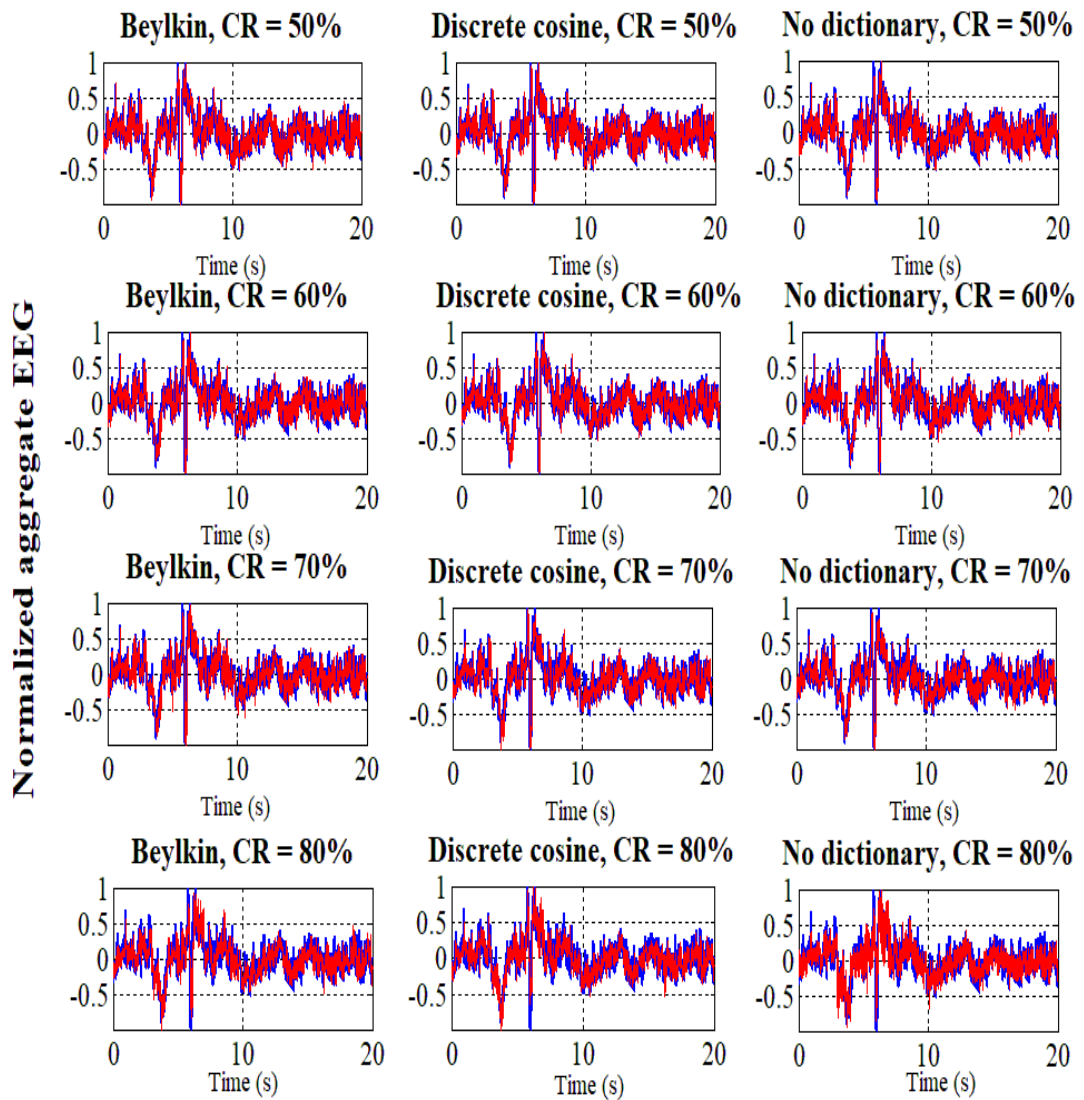


Figure 6.20. Examples of normalised aggregate EEG signal (addition of all 23 channels at a given time) of the original and reconstructed for different values of CR for Beylkin, DCT and the case of using no dictionary. Blue traces show the original while the red traces are the reconstructed. At 80% CR Beylkin outperforms DCT and No dictionary.

Figure 6.20 shows an example of aggregate EEG signals (original and reconstructed upon using different CRs) associated with using Beylkin and DCT as the dictionaries and using no dictionary at all. It is noted that while Beylkin and discrete cosine appear to lead to similar outcome, when using no dictionary the reconstruction is quite poor at higher CRs. There is also a slight indication that Beylkin outperforms DCT at CR=80%.

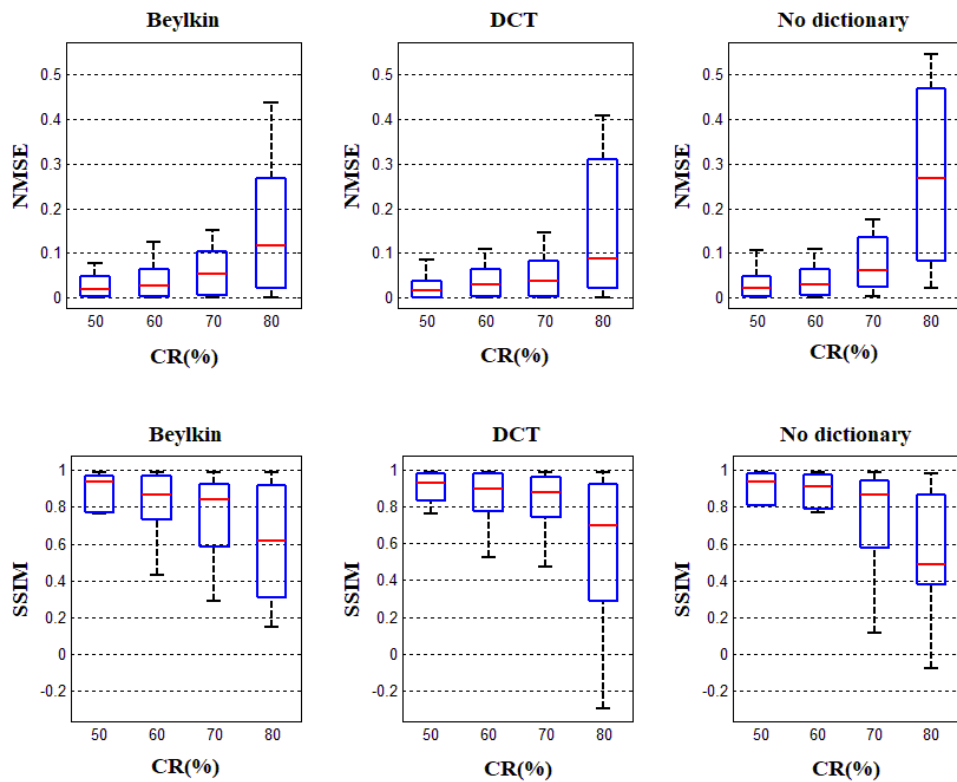


Figure 6.21. The box plot of NMSE and SSIM for different CRs associated with Beylkin and DCT and when no dictionary was used.

Figure 6.21 shows the box plot of NMSE and SSIM comparing the aforementioned three cases. Up to CR=60% the three cases perform at the same level. However, while Beylkin and DCT lead to almost similar performance for CR=70%, using no dictionary deteriorates the performance at this level and higher significantly. At CR=80%, Beylkin outperforms DCT and no dictionary.

6.3.5 Classification Error

Figure 6.22 shows the raster plot of misclassifications of the classification algorithm as calculated for both the original and the reconstructed using Beylkin at CR=50%. Every sample is the recording in a given time instance from 23 channels. The results are pooled together so that the first third of samples are associated with non-epileptic EEG signal and the rest are associated with epileptic EEG. The algorithm leads to 91.7% accuracy of classification on the original test data comparing to 91% accuracy of classification on the reconstructed data. The sample by sample classification difference is 4.7%.

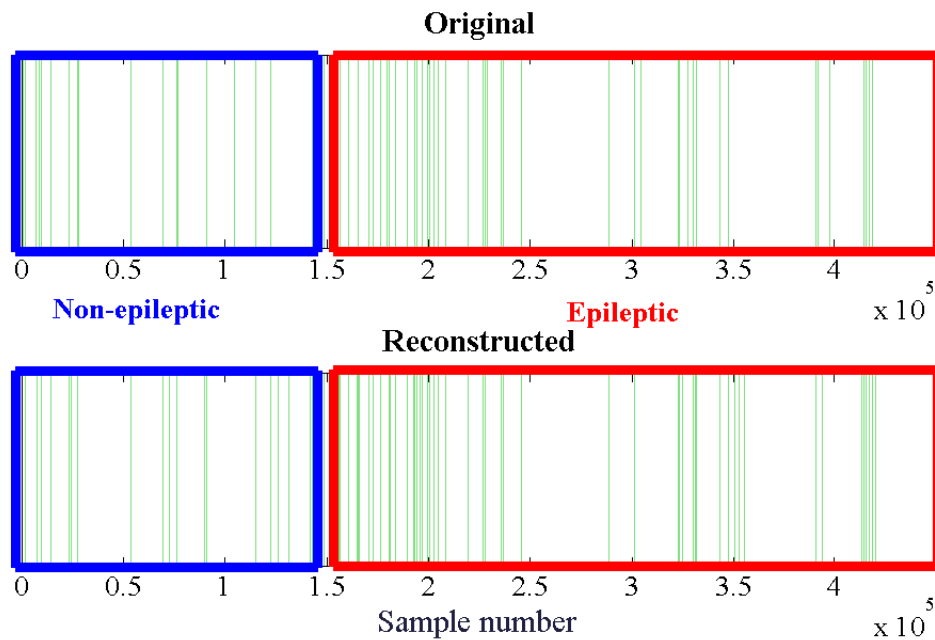


Figure 6.22. The raster plot of misclassification using the classification algorithm is used in this paper in the original training data and the reconstructed test data.

6.4 Discussion

The accurate reconstruction of the EEG signal with CS depends on a suitable dictionary that is maximally incoherent with the sensing basis. The choice of the dictionary is normally based on its ability to represent complex signals given by the number of vanishing moments. A higher number of vanishing moments increases sparsity of a large class of signals being represented by the DWTs. However, incoherence with the sensing matrix also needs to be considered that can affect the quality of reconstructed signal. A high level of incoherence with the sensing matrix is required for accurate

reconstruction of the EEG signal with negligible error. In this study, a suitable DWT dictionary is identified by investigating incoherence with an aim of improving accuracy of reconstruction of the EEG signals. Results indicate that the Beylkin is maximally incoherent with SBM, also yield most accurate reconstruction of the original signal as compared to other DWT dictionaries. Similar higher incoherencies and accurate reconstructions are shown by Symlet-10 and Coiflet-5 DWT dictionaries, even though they may have similar number of vanishing moments. The Debauchies DWT is widely employed for most applications as it has high number of vanishing moments. While Debauchies-10 has equal number of vanishing moments to Symlet-10 and Coiflet-5, it has least incoherence with the SBM yields less accurate results in comparison. Although a high number of vanishing moments indicates an increase in sparsity of a large class of signals, incoherence of the DWT with the sensing matrix antecedence the former for accurate reconstruction of the EEG signal. To reduce the complexity of implementation among those having similar values of incoherence and vanishing moments, dictionaries with lower number of filter coefficients can be implemented to minimize the order of complexity with a view to reduce the power requirements in WBANs.

An interesting demonstration in this thesis is that Beylkin has considerably better performance at higher CRs, compared with DCT and using no sparsifying dictionary. CR=80% would correspond to sampling at 50 Hz which is a substantial reduction. The effect of ensuing errors at this level of CR was not investigated here as the focus of the study is on the specifics of selecting DWT dictionaries. Comparisons of performance with DCT and the case of using no dictionaries were presented merely to demonstrate relevance and for putting the problem into context. For CR=50%, Beylkin led to marginal levels of error using the conventional classification paradigm used. This indicates further the relevance of the effort in arriving at a suitable dictionary to be used in tandem with SBM and ST-SBL algorithm.

6.5 Summary

This chapter provides results of identifying a suitable dictionary for accurate reconstruction of EEG signal in the application of WBAN. It is demonstrated that in selecting the dictionary its incoherence with the sensing matrix as well as its number of vanishing moments should be considered at the same time. Amongst the dictionaries are studied, Baylkin is maximally incoherent with sensing basis and also leads to the best performance in terms of the reconstruction compare to the other dictionaries, though it

has slightly lower vanishing moment. This indicates that incoherence presumably has a slightly stronger impact on the outcome.

Therefore more inform choice for selection of DWT are incoherence which people use separately and Vanishing moment to see DWT in larger variation. The impact is in order to select appropriate DWT both property need to be considered together and classification prove clinical validation.

Chapter 7

Power Consumption Analysis

7.1 Introduction

It is already stated that energy consumption and the high volume of data are major constraints in the transmission of EEG signal over WBAN due to limited battery life and processing capability of sensor nodes. To increase battery life focus on reducing the power of transmission and data rate compressive sensing (CS) is employed (Zhang *et al.*, 2013a; Singh *et al.*, 2014; Liu, Vos & Huffel, 2015; Candes & Wakin, 2008). AS CS can lead to significant computational savings for on-chip implementation with relatively low sampling rates, recently, it has been viewed with considerable interest as a viable technique for the transmission of large data volumes and high data rate signals over WBAN (Zhang *et al.*, 2013a).

In this chapter, the overall energy savings of transmitting EEG signal in WBAN is investigated by exploring the effectiveness of the proposed approach. The investigations are done by numerical experiments following a power model. The results will help to realize the computational complexity and online implementation requirements of CS for transmitting EEG in WBAN.

Section 7.2 presents the necessity of energy efficient sensing system. The wireless sensor nodes types are presented in section 7.3. Multiple hop WBAN system is described in section 7.4. The following section 7.5 provides design of WBAN sensor node. The power consumption analysis of a sensor node is given in section 7.6. Power consumption at different compression rates is presented in section 7.7. Section 7.8 offers further savings of power and the chapter summary is provided in section 7.9.

7.2 The Necessity of Energy Efficient Sensing System

There are various health monitoring applications that require the transfer of biomedical signals over Wireless Body Area Networks (WBAN). Online monitoring of physiological signals over wireless body area networks (WBAN) is challenging due to the high volume of data and power requirements. WBAN sensors should have lightweight, low cost and power consumption while enabling an enhanced analysis of

biomedical signals that involve high data volume for effective monitoring and treatment (Lim, Baumann and Li, 2011; Ivanov *et al.*, 2012; Seyedi *et al.*, 2013; Dharshini and Subashini, 2017).

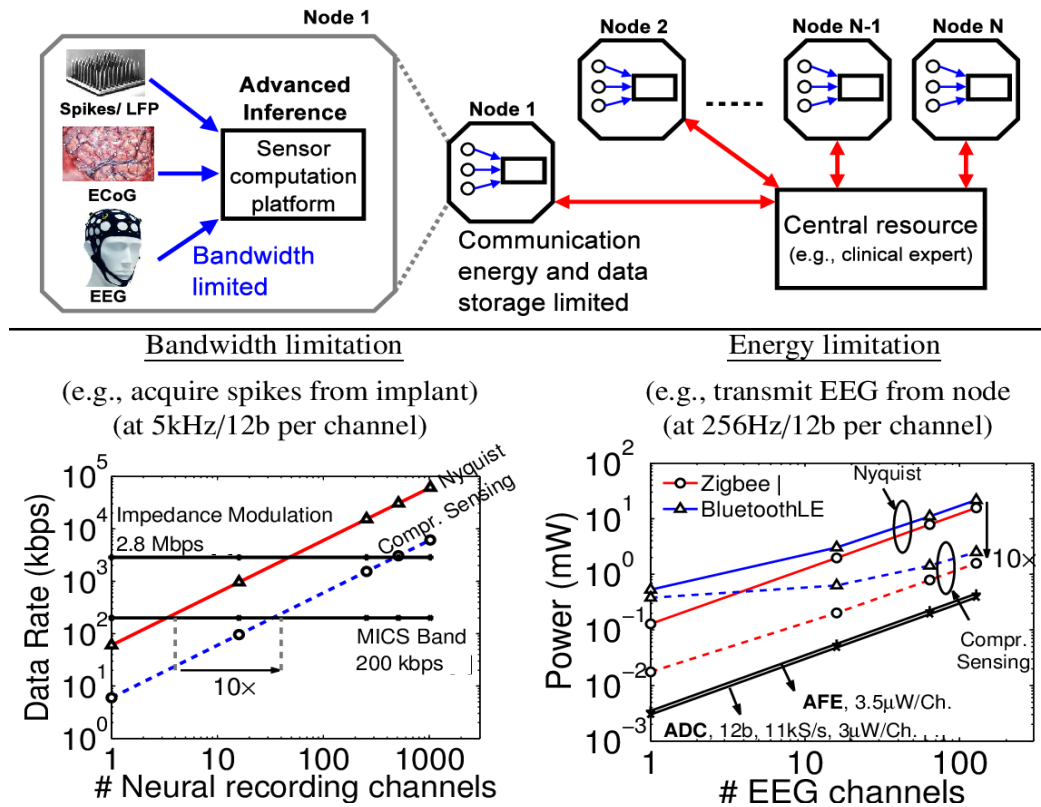


Figure 7.1. Bandwidth and energy constraints for the transmission of EEG signals. Nyquist sampling shows rigid constraints, requiring information to be reduced to a great extent that can possibly be accomplished through effective signal compression techniques like CS. (ECoG: electrocorticogram, LFP: local field potential) (Shoaib, 2013).

The dynamic nature of biomedical signals such as electroencephalographic (EEG) and electrocorticographic (ECoG) traces results in a wide variation in normal and pathologic features in different individuals. The use of manually extracted features for prediction of pathological events is impractical with a large volume of data even for a small number of electrodes, leading to large processing delays.

The major constraints of transmitting physiological signals in wireless sensor networks are illustrated in Figure 7.1(Shoaib, 2013). For instance, transcutaneous or MICS-band

(Medical Implant Communication Service) links are usually used to transmit physiological signals, i.e., neuronal spikes from the energy constrained node to external node (Mandal and Sarpeshkar, 2008; Pandey and Otis, 2011). The top part of Figure 5.1 depicts the data storage capacity and transmission energy limitations in the energy efficient sensor network. The bottom left part of Figure 7.1 shows high data volume requirements with the increments of channels, the bottom right part of shows the power requirements to transmit EEG signals. Therefore, an efficient data processing technique is required to reduce data volume dramatically and thereby reduce power consumption. As an emerging technique, compressed sensing (CS) shows its great potential to minimize the power consumption in the sensor node by compressing the data in a more compact manner (Wang, Song, and Xu, 2014).

7.3 Types of Wireless Sensor nodes

WBAN consists of a number of sensor nodes. On the basis of their implementations the sensor nodes are classified into the following three types (Al-Janabi *et al.*, 2016):

- Implantable node: This kind of node is usually implanted underneath the skin or inside the human body tissue.
- Body surface node: It is placed on the surface of the body.
- External node: This type of node is placed a few centimeters to 5 meters away from the human body (Al-Janabi *et al.*, 2016).

Each sensor node has specific requirements and is utilized for a different purpose. For example, the EEG sensor node is used to detect brain signal, whereas ECG sensor nodes detect heart signal. Sensor nodes communicate with the intermediate node which can be named as a central control unit (CCU). CCU generally consumes less energy and has higher processing capacities (Negra, Jemili and Belghith, 2016). CCU is responsible to transmit physiological signals of the patient to the remote device or medical for real-time diagnostic or health care purposes. The remote terminal is known as a base station which does not consume any energy of the WBAN (Zhang *et al.*, 2013a).

The electronics of the sensor nodes need to be miniaturized, energy-efficient and able to detect physiological signals (Khan and Yuce, 2010).

7.4 Multiple hops WBAN system

Figure 7.2 is showing a multi-hop WBAN. The EEG sensor node acquires brain signal and transmits them to the intermediate unit (CCU) and then the signal is finally sent to the base station. This is a multi-hop network that consists of two networking links; one is between the sensor node and CCU and the other one is between CCU and medical server or base station. CCU can be a smartphone or the user's personal computer (PC). Several technologies, such as Bluetooth, Zigbee, MICS, Ultra Wide Band (UWB), Wifi, and internet are usually used as a networking link (Khan and Yuce, 2010; Negra, Jemili and Belghith, 2016).

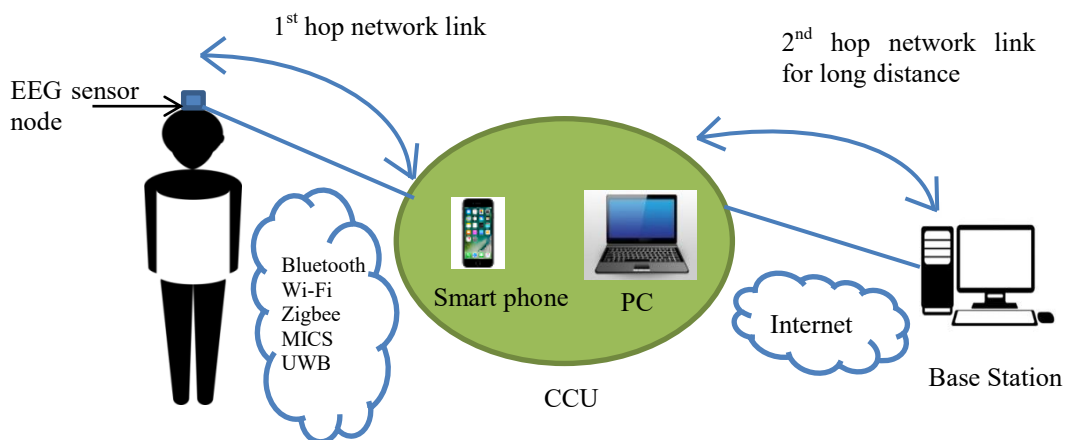


Figure 7.2. Multi-hop EEG based WBAN system.

7.5 Design of WBAN Sensor Node

The sensor node is designed to acquire EEG signal from the user's brain. The sensor node undertakes three tasks: sensing the signal through electrodes, processing (digitizing, controlling) and finally transmission of the signal via a transmitter. Most of the power consumption occurs in the transmitter (Abdulghani, Casson and Rodriguez-Villegas, 2010).

Therefore, methodologies are required for sensing and processing the signal before transmission. In this research, CS being an energy efficient data compression technique is used prior to transmission. As EEG signal is very weak and small (1-100 μ V), first it needs to go through the amplification process as shown in Figure 7.3 (Khan and Yuce, 2010). After amplification, the signal is converted into the digital domain using an analog to digital converter (ADC). Further processing of the signal is done in the

microcontroller. In order to control the power distribution from the battery in an optimized way, microcontroller maintains an energy management method. The compression of the signal is done in this stage. The aim of compression is to reduce the system power consumption by reducing the data volume. Finally, the processed and compressed signal is transmitted to the transmitter.

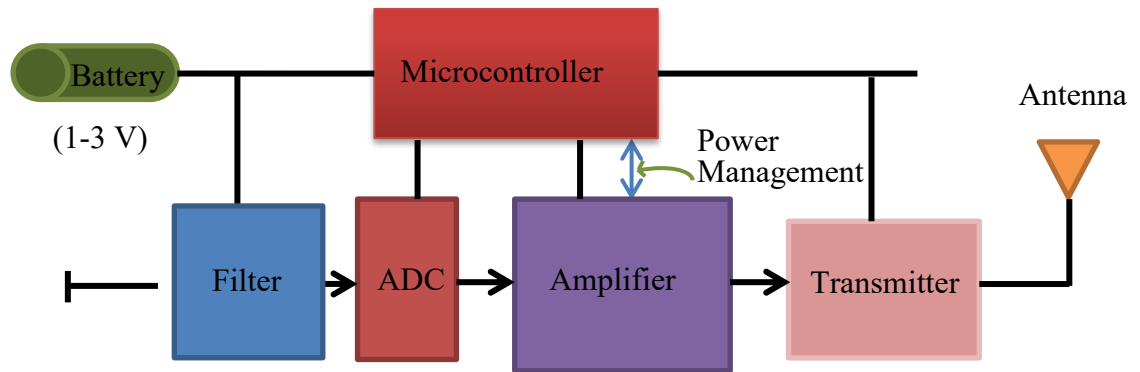


Figure 7.3. Block diagram of a WBAN sensor node.

7.6 Power consumption analysis of a sensor node

It is discussed in chapter 5 that while CS is employed in WBAN, signals are compressed on the sensor node with a reduced number of samples without losing essential information. Only this reduced number of samples is transmitted to the receiver where the original signal is reconstructed offline (Abdulghani, Casson and Rodriguez-Villegas, 2010). Only the compression stage consumes on-chip power in WBAN (Zhang et al., 2013a). At the receiver or server node, the matrix Φ is known to a CS algorithm and the matrix Ψ is determined by a user. This stage does not cause any energy consumption in WBAN (Zhang et al., 2013a). Therefore, the sensor node power consumption is the only concern and investigated here. Figure 7.4 shows the EEG WBAN sensor/server node architecture.

To analyze sensor node power consumption, a power model proposed in (Abdulghani, Casson and Rodriguez-Villegas, 2010) is used in this research. The sensor node incorporates two electrodes (E_1 and E_2) in order to sense EEG signals, an amplifier to amplify the weak EEG signals, an ADC to digitize the signals, a random number generator (RNG) to generate the sensing matrix Φ which is used to select a random set of samples to form the compressed signal y , a Digital signal Processor (DSP) or microcontroller to do the compression and a transmitter to transmit the signal to the receiver.

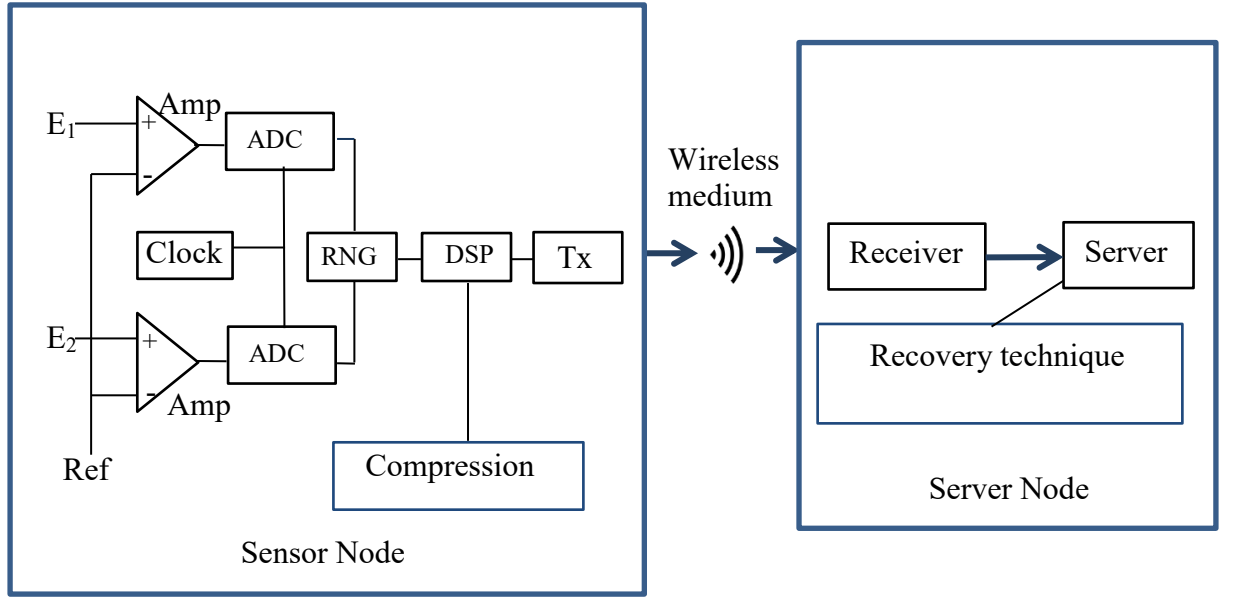


Figure 7.4. The architecture of EEG WBAN sensor/server node.

The total power consumption of the CS-based sensor node is comprised of three parts:

$$P_{sen_CS} = P_{sense} + P_{proc} + P_{trans} \quad (7.1)$$

where $P_{sense} = C(P_{amp} + P_{ADC})$, is the sensing power

$P_{proc} = P_{RNG} + P_{micro}$, is the processing power

$P_{trans} = Cj f_s R$, is the transmission power

where C is the total number of the channels, P_{Amp} is the power consumption in the amplifier, P_{ADC} gives the ADC power consumptions, P_{RNG} is power consumption of the random number generator, P_{micro} is the microcontroller power consumption. Processing power does not depend on the number of channels (Abdulghani, Casson and Rodriguez-Villegas, 2010; Shukla, Majumdar and Ward, 2015), f_s is the sampling frequency of the ADC, R is the number of bits per sample (resolution) and j is the net transmission power per bit.

Thus, the total power consumption by the CS-based EEG sensor node is:

$$P_{sen_CS} = C(P_{amp} + P_{ADC}) + P_{RNG} + P_{micro} + C \frac{M}{N} j f_s R \quad (7.2)$$

The Transmission power requirement has been reduced by a factor of M/N . This corresponds to the compressive sensing in model 5.1 where there is a reduction in dimensionality between x and y .

In order to get an idea about the actual power consumption and savings, the hard values can be established using realistic and state-of-the-art values. Five separate blocks are considered for this which is discussed successively below:

Amplifier: EEG signals are typically in the range of 1-100 μV . Therefore, it is necessary to amplify the signal before it transmits to ADC so that it can match the ADC input range. Moreover, it is assumed that the signal is band-limited to the approximate range of 0.5 Hz to 70 Hz (Abdulghani, Casson and Rodriguez-Villegas, 2010). Considering all the requirements of EEG signals a low power, low noise instrumentation amplifier of 30 Hz bandwidth and 40 dB gain is chosen which consumes 0.9 μW power (Harrison, 2002).

Analogue-to-digital converter (ADC): The ADC is used to digitize the EEG signal for further processing and transmission. Sampling rate and resolution are the two core parameters of interest in ADC. After removal of any d.c. offset in the signal by the instrumentation amplifier a medium resolutions and low sampling rate ADC is generally required for the EEG sensor node. In (Verma and Chandrakasan, 2007) an ultra-low power ADC has been fabricated in a $0.18\mu m$ CMOS technology. A 1V supply is used to power all the circuits. At a resolution of 12-bits, and a sampling rate of 0.5 kS/s (kilo Samples per second), the power consumption of the ADC is 0.2 μW (Verma and Chandrakasan, 2007). The power consumption increases linearly with sampling rate and is measured to be approximately 25 μW (microwatt) at 100 kS/s (Verma and Chandrakasan, 2007). Table 7.1 indicates the change in power consumption of ADC and also the total power consumption of the sensor node using (7.3) with the change of sampling rate. ADC power is directly scaled with the number of channels; it is clear from the Table 7.1 that with the increased number of channels both the ADC power and total power consumption also increased. It is also noticeable that sampling rate up to 0.5 kS/s the power consumption is in the μW range, it increased for higher sampling rate of ADC.

A widely used figure-of-merit (FOM) normalizes the ADC power consumption to the input bandwidth it can digitize and the dynamic range it achieves (Verma and Chandrakasan, 2007):

$$FOM = \frac{P_{ADC}}{2f_{in}2^{ENOB}} \quad (7.3)$$

where f_{in} is the input frequency of the ADC. For 100 kS/s sampling rate f_{in} is 50 kHz.

In 12-bit mode, the ADC samples at 100 kS/s and achieves an effective number of bits (ENOB) of 10.55 bits at its Nyquist rate (Verma & Chandrakasan, 2007).

The ADC also achieves a FOM of 165 fJ per conversion step in its 12-bit mode (Verma and Chandrakasan, 2007):

Table 7.1. Power consumption at different sampling rates of ADC.

R	f_s (kS/s)	P_{ADC} (μW)	Total Power Consumption, P_{total} (for 32 channel)	Total Power Consumption, P_{total} (for 29 channel)	Total Power Consumption, P_{total} (for 23 channel)
12	0.25	0.1	627 μ W	601 μ W	550 μ W
12	0.5	0.2	870 μ W	822 μ W	725 μ W
12	50	2	49 mW	47 mW	35 mW
12	100	25	97 mW	88 mW	70 mW

The resolutions of ADC also affect the power consumption of the ADC and thereby affect the total power consumption. Figure 7.5 shows the change in total power consumption with the varying resolution of ADC (8-12 bits). Table 7.2 summarizes the variation of ADC power consumption and total power consumption with the change of ADC resolution. In this case, the sampling rate is fixed at 100 kS/s.

Table 7.2. Power consumption at different resolution of ADC.

R	f_s (kS/s)	P_{ADC} (μW)	Total Power Consumption, P_{total} (for 32 channel)	Total Power Consumption, P_{total} (for 29 channel)	Total Power Consumption, P_{total} (for 23 channel)
8	100	19	65 mW	59 mW	47 mW
10	100	23	81 mW	74 mW	58 mW
12	100	25	97 mW	88 mW	70 mW

Random number generator: It is used to generate sensing matrix Φ . There is various

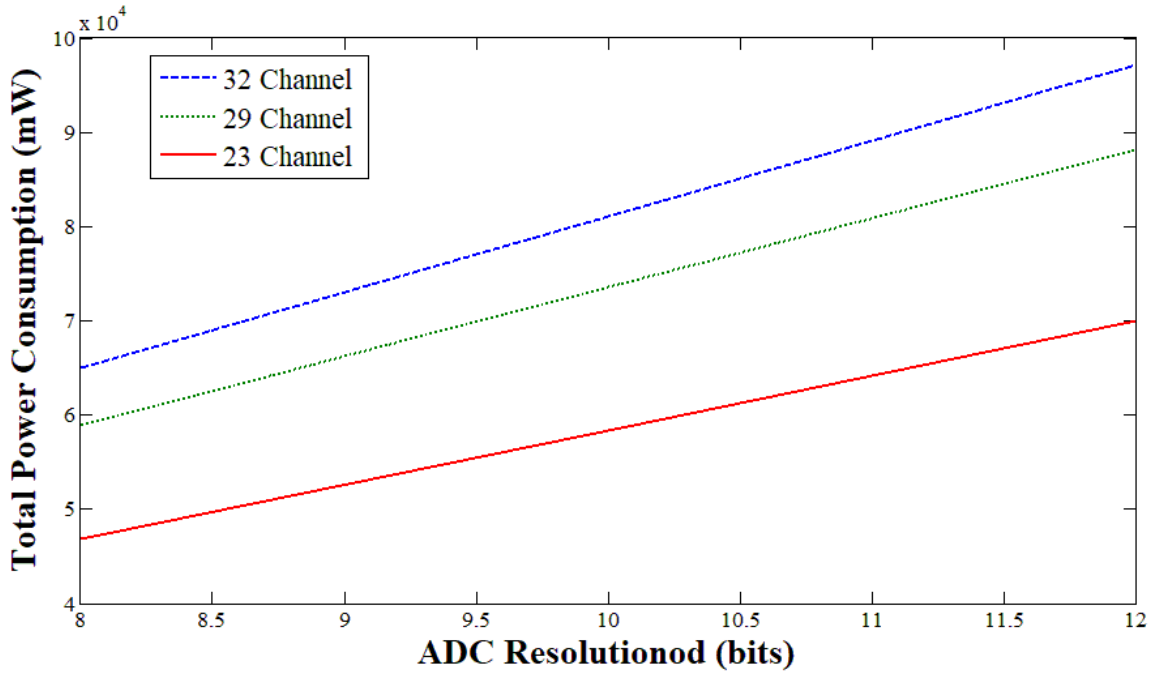


Figure 7.5. Total power consumption Vs ADC Resolution.

type of random number generator (RNG) are available depending on their applications. For example, the RNG that was used in (Holleman *et al.*, 2006) can be used for generating Φ .

matrix (Abdulghani, Casson and Rodriguez-Villegas, 2010). A comparative analysis on the basis of bit rates and power consumption is also made in (Holleman *et al.*, 2006) with other existing RNG. The RNG fabricated on 0.35 μm process and it operates at 5V. It consumes only 2.9 μW power with the output data rate of 500 bps.

Microcontroller or Microprocessor: This is where the compressive sensing is executed by the matrix multiplications. In order to minimize sensor node power consumptions, in this work, a sparse binary matrix (SBM) is used as the sensing matrix Φ with values of 1 and 0 which means each matrix entry is represented by a single bit. This results in reducing the size of the sensing matrix and subsequent matrix multiplication. In addition, SBM requires only accumulator registers for the matrix multiplication operation in the microprocessor. Any other choice of a full rank sensing matrix $M \times N$ would cause additional circuit complexity, data storage, and computation requirements. Moreover, CS with SBM matrix costs less power. During compression of a N number of samples of the signal, a $M \times N (M \ll N)$ Φ matrix is used for multiplications. So, the input data is compressed by M dimension and this compressed data are encoded on the microprocessor, i.e., the processor needs a fewer code

execution. The power requirements of the processor strongly depend on the specifications of the model chosen to be used. Because of its ultra-low power consumption, TI MSP430 family (Texas Instruments, 2013) is a popular choice for sensor nodes. MSP430 operates at clock frequency 1 MHz for a 16-bit resolution of Φ and its active mode power consumption is approximately 352 μ W (Texas Instruments, 2013). Φ can be generated priori in MATLAB using and stored in the memory of MSP430 (Sheng, Yang and Herbordt, 2015).

It is already stated that most power is dissipated in the transmitter of a sensor node; therefore to minimize the power consumption of the sensor node it is necessary to reduce power in the transceiver. The best way of achieving this is to reduce the data volume before transmission. At DSP/microcontroller Φ randomly taking M samples from N samples of signal that's mean it compressed signal by M/N compression ratio so finally the signal is transmitting to the receiver at a highly reduced rate ($f_s \frac{M}{N}$; here, $f_s = 250, M = 128, N = 256$;); which means data is compressed at 0.63 nyquist rate of EEG (EEG nyquist rate is 200 Hz). Compressing signal such a below nyquist rate also increase the processing and transmission sleep time. Thus it is possible to transmit signal only when it is required.

Figure 7.6 shows the circuitry for the sensor node illustrating the reduced data rate by the microcontroller. Figure 7.7 depicts the total power consumption of the sensor node with the variation of different nyquist rate of compression. It is clear from the Figure 7.7 that at nyquist rate 0.63 the total power consumption by the sensor node is lowest in comparison to other rates. It is also noted that this rate is used across this research to compress various types of EEG signal.

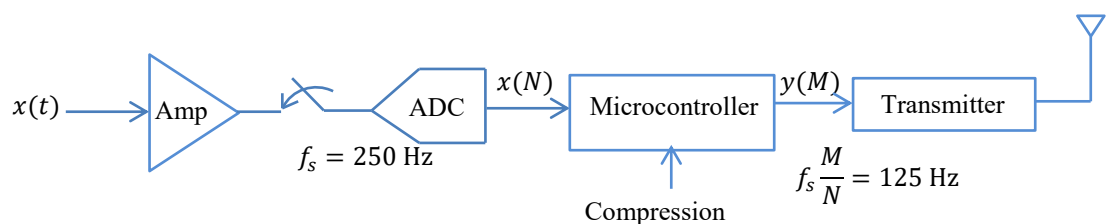


Figure 7.6. The circuitry of a sensor node.

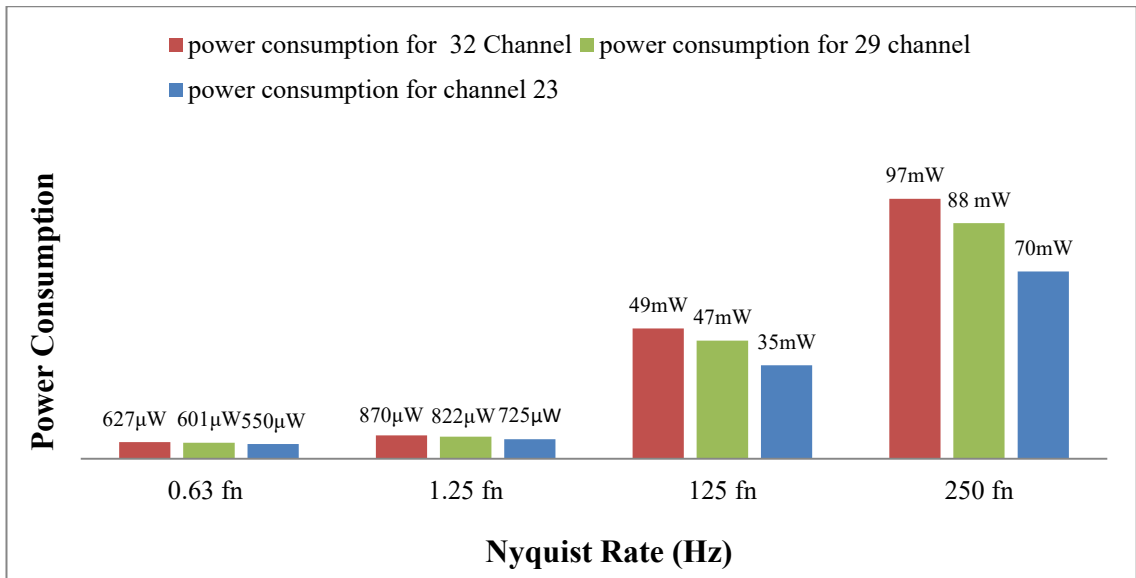


Figure 7.7. Power consumption Vs EEG Nyquist rate.

Transmitter: The performances of several off-the-shelf transmitters are analysed in (Yates and Rodriguez-Villegas, 2007). Two figures for energy per bit (j) are considered and analysed briefly in that paper. One figure is 50 nJ/b, which is considered on the performance basis of 2.4 - 2.5 GHz (The Industrial, Scientific and Medical) ISM radio transceiver nRF2401 (Nordiac semiconductor, 2004) and Bluetooth Specification v1.2 solution BRF6150 (Texas Instruments, 2003). On the other hand based on the performance of UWB devices such as the XS110 (Freescale Semiconductor, 2004) second figure 5 nJ/b is taken. In (Khan and Yuce, 2010) UWB is used as a high data rate transmission link for WBAN sensor node. As 5 nJ/b is already used as a considerable j figure for UWB device. In this work, 5 nJ/b is used as j value.

All the parameters that are used for power consumption calculation are summarized in Table 7.3.

Table 7.3. Summary of the parameters used in power consumption analysis.

Parameter	Symbol	Value
Amplifier Power	P_{AMP}	0.9 μ W
ADC Power	P_{ADC}	.1 μ W
Random Number Generator Power	P_{RNG}	2.9 μ W
Matrix Multiplication Power,	P_{MULT}	352 μ W
Transmission Power per bit,	j	5 nj/b
Total Number of Sample	N	256
Number of samples taken	M	128
Nyquist Sampling Frequency	f_s	0.25 kS/s
ADC Sampling Resolution	R	12
Number of Channels in the system	C	Variable

7.7 Power Consumption at different CR

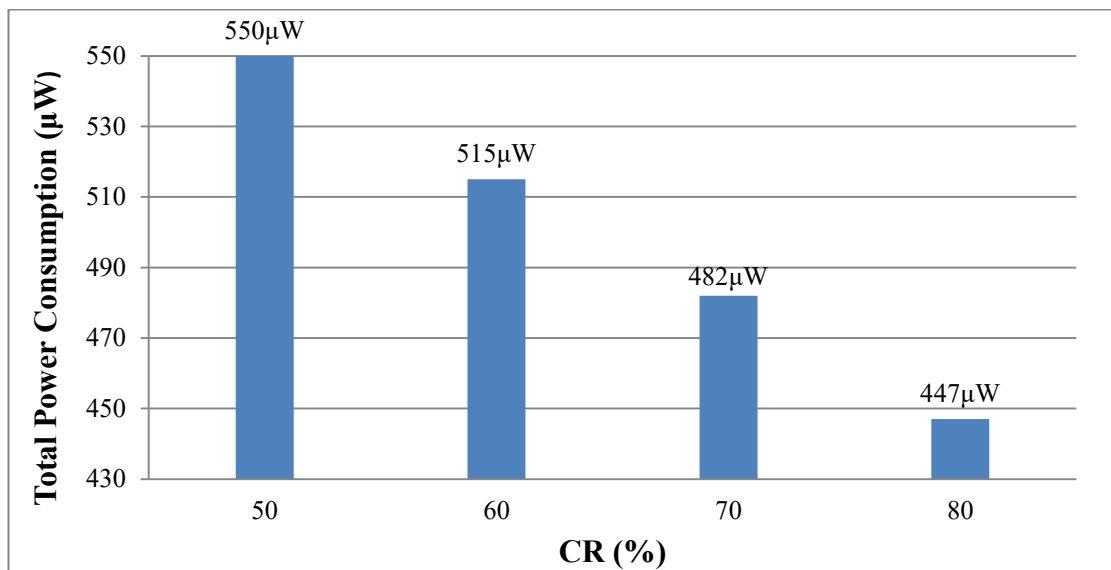


Figure 7.8. Power consumption at different CR, while ADC sampling rate is 250 Hz.

Figure 7.8 shows the power consumption in terms of CR at a variety of ranges (50%-80%). The outcome indicates that at each CR level the amount of power consumption is strict into μW range. This is because the data is under sampled at very below Nyquist rate. The findings indicate that by compressing signal at 50% it is possible to achieve a reduced rate of (at μW range) power consumption even without sacrificing performances. As it is demonstrated in the previous chapter that at 80% CR the reconstruction error is a bit high still if necessary system can use 80% compression to save about 97 μW of energy by sacrificing the reconstruction accuracy.

7.8 Further Power Savings in WBAN

The ST-SBL framework can further decrease the power consumption without affecting the reconstruction accuracy. It is shown in section 6.3.1 that the variation in the entries of d (number of non-zero entries in the columns of SBM) does not affect the reconstruction performance. Therefore, further savings of power is possible by using a lower value of d , for example, 2 can be used instead of 30 as d in each column of SBM which will reduce the number of computation and execution time to a great extent.

The experimental outcomes in (Mamaghanian *et al.*, 2011; Zhang *et al.*, 2013b) indicate that the performances of other algorithms are affected by the variation of d . In (Zhang *et al.*, 2013b) it is stated that only SBL algorithms can sampled signal using a SBM of such a less number of non-zero entries and can contribute to the further energy savings.

7.9 Summary

The development of WBAN based EEG sensor node is crucial in facilitating the distant monitoring of a patient in their everyday environment. The critical factor in realizing the benefit of wireless sensor nodes is its power consumption. Minimizing the battery size which determines the device size and power consumption of the EEG sensor node is key to its success (Imtiaz, Casson and Rodriguez-Villegas, 2014). In order to minimize the size and power consumption, some data reduction strategy is required at the sensor node (Chen, Chandrakasan and Stojanovic, 2012). It is widely accepted that CS has its significant use in simplifying the operation of wireless EEG sensor nodes from physically small batteries over a long period of time. Thus it ensures the reliability and robustness of the total system as the device is easier to use and more comfortable to wear. CS is a signal sampling paradigm that effectively samples a signal at a sampling

rate much lower than the Nyquist rate (Sheng, Yang and Herbordt, 2015; Donoho, 2006) and still ensures accurate reconstruction of the signal. The signal reconstruction is described in the previous chapter. This chapter has analyzed the feasibility of the proposed framework to enable online data reduction, from the power point of view. The power requirements for the proposed framework based EEG sensor node are quantified in this chapter following a power model. It is shown that at a data compression ratio of 50% (0.63 of nyquist rate), the proposed approach enables the energy savings budget well into the microwatts range which ensures a significant savings of battery life and overall system's power. Further reduction of the power consumption is also possible by reducing the number of non-zero elements in SBM.

Therefore, the findings indicate that the proposed strategy can help to save power, execution time and lessen the requirements of computation, transmission and storage in WBANs sensor nodes.

Chapter 8

Conclusion and Future Research Scopes

8.1 Conclusion

As a conclusion of the dissertation, this chapter emphasizes the primary contributions and its effect in the associate research area. Furthermore, the possible directions of further study are also suggested in the end.

WBAN is intended to help human's regular life and also enhance the quality of life. A numbers of studies have been accomplished over the past few years to integrate sensor nodes in WBANs which an individual can carry easily. This allows a variety of biomedical applications, for example, detection of epilepsy, transmission and monitoring of EEG signals, ECG signal, blood pressure, temperature etc. Thus WBAN can help people (especially disabled people who are not able to visit hospitals regularly) in their daily lives by recording their health status and tele-monitoring them in an outpatient setting.

The aim of this study is the low power transmission of EEG signal over WBAN and its accurate reconstruction at the receiver to ensure continuous EEG record monitoring and real time feedback to the patients from the medical experts.

The high volume of data and power consumption are the main limitations in transmission of EEG signal over WBAN, because of the short life of battery and processing capability of wireless sensor nodes. It is found that most of the energy consumptions occur during transmission of the signal. Therefore, methodologies are required for sensing and processing the signal before transmission. In this research, CS being an energy efficient data compression technique is applied prior to the transmission.

A requirement of CS is that the signal has to be sparse in the domain where it is compressed. EEG signal, however, is not sparse in time or the frequency domains. A challenge, therefore, in employing CS for the EEG signal is to identify the domain known as the dictionary in which the EEG signal is sufficiently sparse. This leads to another sufficient requirement for CS which is the incoherence between the dictionary and the sensing basis matrix. The aim of this study is to identify a suitable DWT dictionary by investigating incoherence with an aim

of improving accuracy of reconstruction of the EEG signals. Although state-of-the-art approaches show accurate reconstruction of EEG, however the specific features that make these suitable dictionaries have not investigated.

It is demonstrated in this work that there are two key criteria for an appropriate selection of the DWT are the number of vanishing moments, indicating to what extent it can represent complex signals sparsely; and with respect to CS, incoherence of the dictionary with the sensing basis, denoting how accurately the original signal may then be reconstructed. In this thesis, the relationship between incoherence of the DWTs and the ensuing reconstructed signal is investigated for a range of DWTs while using sparse binary matrix (SBM) as the sensing basis. SBM, owing to its low power features, is suitable for WBAN. Results indicate that DWTs that are more incoherent with the SBM lead to lower errors in reconstruction and that the accuracy in reconstruction is a stronger function of incoherence compared with vanishing moments. The experimental result shows that Beylkin among all the DWT is maximally incoherent with SBM. The reconstruction results of the signal also show that best reconstructions are also obtained with Beylkin. Further analysis of the results with vanishing moments and coherence shows that Beylkin has higher incoherence with SBM but slightly lower number of vanishing moments compared to other DWTs but the overall performance associated with Beylkin is better. Moreover, Beylkin has least number of filter coefficients in comparison to others which also increase the computational efficiency.

In addition, the overall energy savings of transmitting EEG signal in WBAN are investigated by exploring the effectiveness of the proposed approach. The investigations are done by numerical experiments following a power model. In order to get an idea about the actual power consumption and savings, the hard values are established using realistic and state-of-the-art values. The results will help to realize the computational complexity and online implementation requirements of CS for transmitting EEG in WBAN. It is stated that the most energy consumption part of WBAN is transmission. Therefore, the Transmission power requirement has been reduced by a factor of M/N using CS. This is the advantage of CS that it compresses signal at a below rate of Nyquist. In this work the sampling rate is much below than Nyquist rate which assists to keep the power consumption in μW range.

Thus, proposed approach enables energy savings-reconstruction quality trade-off in the system.

8.2 Future Research Scopes

There are many possible scopes of further research of the work presented in this dissertation. Several possible directions are highlighted below:

Clinical evaluation

One possible scope of the work is applying the given approach for clinically evaluating EEG Signal to detect epilepsy or sleep apnea or any other brain diseases by employing appropriate classification method to the reconstructed signal in proposed framework. Thus, this will assist WBAN system to detect disease through tele-monitoring and will improve and ease the treatment process.

Since the nature of EEG, ECG, EMG signals are almost similar, the proposed concept can be applied for these physiological signals which requires compression and transmission over WBAN to see the feasibility that can it be done and then followed by clinical evaluation.

Hardware implementations

Another possible extension of the work is to implement the proposed approach in hardware to check its performances and efficiency. The proposed framework offers a broad range of opportunities to improve the implementation of hardware. Furthermore, during designing SBM, there are scopes of further algorithmic improvements which can contribute to the system's overall efficiency.

Exploiting other features of EEG

This work is focused on the correlation structures of EEG signals among channels. There are scopes of exploring other structures of EEG signal, such as group structure, tree structure and so on. By employing different methods in the proposed approach these features of EEG can be explored.

Employing other methods

In addition, there have been efforts to develop data-driven schemes for learning the best sparsifying dictionaries as well as using Deep Neural Network (DNN) for reconstructing the compressed signals (Hamner, Chavarriaga and Millan, 2011; Majumdar and Ward, 2016; Palangi, Ward, and Deng, 2016; Tour *et al.*, 2018). Considering these methods for further benchmarking could be a promising direction for future research.

References and Bibliography

References

- Abdulghani, A.M., Casson, A.J. and Rodriguez-Villegas, E. (2010) 'Quantifying the performance of compressive sensing on scalp EEG signals', *3rd International Symposium on Applied Sciences in Biomedical and Communication Technologies (ISABEL 2010)*, Rome, 7-10 November, pp. 1-5. doi: 10.1109/ISABEL.2010.5702814.
- Adeli, H., Zhou, Z. and Dadmehr, N. (2003) 'Analysis of EEG records in an epileptic patient using wavelet transform', *Journal of Neuroscience Methods*, 123(1), pp. 69-87. doi:10.1016/s0165-0270(02)00340-0.
- Al-Janabi, S., Al-Shourbaji, I., Shojafar, M. and Shamshirband, S. (2016) 'Survey of main challenges (security and privacy) in wireless body area networks for healthcare applications' *Egyptian Informatics Journal*, 16(2), pp. 113-122. doi: 10.1016/j.eij.2016.11.011.
- Antoniol, G. and Tonella, P. (1997) 'EEG data compression techniques', *IEEE Transactions on Biomedical Engineering*, 44(2), pp. 105-114. doi: 10.1109/10.552239.
- Aviyente, S. (2007) 'Compressed Sensing Framework for EEG Compression', *IEEE/SP 14th Workshop on Statistical Signal Processing*, Madison, WI, USA, 26-29 August, pp. 181-184. doi: 10.1109/SSP.2007.4301243.
- Balouchestani, M., Raahemifar, K. and Krishnan, S. (2012a) 'Low Power Wireless Body Area Networks with Compressed sensing theory' *IEEE 55th International Midwest Symposium on Circuits and Systems (MWSCAS)*, Boise, ID, 5-8 August, pp. 916-919. doi: 10.1109/MWSCAS.2012.6292170.
- Balouchestani, M., Raahemifar, K. and Krishnan, S. (2012b) 'Wireless Body Area Networks with compressed sensing theory', *ICME International Conference on Complex Medical Engineering (CME)*, Kobe, 1-4 July, pp. 364-369. doi: 10.1109/ICCME.2012.6275663.
- Buckheit, J.B. and Donoho, D.L. (1995) 'WaveLab and Reproducible Research', In: Antoniadis A., Oppenheim G. (eds) *Wavelets and Statistics*. Lecture Notes in Statistics, (103). Springer, New York, NY. doi: https://doi.org/10.1007/978-1-4612-2544-7_5.
- Büsze, B., Bouwens, F., Konijnenburg, M., Nil, M.D., Ashouei, M., Hulzink, J., Zhou, J., Stuyt, J., Huisken, J., Groot, H.D., Santana, O., Abbo, A., Yseboodt, L., Meerbergen, J.V. and Bennebroek, M., (2010) 'Ultra Low Power programmable biomedical SoC for on-body ECG and EEG processing', *IEEE Asian Solid-State Circuits Conference*, Beijing, 8-10 November, pp. 1-4. doi: 10.1109/ASSCC.2010.5716625.
- Casson, A.J. and Rodriguez-Villegas, E. (2012) 'Signal agnostic compressive sensing for Body Area Networks: Comparison of signal reconstructions', *Annual International Conference of the IEEE Engineering in Medicine and Biology Society*,

- San Diego, CA, 28 August-1 September, pp. 4497-4500. doi: 10.1109/EMBC.2012.6346966.
- Candes, E.J. and Wakin, M.B. (2008) 'An introduction to compressive sampling', *IEEE Signal Processing Magazine*, 25(2), pp. 21-30. doi: 10.1109/MSP.2007.91473.
- Craven, D., McGinley, B., Kilmartin, L., Glavin, M. and Jones, E. (2015) 'Compressed Sensing for Bioelectric Signals: A Review', *IEEE Journal of Biomedical and Health Informatics*, 19(2), pp. 529-540, doi: 10.1109/JBHI.2014.2327194.
- Chen, F., Chandrakasan, A.P. and Stojanovic, V.M. (2012) 'Design and Analysis of a Hardware-Efficient Compressed Sensing Architecture for Data Compression in Wireless Sensors', *IEEE Journal of Solid-State Circuits*, 47(3), pp. 744-756, doi: 10.1109/JSSC.2011.2179451.
- Chitra, S., Deborah, S. and Sreeja, G.B. (2015) 'EEG Signal Compression Using Wavelet Based Arithmetic Coding', *International Journal of Science, Engineering and Technology Research (IJSETR)*, 4(4), pp. 898-902.
- Crystal Blue Enterprises (2015) *Brain Waves*. Available at: <http://www.crystalblueent.com/brain-waves.html> (Accessed: 25 July 2019).
- Dharshini, S. and Subashini, M.M. (2017) 'An overview on wireless body area networks', *2017 Innovations in Power and Advanced Computing Technologies (i-PACT)*, Vellore, 21-22 April, pp. 1-10. doi: 10.1109/IPACT.2017.8244985.
- Dehkordi, V.R., Daou, H. and Labeau, F. (2011) 'A Channel Differential EZW Coding Scheme for EEG Data Compression', *IEEE Transactions on Information Technology in Biomedicine*, 15(6), pp. 831-838. doi: 10.1109/TITB.2011.2171703.
- Delorme, A. and Makeig, S. (2004) 'EEGLAB: an open source toolbox for analysis of single-trial EEG dynamics including independent component analysis', *Journal of Neuroscience Methods*, 134, pp.9-21.
- Djelouat, H., Baali, H., Amira, A. and Bensaali, F. (2017) 'Joint sparsity recovery for compressive sensing based EEG system', *IEEE 17th International Conference on Ubiquitous Wireless Broadband (ICUWB)*, Salamanca, 12-15 September, pp. 1-5. doi: 10.1109/ICUWB.2017.8251001.
- Donoho, D.L. (2006) 'Compressed sensing', *IEEE Transactions on Information Theory*, 52(4), pp. 1289-1306. doi: 10.1109/TIT.2006.871582.
- Fira, M. and Goras, L. (2010) 'Biomedical Signal Compression based on Basis Pursuit', *International Journal of Advanced Science and Technology*, 14, pp. 53-64.
- Freescale Semiconductor (2004) *XS110 UWB Solution for Media-Rich Wireless Applications*. Available at: <http://www.uta.edu/rfmems/Telemetry/UWB/UWBFS.pdf> (Accessed: 13 June 2019).
- Gangopadhyay, D., Allstot, E.G., Dixon, A.M.R. and Allstot, D.J. (2011) 'System considerations for the compressive sampling of EEG and ECoG bio-signals', *IEEE Biomedical Circuits and Systems Conference (BioCAS)*, San Diego, CA, 10-12 November, pp. 129-132. doi: 10.1109/BioCAS.2011.6107744.

- Gil, Y., Li, G., Chen, H. and Lee, J. (2011) 'A wireless EEG monitor system based on BSN node', 24th International Symposium on Computer-Based Medical Systems (CBMS), Bristol, 27-30 June, pp. 1-7. doi: 10.1109/CBMS.2011.5999039.
- Gogna, A., Majumdar, A. and Ward, R. (2017) 'Semi-supervised Stacked Label Consistent Autoencoder for Reconstruction and Analysis of Biomedical Signals', *IEEE Transactions on Biomedical Engineering*, 64(9), pp. 2196-2205. doi: 10.1109/TBME.2016.2631620.
- Hamner, B., Chavarriaga, R. and Millan, J.D.R. (2011) 'Learning dictionaries of spatial and temporal EEG primitives for brain-computer interfaces', Presented at Workshop on Structured Sparsity: Learning and Inference, *International Conference Machine Learning, ICML*, June.-July. 2011.
- Hanafy, M.A., Ali, H.S. and Shaalan, A.A. (2017) 'Compressed sensing for reliable body area propagation with efficient signal reconstruction', *29th International Conference on Microelectronics (ICM)*, Beirut, 10-13 December, pp. 1-4. doi: 10.1109/ICM.2017.8268855.
- Harati, A., López, S., Obeid, I., Picone, J., Jacobson, M.P. and Tobochnik, S. (2014) 'The TUH EEG CORPUS: A big data resource for automated EEG interpretation', *IEEE Signal Processing in Medicine and Biology Symposium (SPMB)*, Philadelphia, PA, 13 December, pp. 1-5. doi: 10.1109/SPMB.2014.7002953.
- Harrison, R.R. (2002) 'A low-power, low-noise CMOS amplifier for neural recording applications', *IEEE International Symposium on Circuits and Systems. Proceedings (Cat. No.02CH37353)*, Phoenix-Scottsdale, AZ, USA, 26-29 May, pp. 958-965. doi: 10.1109/ISCAS.2002.1010674.
- Higgins, G., Faul, S., McEvoy, R.P. and McGinley, B. (2010) 'EEG compression using JPEG2000: How much loss is too much?', Annual International Conference of the IEEE Engineering in Medicine and Biology, Buenos Aires, 31 August-4 September, pp. 614-617. doi: 10.1109/IEMBS.2010.5628020.
- Higgins, G., Ginley, B.M., Glavin, M. and Jones, E. (2010) 'Low power compression of EEG signals using JPEG2000' *4th International Conference on Pervasive Computing Technologies for Healthcare*, Munich, 22-25 March, pp. 1-4. doi: 10.4108/ICST.PERVASIVEHEALTH2010.8861.
- Hilton, M.L., Jawerth, B.D. and Sengupta, A. (1994) 'Compressing Still and Moving Images with Wavelets', *Multimedia Systems*, 2(3), pp. 218 – 227.
- Holleman, J., Otis, B., Bridges, S., Mitros, A. and Diorio, C. (2006) 'A 2.92 μ W Hardware Random Number Generator', *Proceedings of the 32nd European Solid-State Circuits Conference*, Montreux, 19-21 September, pp. 134-137. doi: 10.1109/ESSCIR.2006.307549.
- Hosseini, M., Pompili, D., Elisevich, K. and Soltanian-Zadeh, H. (2017) 'Optimized Deep Learning for EEG Big Data and Seizure Prediction BCI via Internet of Things' *IEEE Transactions on Big Data*, 3(4), pp. 392-404. doi: 10.1109/TBDATA.2017.2769670.
- Hussein, R., Mohamed, A. and Alghoniemy, M. (2015) 'Energy-efficient on-board processing technique for wireless epileptic seizure detection systems', *International*

- Conference on Computing, Networking and Communications (ICNC)*, Garden Grove, CA, 16-19 February, pp. 1116-1121. doi: 10.1109/ICCNC.2015.7069506.
- Imtiaz, S.A., Casson, A. J. and Rodriguez-Villegas, E. (2014) ‘Compression in Wearable Sensor Nodes: Impacts of Node Topology’, *IEEE Transactions on Biomedical Engineering*, 61(4), pp. 1080-1090. doi: 10.1109/TBME.2013.2293916.
- Ivanov, S., Foley, C., Balasubramaniam, S. and Botvich, D. (2012) ‘Virtual Groups for Patient WBAN Monitoring in Medical Environments’, *IEEE Transactions on Biomedical Engineering*, 59(11), pp. 3238-3246. doi: 10.1109/TBME.2012.2208110.
- Jasper, H.H. (1958) ‘The ten-twenty electrode system of the International Federation’, *Electroencephalography and Clinical Neurophysiology*. 10, pp. 367-380.
- Kamal, M.H., Shoaran, M., Leblebici, Y., Schmid, A. and Vandergheynst, P. (2013) ‘Compressive multichannel cortical signal recording’, *IEEE International Conference on Acoustics, Speech and Signal Processing*, Vancouver, BC, 26-31 May, pp. 4305-4309. doi: 10.1109/ICASSP.2013.6638472.
- Kamat, S.U., Raveendra, M. and Inamdar, N. (2013) ‘Improved compression of EEG Data Using Wavelets’, *International Journal of Advanced Research in Electronics and Communication Engineering (IJARECE)*, 2(5), pp. 583-588.
- Kaliannan, B. and Pasupureddi, V.S.R. (2016) ‘A low power charge mode compressive acquisition of multichannel EEG signals’, *IEEE International Symposium on Circuits and Systems (ISCAS)*, Montreal, QC, 22-25 May, pp. 518-521. doi: 10.1109/ISCAS.2016.7527291.
- Khan, J.Y. and Yuce, M. R. (2010) ‘Wireless Body Area Network (WBAN) for Medical Applications’, Campolo, D. *New Developments in Biomedical Engineering*, IntechOpen, pp. 591-627. doi: 10.5772/7598.
- Klem, G.H., Lüders, H.O., Jasper, H.H. and Elger, C. (1999) ‘The ten-twenty electrode system of the International Federation’, *Electroencephalography and Clinical Neurophysiology*. 52, pp. 3-6.
- Kumar, J.S. and Bhuvaneshwari, P. (2012) ‘Analysis of Electroencephalography (EEG) Signals and Its Categorization—A Study’, *International Conference on Modelling Optimization and Computing*, Elsevier Ltd, pp. 2525-2536. doi: 10.1016/i.proeng.2012.06.298.
- Lalos, A.S., Antonopoulos, A., Kartsakli, E., Renzo. M.D., Tennina, S., Alonso, L. and Verikoukis, C. (2014) ‘Cooperative compressed sensing schemes for telemonitoring of vital signals in WBANs’, *IEEE Global Communications Conference*, Austin, TX, 8-12 December, pp. 2387-2392. doi: 10.1109/GLOCOM.2014.7037165.
- Lalos, A.S., Antonopoulos, A., Kartsakli, E., Renzo. M.D., Tennina, S., Alonso, L. and Verikoukis, C. (2015) ‘RLNC-Aided Cooperative Compressed Sensing for Energy Efficient Vital Signal Telemonitoring’, *IEEE Transactions on Wireless Communications*, 14(7), pp. 3685-3699. doi: 10.1109/TWC.2015.2409841.
- Lim, H.B., Baumann, D. and Li, E. (2011) ‘A Human Body Model for Efficient Numerical Characterization of UWB Signal Propagation in Wireless Body Area Networks’, *IEEE Transactions on Biomedical Engineering*, 58(3), pp. 689-697. doi: 10.1109/TBME.2010.2091128.

- Lin, C.-L., Wu, R.-C., Liang, S.-F., Chao, W.-C., Chen, Y.-J. and Jung, T.-P. (2005) 'EEG-based drowsiness estimation for safety driving using independent component analysis', *IEEE Transactions on Circuits and Systems I: Regular Papers*, 52(12), pp. 2726-2738. doi: 10.1109/TCSI.2005.857555.
- Liu, Y., Vos, M.D. and Huffel, S.V. (2015) 'Compressed Sensing of Multichannel EEG Signals: The Simultaneous Cosparsity and Low-Rank Optimization', *IEEE Transactions on Biomedical Engineering*, 62(8), pp. 2055-2061. doi: 10.1109/TBME.2015.2411672.
- Mahajan, R. and Bansal, D. (2014) 'Hybrid multichannel EEG compression scheme for tele-health monitoring' *Proceedings of 3rd International Conference on Reliability, Infocom Technologies and Optimization*, Noida, 8-10 October, pp. 1-6. doi: 10.1109/ICRITO.2014.7014672.
- Mahmoodin, Z., Jalalludin, N.S., Mansor, W., Lee, K.Y. and Mohamad, N.B. (2015) 'Selection of Symlets wavelet function order for EEG signal feature extraction in children with dyslexia', *IEEE Student Symposium in Biomedical Engineering & Sciences (ISSBES)*, Shah Alam, 4 November, pp. 113-117. doi: 10.1109/ISSBES.2015.7435879.
- Mahrous, H. and Ward, R. (2016a) 'A low power Dirac basis compressed sensing framework for EEG using a Meyer wavelet function dictionary', *IEEE Canadian Conference on Electrical and Computer Engineering (CCECE)*, Vancouver, BC, 15-18 May, pp. 1-6. doi: 10.1109/CCECE.2016.7726836.
- Mahrous, H. and Ward, R. (2016b) 'Block sparse compressed sensing of electroencephalogram (EEG) signals by exploiting linear and non-linear dependencies', *Sensors*, 16(2) pp. 1-16.
- Mallat, S (2008) 'A Wavelet Tour of Signal Processing', *Sparse Representation*, Burlington: Elsevier Academic Press, pp. 1-21.
- Mamaghanian, H. Khaled, N., Atienza, D. and Vandergheynst, P. (2011) 'Compressed Sensing for Real-Time Energy-Efficient ECG Compression on Wireless Body Sensor Nodes', *IEEE Transactions on Biomedical Engineering*, 58(9), pp. 2456-2466. doi: 10.1109/TBME.2011.2156795.
- Majumdar, A., Gogna, A. and Ward, R. (2014) 'A low-rank matrix recovery approach for energy efficient EEG acquisition for a Wireless Body Area Network', *Sensors*, 14, pp. 15729-15748. doi:10.3390/s140915729.
- Majumdar, A. and Ward, R. (2015) 'Energy efficient EEG sensing and transmission for wireless body area networks: A blind compressed sensing approach', *Biomedical Signal Processing and Control, Elsevier*, 20, pp. 1-9. doi.org/10.1016/j.bspc.2015.03.002.
- Majumdar, A. and Ward, R. (2016) 'Real-time reconstruction of EEG signals from compressive measurements via deep learning', *International Joint Conference on Neural Networks (IJCNN)*, Vancouver, BC, 24-29 July, pp. 2856-2863. doi: 10.1109/IJCNN.2016.7727560.
- Mandal, S. and Sarpeshkar, R. (2008) 'Power-Efficient Impedance-Modulation Wireless Data Links for Biomedical Implants', *IEEE Transactions on Biomedical Circuits and Systems*, 2(4), pp. 301-315. doi: 10.1109/TBCAS.2008.2005295.

- Mansor, W., Rani, M.S.A. and Wahy, N. (2011) 'Integrating Neural Signal and Embedded System for Controlling Small Motor', in Martinez-Alfar, H. (ed.) *Advances in Mechatronics*. InTech, pp. 31-42.
- Memon, N., Kong, X. and Cinkler, J. (1999) 'Context-based lossless and near-lossless compression of EEG signals', *IEEE Transactions on Information Technology in Biomedicine*, 3(3), pp. 231-238. doi: 10.1109/4233.788586.
- Men, H., Li, X., Wang, J. and Gao, J. (2007) 'Applies of Neural Networks to Identify Gases Based on Electronic Nose' *IEEE International Conference on Control and Automation*, Guangzhou, 30 May-1June, pp. 2699-2704. doi: 10.1109/ICCA.2007.4376852.
- Meng, Y., Qin, T. and Xing, J. (2014) 'Sensor Cooperation Based on Network Coding in Wireless Body Area Networks', *International Conference on Wireless Communication and Sensor Network*, IEEE, Wuhan, 13-14 December, pp. 358-361. doi: 10.1109/WCSN.2014.80.
- Misiti, M., Misiti, Y., Oppenheim, G. and Poggi, J.-M. (2004) 'Wavelet Toolbox', *Wavelets: A New Tool for Signal Analysis*. Natick, MA: The MathWorks, Inc, pp. 2-42.
- Mishra, A., Thakkar, F., Modi, C. and Kher, Rahul (2012) 'Comparative analysis of wavelet basis functions for ECG signal compression through compressive sensing', *International Journal of Computer Science and Telecommunications*, 3(5), pp. 23-31.
- Negra, R., Jemili, I. and Belghith, A. (2016) 'Wireless Body Area Networks: Applications and Technologies', *Procedia Computer Science*, 83(2016), pp. 1274-1281. doi: .org/10.1016/j.procs.2016.04.266.
- Nordiac semiconductor (2004) *Single chip 2.4 GHz Transceiver*. Available at: https://www.sparkfun.com/datasheets/Components/SMD/nRF24L01Pluss_Preliminary_Product_Specification_v1_0.pdf (Accessed: 13 June 2019).
- Nuwer, M.R., Comi, G., Emerson, R., Fuglsang-Frederiksen, A., Guerit J.-M., Hinrichs, H., Ikeda, A., Luccas, F.J.C. and Rappelsburger, P., (1998) 'IFCN standards for digital recording of clinical EEG', *Electroencephalography and Clinical Neurophysiology*, 106(3), pp. 259-261. doi: org/10.1016/S0013-4694(97)00106-5.
- Palangi, H., Ward, R., and Deng, L. (2016) 'Exploiting correlations among channels in distributed compressive sensing with convolutional deep stacking networks', *IEEE International Conference on Acoustics, Speech and Signal Processing (ICASSP)*, Shanghai, 20-25 March, pp. 2692-2696. doi: 10.1109/ICASSP.2016.7472166.
- Pandey, J. and Otis, B.P. (2011) 'A Sub-100 μ W MICS/ISM Band Transmitter Based on Injection-Locking and Frequency Multiplication', *IEEE Journal of Solid-State Circuits*, 46(5), pp. 1049-1058. doi: 10.1109/JSSC.2011.2118030.
- Panessai, I.Y. and Abdulbaqi, A.S. (2019) 'An Efficient Method of EEG Signal Compression and Transmission Based Telemedicine', *Journal of Theoretical and Applied Information Technology*, 97(4), pp. 1061-1070.
- Pei, Z. and Wang, Y. (2017) 'Energy Efficient Compressed Sensing of Bio-Signals with Sparse Binary Matrix', *4th International Conference on Information Science and*

- Control Engineering (ICISCE)*, Changsha, 21-23 July, pp. 1492-1496. doi: 10.1109/ICISCE.2017.311.
- Pereira, M.P., Lovisolio, L., Silva, E.A.D. and Campos, M.L.R.D. (2014) ‘On the design of maximally incoherent sensing matrices for compressed sensing using orthogonal bases and its extension for biorthogonal bases case’, *Elsevier*, 27, pp.12-22.
- Sazgar, M. and Young, M.G. (2019) ‘Overview of EEG, Electrode Placement, and Montages’, *Absolute Epilepsy and EEG Rotation Review*. Springer, Cham, pp.117-125.
- Selesnick, I.W. (2004) ‘The Double-Density Dual-Tree DWT’, *IEEE Transection on Signal Processing*, 52(5), pp. 1304-1313. doi: 10.1109/TSP.2004.826174.
- Seyedi, M., Kibret, B., Lai, D.T.H. and Faulkner, M. (2013) ‘A Survey on Intrabody Communications for Body Area Network Applications’, *IEEE Transactions on Biomedical Engineering*, 60(8), pp. 2067-2079. doi: 10.1109/TBME.2013.225471.
- Sheng, J., Yang, C. and Herbordt, M.C. (2015) ‘Hardware-efficient compressed sensing encoder designs for WBSNs’ *IEEE High Performance Extreme Computing Conference (HPEC)*, Waltham, MA, 15-17 September, pp. 1-7. doi: 10.1109/HPEC.2015.7322437.
- Shukla, A. (2014) *Signal Processing Techniques to Reduce Energy Consumption in EEG Acquisition and Transmission for WBAN*. MTech thesis. Indraprastha Institute of Institute of Information Technology, New Delhi. Available at: <https://pdfs.semanticscholar.org/bad6/b87075bb1f9ff7faf826332cd2fc9a340bbc.pdf> (Accessed: 8 May 2019).
- Shukla, A., Majumdar, A. and Ward, R. (2015) ‘A Kronecker Compressed Sensing Formulation for Energy Efficient EEG sensing’, *Eighth International Conference on Advances in Pattern Recognition (ICAPR)*, Kolkata, 4-7 January, pp. 1-6. doi: 10.1109/ICAPR.2015.7050682.
- Shoaib, M. (2013) *Design of Energy-efficient Sensing Systems with Direct Computations on Compressively-sensed Data*. PhD thesis. Princeton University. Available at: https://www.microsoft.com/en-us/research/wp-content/uploads/2016/02/Shoaib_Princeton_Thesis.pdf (Accessed: 26 May 2019).
- Singh, W., Shukla, A., Deb, S. and Majumdar, A. (2014) ‘Energy efficient acquisition and reconstruction of EEG signals’, *36th Annual International Conference of the IEEE Engineering in Medicine and Biology Society*, Chicago, IL, 26-30 August. pp. 1274-1277. doi: 10.1109/EMBC.2014.6943830.
- Singh, W., Shukla, A., Deb, S. and Majumdar, A. (2017) ‘Energy efficient EEG acquisition and reconstruction for a wireless body area network,” *J. Integration VLSI*, 58, pp. 285-302, doi.org/10.1016/j.vlsi.2016.08.006.
- Sornmo, L. and Laguna, P. (2005) ‘Evoked Potential’, *Bioelectrical Signal Processing in Cardiac and Neurological Applications*. Burlington: Elsevier Academic Press, pp. 286-306.
- Sriraam, N. and Eswaran, C. (2008) ‘Performance Evaluation of Neural Network and Linear Predictors for Near-Lossless Compression of EEG Signals’, *IEEE Transactions on Information Technology in Biomedicine*, 12(1), pp. 87-93. doi: 10.1109/TITB.2007.899497.

- Sriraam, N. (2012) 'A High-Performance Lossless Compression Scheme for EEG Signals Using Wavelet Transform and Neural Network Predictors' *International Journal of Telemedicine and Applications*, 2012, pp. 1-8. doi:10.1155/2012/302581.
- Stanford University (2005) *WAVELAB 850*. Available at: http://statweb.stanford.edu/~wavelab/Wavelab_850/Links.html (Accessed: 20 December 2015).
- Taywade, S.A. and Raut, R.D., (2012) 'A Review: EEG Signal Analysis With Different Methodologies', *National Conference on Innovative Paradigms in Engineering & Technology*, International Journal of Computer Applications, pp. 29-31.
- Teplan, M. (2002) 'Fundamental of EEG Measurement', *Measurement Science Review*, 2(2).
- Tiwari, V., Bansod, P.P. and Kumar, A. (2015) 'Designing sparse sensing matrix for compressive sensing to reconstruct high resolution medical image', *Cogent Engineering*, 2(1).
- Texas Instruments (2013) *Mixed Signal Microcontroller*. Available at: <http://www.ti.com/lit/ds/symlink/msp430g2553.pdf> (Accessed: 31 January 2019).
- Texas Instruments (2003) *BRF6150 Bluetooth v1.2 single-chip solution for mobile terminals*. Available at: <http://www.ti.com/pdfs/vf/wireless/brf6150bulletin.pdf> (Accessed: 13 June 2019).
- The Institute for Signal and Information Processing (1994) *Temple University Hospital EEG (TUH EEG) Resources*. Available at: https://www.isip.piconepress.com/projects/tuh_eeg/downloads/tuh_eeg_epilepsy/ (Accessed: 25 April 2019).
- Tour, T.D.L., Moreau, T., Jas, M. and Gramfort, X. (2018) 'Multivariate Convolutional Sparse Coding for Electromagnetic Brain Signals', *32nd Conference on Neural Information Processing Systems (NeurIPS 2018)*, Montreal, Canada.
- Unser, M. (1996) 'Vanishing moments and the approximation power of wavelet expansions', *Proceedings of 3rd IEEE International Conference on Image Processing, Lausanne, Switzerland*, 1, 19 September, pp. 629-632. doi: 10.1109/ICIP.1996.559575.
- Veloso, L., McHugh, J., Weltin, E.V., Lopez, S., Obeid, I. and Picone, J. (2017) 'Big data resources for EEGs: Enabling deep learning research' *IEEE Signal Processing in Medicine and Biology Symposium (SPMB)*, Philadelphia, PA, 2 December, pp. 1-3. doi: 10.1109/SPMB.2017.8257044.
- Verma, N. and Chandrakasan, A.P. (2007) 'An Ultra Low Energy 12-bit Rate-Resolution Scalable SAR ADC for Wireless Sensor Nodes' *IEEE Journal of Solid-State Circuits*, 42(6), pp. 1196-1205. doi: 10.1109/JSSC.2007.897157.
- Waltz, E. (2017) 'A Wearable chip to predict seizures', *IEEE Spectrum*, 6 December. Available at: <https://spectrum.ieee.org/the-human-os/biomedical/devices/a-wearable-chip-to-predict-seizures> (Accessed: 17 July 2019).
- Wang, A., Song, C. and Xu, W. (2014) 'A configurable quantized compressed sensing architecture for low-power tele-monitoring', *International Green Computing Conference*, Dallas, TX, 3-5 November, pp. 1-10. doi: 10.1109/IGCC.2014.7039153.

- Wang, Z., Bovik, A.C., Sheikh, H.R. and Simoncelli, E.P. (2004) 'Image quality assessment: from error visibility to structural similarity', *IEEE Transactions on Image Processing*, 13(4), pp. 600-612, doi: 10.1109/TIP.2003.819861.
- Yates, D.C. and Rodriguez-Villegas, E. (2007) 'A Key Power Trade-off in Wireless EEG Headset Design' *3rd International IEEE/EMBS Conference on Neural Engineering*, Kohala Coast, HI, 2-5 May, pp. 453-456. doi: 10.1109/CNE.2007.369707.
- Yger, F. and Rakotomamonjy, A. (2011) 'Wavelet Kernel Learning', *Pattern Recognition*. doi:10.1016/j.patcog.2011.03.006.
- Zhang, Z. and Rao, B.D. (2011) 'Exploiting correlation in sparse signal recovery problems: Multiple measurement vectors, block sparsity, and time-varying sparsity', *ICML Workshop on Structured Sparsity: Learning and Inference*.
- Zhang, Z. and Rao, B.D. (2013) 'Extension of SBL Algorithms for the Recovery of Block Sparse Signals With Intra-Block Correlation', *IEEE Transactions on Signal Processing*, 61(8), pp. 2009-2015, doi: 10.1109/TSP.2013.2241055.
- Zhang, Z., Jung, T.-P., Makeig, S. and Rao, B.D. (2013a) 'Compressed Sensing of EEG for Wireless Telemonitoring With Low Energy Consumption and Inexpensive Hardware', *IEEE Transactions on Biomedical Engineering*, 60(1), pp. 221-224. doi: 10.1109/tbme.2012.2217959.
- Zhang, Z., Jung, T.-P., Makeig, S. and Rao, B.D. (2013b), 'Compressed Sensing for Energy-Efficient Wireless Telemonitoring of Noninvasive Fetal ECG Via Block Sparse Bayesian Learning', *IEEE Transactions on Biomedical Engineering*, 60(2), pp. 300-309, Feb. 2013. doi: 10.1109/TBME.2012.2226175.
- Zhang, Z., Rao B.D. and Jung T.-P. (2013) 'Compressed sensing for energy-efficient wireless telemonitoring: Challenges and opportunities', *Asilomar Conference on Signals, Systems and Computers*, Pacific Grove, CA, 3-6 November, pp. 80-85. doi: 10.1109/ACSSC.2013.6810234.
- Zhang, Z., Jung, T.-P., Makeig, S. and Rao, B.D. (2014) 'Spatiotemporal Sparse Bayesian Learning With Applications to Compressed Sensing of Multichannel Physiological Signals', *IEEE Transactions on Neural Systems and Rehabilitation Engineering*, 22(6), pp. 1186-1197, doi: 10.1109/TNSRE.2014.2319334.

Bibliography

- Bertoni, N., Senevirathna, B., Pareschi, F., Mangia, M., Rovatti, R., Abshire, P., Simon, J.Z. and Setti, G. (2016) 'Low-power EEG monitor based on compressed sensing with compressed domain noise rejection', *IEEE International Symposium on Circuits and Systems (ISCAS)*, Montreal, QC, 22-25 May, pp. 522-525. doi: 10.1109/ISCAS.2016.7527292.
- Chuang, A.Y., Ward, R.K. and Birch, G.E. (2009) 'Rapid detection of voluntary movements in a self-paced brain-computer interface via compressive sensing', *4th*

- International IEEE/EMBS Conference on Neural Engineering*, Antalya, 29 April-2 May, pp. 335-338. doi: 10.1109/NER.2009.5109301.
- Graps, A. (1995) 'An introduction to wavelets' *IEEE Computational Science and Engineering*, 2(2), pp. 50-61. doi: 10.1109/99.388960.
- Hu, D., Mao, S. and Billor, N. (2012) 'On balancing energy efficiency and estimation error in compressed sensing' *IEEE Global Communications Conference (GLOBECOM)*, Anaheim, CA, 3-7 December, pp. 4278-4283. doi: 10.1109/GLOCOM.2012.6503790.
- Hussein, R., Mohamed, A. and Alghoniemy, M. (2013) 'Adaptive compression and optimization for real-time energy-efficient wireless EEG monitoring systems' *The 6th 2013 Biomedical Engineering International Conference*, Amphur Muang, 23-25 October, pp. 1-5. doi: 10.1109/BMEiCon.2013.6687691.
- Kim, D.-G., Hong, K.-S. and Chung, K.-W. (2012) 'Implementation of portable multi-channel EEG and head motion signal acquisition system', *8th International Conference on Computing and Networking Technology (INC, ICCIS and ICMIC)*, Gueongju, 27-29 August, pp. 370-375.
- Mainoddin, K. and Usha, S.A. (2014) 'Design and Development of Low Power Signal Conditioning and Processing Electronic System Using TIOPA4131 and MSP430', *International Journal of Innovative Research in Advanced Engineering (IJIRAE)*, 1(10), pp. 196-204.
- Majumdar, A., Shukla, A. and Ward, R. (2015) 'Combining sparsity with rank-deficiency for energy efficient EEG sensing and transmission over Wireless Body Area Network', *IEEE International Conference on Acoustics, Speech and Signal Processing (ICASSP)*, Brisbane, QLD, 19-24 April, pp. 837-841. doi: 10.1109/ICASSP.2015.7178087.
- Nassir, A., and Barnea, O. (2012) 'Wireless body-area network for detection of sleep disorders', *IEEE 27th Convention of Electrical and Electronics Engineers in Israel*, Eilat, 14-17 November, pp. 1-5. doi: 10.1109/EEEL.2012.6377041.
- Nia, A.M., Mozaffari-Kermani, M., Sur-Kolay, S., Raghunathan, A. and Jha, N.K. (2015) 'Energy-Efficient Long-term Continuous Personal Health Monitoring', *IEEE Transactions on Multi-Scale Computing Systems*, 1(2), pp. 85-98. doi: 10.1109/TMSCS.2015.2494021.
- Rahim, A. and Karmakar, N.C. (2013) 'Sensor cooperation in wireless body area network using network coding for sleep apnoea monitoring system' *IEEE Eighth International Conference on Intelligent Sensors, Sensor Networks and Information Processing*, Melbourne, VIC, 2-5 April, pp. 432-436. doi: 10.1109/ISSNIP.2013.6529829.
- Sangavi, J. and Hemalatha, M. (2018) 'Design of a Low Power and Area Efficient Architecture for the Detection of Audio Biological Signals', *International Journal for Research in Applied Science & Engineering Technology (IJRASET)*, 6(IV), pp. 4215-4225.
- Servín-Aguilar, J.G., Rizo-Dominguez, L. and Pardiñas-Mir, J.A. (2016) 'A comparison between wavelet families to compress an EEG signal', *IEEE ANDESCON*, Arequipa, 19-21 October, pp. 1-4. doi: 10.1109/ANDESCON.2016.783619.

- Shin, Y., Lee, S., Ahn, M., Jun, S.C. and Lee, H. (2011) ‘Motor imagery based BCI classification via sparse representation of EEG signals’, *8th International Symposium on Noninvasive Functional Source Imaging of the Brain and Heart and the 2011 8th International Conference on Bioelectromagnetism*, Banff, AB, 13-16 May, pp. 93-97. doi: 10.1109/NFSI.2011.5936827.
- Shin, Y., Lee, S., Woo, S. and Lee, H. (2013) ‘Performance increase by using a EEG sparse representation based classification method’, *IEEE International Conference on Consumer Electronics (ICCE)*, Las Vegas, NV, 11-14 January, pp. 201-203. doi: 10.1109/ICCE.2013.6486858.
- Shoaib, M., Lee, K.H. Jha, N.K. and Verma, N. (2014) ‘A 0.6–107 μ W Energy-Scalable Processor for Directly Analyzing Compressively-Sensed EEG’, *IEEE Transactions on Circuits and Systems I: Regular Papers*, 61(4), pp. 1105-1118, doi: 10.1109/TCSI.2013.2285912.
- Suo, Y., Zhang, J., Xiong, T., Chin, P.S., Etienne-Cummings, R. and Tran, T.D. (2014) ‘Energy-Efficient Multi-Mode Compressed Sensing System for Implantable Neural Recordings’, *IEEE Transactions on Biomedical Circuits and Systems*, 8(5), pp. 648-659, Oct. 2014. doi: 10.1109/TBCAS.2014.2359180.
- Trakimas, M., Hancock, T. and Sonkusale, S. (2012) ‘A Compressed sensing analog-to-information converter with edge-triggered SAR ADC Core’, *IEEE International Symposium on Circuits and Systems (ISCAS)*, Seoul, 22-23 May, pp. 3162-3165. doi: 10.1109/ISCAS.2012.6271993.
- Xiang, L., Luo, J. and Rosenberg, C. (2013) ‘Compressed Data Aggregation: Energy-Efficient and High-Fidelity Data Collection’, *IEEE/ACM Transactions on Networking*, 21(6), pp. 1722-1735. doi: 10.1109/TNET.2012.2229716.
- Yamaguchi, T., Fujio, M., Inoue, K. and Pfurtscheller, G. (2008) ‘Wavelet analysis of EEG signals during motor imagery’, *2008 International Conference on Wavelet Analysis and Pattern Recognition*, Hong Kong, 30-31 August, pp. 454-459. doi: 10.1109/ICWAPR.2008.4635822.
- Yu, H., Lu, H., Ouyang, T., Liu, H. and Lu, H. (2010) ‘Vigilance detection based on sparse representation of EEG’, *Annual International Conference of the IEEE Engineering in Medicine and Biology*, Buenos Aires, 31 August-4 September, pp. 2439-2442. doi: 10.1109/IEMBS.2010.5626084.

Appendix: MATLAB Code

%% Generate DWT Dictionary using Wavelab toolbox

% DWT generates using QMF filter bank

```
qmf = MakeONFilter('Beylkin');
N=256;
XI=eye(N);
W=zeros(N);
```

```

for i=1:N,
    W(:,i)=IWT_PO(XI(:,i),1,qmf);
end

%% Figure Mother Wavelets

subplot(5,3,1);
plot(db6,'b','LineWidth',2,'MarkerSize',12);
title('db3 ');

subplot(5,3,2);
plot(db8,'b','LineWidth',2,'MarkerSize',12);
title('db4');

subplot(5,3,3);
plot(db16,'b','LineWidth',2,'MarkerSize',12);
title('db8');

subplot(5,3,4);
plot(db20,'b','LineWidth',2,'MarkerSize',12);
title('db10');

subplot(5,3,5);
plot(Haar,'b','LineWidth',2,'MarkerSize',12);
title('Haar');

subplot(5,3,6);
plot(Vaidyanathan,'b','LineWidth',2,'MarkerSize',12);
title('Vaidyanathan');

subplot(5,3,7);
plot(Battle1,'b','LineWidth',2,'MarkerSize',12);
title('Battle1');

subplot(5,3,8);
plot(Battle3,'b','LineWidth',2,'MarkerSize',12);
title('Battle3');

subplot(5,3,9);
plot(Sym10,'b','LineWidth',2,'MarkerSize',12);
title('Sym10');

subplot(5,3,10);
plot(coif1,'b','LineWidth',2,'MarkerSize',12);
title('coif1 ');

subplot(5,3,11);
plot(coif2,'b','LineWidth',2,'MarkerSize',12);
title('coif2 ');

subplot(5,3,12);
plot(coif3,'b','LineWidth',2,'MarkerSize',12);

```

```

title('coif3');

subplot(5,3,13);
plot(coif4,'b','LineWidth',2,'MarkerSize',12);
title('coif4');

subplot(5,3,14);
plot(coif5,'b','LineWidth',2,'MarkerSize',12);
title('coif5');

subplot(5,3,15);
plot(Beylkin,'b','LineWidth',2,'MarkerSize',12);
title('Beylkin');

```

%% Coherence of SBM with DWT dictionary

```

close all;
clear all;

% Load DWT Dictionary
load W_Beylkin.mat;

% generate SBM (128 by 256)
M = 128;
N = 256;
%
while(1)
    [Phi,flag] = genPhi(M,N,30);
    if flag == 1, break; end;
end

%Normalized data
Phi=Phi/norm(Phi);
W_Beylkin =W_Beylkin/norm(W_Beylkin);

% Calculate Crosscorelation
xc = abs(Phi * W_Beylkin');

% Get the maximum
result = max(max(abs(Phi * W_Beylkin')));

% Measure Coherency
n=256;
N=sqrt(n);
coherency = N*result

/*****

* Title: Spatio-Temporal Sparse Bayesian Learning
* Author: Zhang, Z

```

* Date: 2014
 * Code version: 1.0
 * Availability: <https://sites.google.com/site/researchbyzhang/software>

*****/

```
function [Phi,flag] = genPhi(M,N,D)
% generate the sensing matrix Phi, which is a sparse binary matrix.
% Input:
%   M - row number of the matrix
%   N - column number of the matrix
%   D - number of nonzero entries of value 1 in each column of Phi
%
% Output
%   Phi - the generated sparse binary matrix
%   flag - if the generated Phi matrix is full rank, then flag = 1;
%         otherwise, flag= 0.
```

```
if M>N,
    error('M should <= N\n');
end
```

```
Phi = zeros(M,N);
```

```
for i = 1 : N
    ind = randperm(M);
    indice = ind(1:D);
    col = zeros(M,1);
    col(indice) = ones(D,1);
    Phi(:,i) = col;
end
```

```
if rank(Phi) == M
    flag = 1;
else
    flag = 0;
end
```

% STSBL-EM: Spatio-temporal Sparse Bayesian Learning Based on the EM Method

% Describe:

% The algorithm solves the following inverse problem

$$Y = \Phi * X + V$$
 % where Y is N by L known matrix, Phi is N by M known matrix,
 % X is M by L unknown matrix, V is N by L unknown noise matrix. Each
 % column in X has the same block structure (defined by input variable
 % 'blkStartLoc'); the locations of nonzero blocks in each column are
 % identical. X may have both intra-column correlation and inter-column
 % correlation, which are exploited to improve the algorithm's performance.

=====
 % INPUTS =====
 % Phi : N X M known matrix

```

%
% y      : N X L measurement vector
%
% blkStartLoc : Start location of each block
%
% LearnLambda : (1) If LearnLambda = 1, use the lambda learning rule for generally
% noisy
%             cases (SNR<=20dB) (thus the input lambda is just as initial value)
%             (2) If LearnLambda = 2, use the lambda learning rule for high SNR cases
%             (SNR>20dB)
%             (3) If LearnLambda = 0, do not use the lambda learning rule, but use the %
%             input
%             lambda value (or the default lambda value).
%
% [varargin values -- in most cases you can use the default values]
%
% 'LEARNTYPE' : LEARNTYPE = 0: Ignore intra-column correlation (but
%             still exploits inter-column correlation)
%             LEARNTYPE = 1: Exploit intra-block correlation
%             [ Default: LEARNTYPE = 1 ]
%
% 'PRUNE_GAMMA' : threshold to prune out small gamma_i
%             (generally, 10^{-3} or 10^{-2})
%
% 'LAMBDA'     : user-input value for lambda
%             [ Default: LAMBDA=1e-14 when LearnLambda=0;
%             LAMBDA=std(y)*1e-2 in noisy cases ]
%
% 'MAX_ITERS'  : Maximum number of iterations.
%             [ Default value: MAX_ITERS = 800 ]
%
% 'EPSILON'    : Solution accuracy tolerance parameter
%             [ Default value: EPSILON = 1e-6 ]
%
% 'PRINT'      : Display flag. If = 1: show output; If = 0: supress output
%             [ Default value: PRINT = 0 ]
%
% ===== OUTPUTS =====
% Result : A structured data with:
% Result.x      : the estimated X
% Result.gamma_used : indexes of nonzero groups in the sparse signal
% Result.gamma_est : the gamma values of all the groups of the signal
% Result.count   : iteration times
% Result.lambda  : the final value of lambda
% Scaling (will be re-scaling back in the end of the code)
% This step is to make those default values effective

scl = mean(std(y));
if (scl < 0.4) | (scl > 1)
    y = y/scl*0.4;
end

```

```

% get problem dimension
[N,M] = size(Phi);
L = size(y,2);

% Default Parameter Values for Any Cases
EPSILON    = 1e-6;    % solution accuracy tolerance
MAX_ITERS   = 800;    % maximum iterations
PRINT      = 0;      % don't show progress information
LEARNTYPE   = 1;      % adaptively estimate the covariance matrix B

if LearnLambda == 0
    lambda = 1e-12;
    PRUNE_GAMMA = 1e-3; MatrixReg = zeros(L);
elseif LearnLambda == 2
    lambda = 1e-3;
    PRUNE_GAMMA = 1e-2; MatrixReg = eye(L) * 0.5;
elseif LearnLambda == 1
    lambda = 1e-3;
    PRUNE_GAMMA = 1e-2; MatrixReg = eye(L) * 2;
else
    error(['Unrecognized Value for Input Argument "LearnLambda"']);
end

if(mod(length(varargin),2)==1)
    error('Optional parameters should always go by pairs\n');
else
    for i=1:2:(length(varargin)-1)
        switch lower(varargin{i})
            case 'learntype'
                LEARNTYPE = varargin{i+1};
                if LEARNTYPE ~= 1 & LEARNTYPE ~= 0
                    error(['Unrecognized Value for Input Argument "LEARNTYPE"']);
                end
            case 'prune_gamma'
                PRUNE_GAMMA = varargin{i+1};
            case 'lambda'
                lambda = varargin{i+1};
            case 'epsilon'
                EPSILON = varargin{i+1};
            case 'print'
                PRINT = varargin{i+1};
            case 'max_iters'
                MAX_ITERS = varargin{i+1};
            otherwise
                error(['Unrecognized parameter: "' varargin{i} '"']);
        end
    end
end

if PRINT

fprintf("\n===== \n");

```

```

fprintf('      Running STSBL_EM..... \n');
fprintf('      Information about parameters...\n');
fprintf('===== \n');
fprintf('PRUNE_GAMMA : %e\n',PRUNE_GAMMA);
fprintf('lambda      : %e\n',lambda);
fprintf('LearnLambda  : %d\n',LearnLambda);
fprintf('LearnType    : %d\n',LEARNTYPE);
fprintf('EPSILON      : %e\n',EPSILON);
fprintf('MAX_ITERS    : %d\n\n',MAX_ITERS);
end

%% Initialization

y0 = y;
Phi0 = Phi;
blkStartLoc0 = blkStartLoc;
p = length(blkStartLoc); % block number
for k = 1 : p-1
    blkLenList(k) = blkStartLoc(k+1)-blkStartLoc(k);
end
blkLenList(p) = M - blkStartLoc(end)+1;
maxLen = max(blkLenList);
if sum(blkLenList == maxLen) == p,
    equalSize = 1;
else
    equalSize = 0;
end

for k = 1 : p
    Sigma0{k} = eye(blkLenList(k));
end

gamma = ones(p,1);
keep_list = [1:p]';
usedNum = length(keep_list);
mu_t = zeros(M,L);
count = 0;

B = eye(L);

%% Iteration
while (1)
    count = count + 1;

    %===== Prune weights as their hyperparameters go to zero =====
    if (min(gamma) < PRUNE_GAMMA)
        index = find(gamma > PRUNE_GAMMA);
        usedNum = length(index);
        keep_list = keep_list(index);
        if isempty(keep_list),

fprintf('\n===== \n');

```

```

        fprintf('x becomes zero vector. The solution may be incorrect. \n');
        fprintf('Current "prune_gamma" = %g, and Current "EPSILON" =
%g.\n',PRUNE_GAMMA,EPSILON);
        fprintf("Try smaller values of "prune_gamma" and "EPSILON" or normalize "y"
to unit norm.\n");

fprintf('=====\n\n');
    break;
end;
blkStartLoc = blkStartLoc(index);
blkLenList = blkLenList(index);

% prune gamma and associated components in Sigma0
gamma = gamma(index);
temp = Sigma0;
Sigma0 = [];
for k = 1 : usedNum
    Sigma0{k} = temp{index(k)};
end

% construct new Phi
temp = [];
for k = 1 : usedNum
    temp = [temp, Phi0(:,blkStartLoc(k):blkStartLoc(k)+blkLenList(k)-1)];
end
Phi = temp;
%clear temp;
end

% ===== Spatially Whitening =====
y = y0 * sqrtm(inv(B));

%===== Compute new weights =====
PhiAPhi = zeros(N);
currentLoc = 0;
for i = 1 : usedNum

    currentLen = size(Sigma0{i},1);
    currentLoc = currentLoc + 1;
    currentSeg = currentLoc : 1 : currentLoc + currentLen - 1;

    PhiAPhi = PhiAPhi + Phi(:, currentSeg)*Sigma0{i}*Phi(:, currentSeg)';
    currentLoc = currentSeg(end);
end

H = Phi'/(PhiAPhi + lambda * eye(N));
Hy = H * y;
HPhi = H * Phi;

mu_x = zeros(size(Phi,2),L);
Sigma_x = [];
Cov_x = [];

```

```

A = []; invA = []; A0 = zeros(maxLen); r0 = zeros(1); r1 = zeros(1);

currentLoc = 0;
for i = 1 : usedNum

    currentLen = size(Sigma0{i},1);
    currentLoc = currentLoc + 1;
    seg = currentLoc : 1 : currentLoc + currentLen - 1;

    mu_x(seg,:) = Sigma0{i} * Hy(seg,:);    % solution
    Sigma_x{i} = Sigma0{i} - Sigma0{i} * HPhi(seg,seg) * Sigma0{i};
    %Cov_x{i} = Sigma_x{i} + mu_x(seg,:) * mu_x(seg,:);

    currentLoc = seg(end);

    %===== Learn intra-block correlation within columns =====
    % do not consider correlation structure in each block
    if LEARNATYPE == 0
        A{i} = eye(currentLen);
        invA{i} = eye(currentLen);

    % constrain all the blocks have the same correlation structure
    elseif LEARNATYPE == 1
        if equalSize == 0
            if currentLen > 1
                %temp = Cov_x{i}/gamma(i);
                temp = Sigma_x{i}/gamma(i) + mu_x(seg,:)*mu_x(seg,:)/L/gamma(i);

                r0 = r0 + mean(diag(temp));
                r1 = r1 + mean(diag(temp,1));
            end
        elseif equalSize == 1
            %A0 = A0 + Cov_x{i}/gamma(i);
            A0 = A0 + Sigma_x{i}/gamma(i) + mu_x(seg,:)*mu_x(seg,:)/L/gamma(i);
        end
    end % end of learnType

end % end of usedNum

%===== Learn the intra-block correlation with regularization =====
% If blocks have the same size
if (equalSize == 1) & (LEARNATYPE == 1)

    % Constrain all the blocks have the same correlation structure
    % (an effective strategy to avoid overfitting)
    b = (mean(diag(A0,1))/mean(diag(A0)));
    if abs(b) >= 0.99, b = 0.99*sign(b); end;
    bs = [];
    for j = 1 : maxLen, bs(j) = (b)^(j-1); end;

```

```

A0 = toeplitz(bs);

for i = 1 : usedNum

    A{i} = A0;
    invA{i} = inv(A{i});
end

% if blocks have different sizes
elseif (equalSize == 0) & (LEARNTYPE == 1)
    r = r1/r0; if abs(r) >= 0.99, r = 0.99*sign(r); end;

    for i = 1 : usedNum
        currentLen = size(Sigma_x{i},1);

        bs = [];
        for j = 1 : currentLen, bs(j) = r^(j-1); end;
        A{i} = toeplitz(bs);
        invA{i} = inv(A{i});
    end
end

% estimate gamma(i) and lambda
if LearnLambda == 1 % this learning rule is suitable for general noisy cases
(SNR<=20dB)
    gamma_old = gamma;
    lambdaComp = 0;
    currentLoc = 0;
    for i = 1 : usedNum

        currentLen = size(Sigma_x{i},1);
        currentLoc = currentLoc + 1;
        currentSeg = currentLoc : 1 : currentLoc + currentLen - 1;
        lambdaComp = lambdaComp +
trace(Phi(:,currentSeg)*Sigma_x{i}*Phi(:,currentSeg)');
        currentLoc = currentSeg(end);

        %gamma(i) = trace(invA{i} * Cov_x{i})/currentLen;
        gamma(i) = trace(invA{i}*Sigma_x{i})/currentLen ...
            + sum( sum( (mu_x(currentSeg,:)'*invA{i})*mu_x(currentSeg,:)
,2))/(L*currentLen);

        Sigma0{i} = A{i} * gamma(i);

    end
    lambda = norm(y - Phi*mu_x,'fro')^2/(N*L) + lambdaComp/N;

elseif LearnLambda == 2 % this learning rule is suitable for high SNR cases
(>20dB)
    gamma_old = gamma;
    lambdaComp = 0;

```

```

currentLoc = 0;
for i = 1 : usedNum
    lambdaComp = lambdaComp + trace(Sigma_x{i}*invA{i})/gamma(i);

    currentLen = size(Sigma_x{i},1);
    currentLoc = currentLoc + 1;
    currentSeg = currentLoc : 1 : currentLoc + currentLen - 1;

    gamma(i) = trace(invA{i}*Sigma_x{i})/currentLen ...
        + sum( sum( (mu_x(currentSeg,:)'*invA{i})*mu_x(currentSeg,:)
,2))/(L*currentLen);
    Sigma0{i} = A{i} * gamma(i);

    currentLoc = currentSeg(end);
end
lambda = norm(y - Phi * mu_x,'fro')^2/(N*L) + lambda * (length(mu_x) -
lambdaComp)/N;

else % only estimate gamma(i)
    gamma_old = gamma;
    currentLoc = 0;
    for i = 1 : usedNum
        currentLen = size(Sigma_x{i},1);
        currentLoc = currentLoc + 1;
        currentSeg = currentLoc : 1 : currentLoc + currentLen - 1;

        gamma(i) = trace(invA{i}*Sigma_x{i})/currentLen ...
            + sum( sum( (mu_x(currentSeg,:)'*invA{i})*mu_x(currentSeg,:)
,2))/(L*currentLen);

        Sigma0{i} = A{i} * gamma(i);

        currentLoc = currentSeg(end);
    end
end

% ===== Learn Spatial (inter-column) Covariance Matrix B =====
mu_old = mu_t;
mu_t = mu_x * sqrtm(B);
B = zeros(L); currentLoc = 0;
for i = 1 : usedNum

    currentLoc = currentLoc + 1;
    currentLen = size(Sigma0{i},1);
    seg = currentLoc : 1 : currentLoc + currentLen - 1;

    B = B + mu_t(seg,:)' * invA{i} * mu_t(seg,:)/gamma_old(i);
    % invA should choose the previous value, but it can use the updated
    % value since the value of invA changes slowly.

    currentLoc = seg(end);

```

```

end
B = B/norm(B,'fro');
B = B + MatrixReg;
B = B./norm(B);
if size(Phi,2) <= size(Phi,1), B = eye(L); end;

% ===== Check stopping conditions, etc. =====

% check convergence
if (size(mu_t) == size(mu_old))
    dmu = max(max(abs(mu_old - mu_t)));
    if (dmu < EPSILON) break; end;
end;
if (PRINT)
    disp([' iters: ', num2str(count), ...
        ' num coeffs: ', num2str(usedNum), ...
        ' min gamma: ', num2str(min(gamma)), ...
        ' gamma change: ', num2str(max(abs(gamma - gamma_old))), ...
        ' mu change: ', num2str(dmu)]);
end;
if (count >= MAX_ITERS), if PRINT, fprintf('Reach max iterations. Stop\n\n');
end; break; end;
% end

end;

%% Expand hyperparameters
gamma_used = sort(keep_list);
gamma_est = zeros(p,1);
gamma_est(keep_list,1) = gamma;

%% reconstruct the original signal
x = zeros(M,L);
currentLoc = 0;
for i = 1 : usedNum

    currentLen = size(Sigma0{i},1);
    currentLoc = currentLoc + 1;
    seg = currentLoc : 1 : currentLoc + currentLen - 1;

    realLocs = blkStartLoc0(keep_list(i)) : blkStartLoc0(keep_list(i))+currentLen-1;

    x( realLocs,:) = mu_t( seg,: );
    currentLoc = seg(end);
end

if (scl < 0.4) | (scl > 1)
    Result.x = x * scl/0.4;
else
    Result.x = x;
end

```

```

%Result.x = Result.x * sqrtm(B);
Result.gamma_used = gamma_used;
Result.gamma_est = gamma_est;
Result.A = A;
Result.count = count;
Result.lambda = lambda;
return;

```

%% Reconstruction of EEG using ST-SBL Method

```
clear; clc;
```

```
% Load Eppilepsy_Subject1
load Eppilepsy_Subject1; % 250 Hz
```

```
% generate SBM (128 by 256)
M = 128;
N = 256;
%
while(1)
    [Phi,flag] = genPhi(M,N,30);
    if flag == 1, break; end;
end
```

```
% Load Dictionary
load W_Beylkin.mat;
```

```
% Block size
blkLen = 16;
groupStartLoc = 1:blkLen:N;
```

```
% variable for storing reconstructed Eppilepsy_Subject1 set
X_hat = zeros(size(Eppilepsy_Subject1));
segNb = floor(size(Eppilepsy_Subject1,2)/N);
```

```
% run....
for j = 1 : segNb
```

```
    % Signal Compression
    y = Phi * Eppilepsy_Subject1(:,(j-1)*N+1:j*N);
```

```
    % Signal Reconstruction
```

```
    Result = STSBL_EM(Phi* W_Beylkin',y,groupStartLoc,0,'prune_gamma',-1,
'max_iters',40);
```

```
    signal_hat = W_Beylkin' * Result.x;
```

```
    % Reconstructed EEG epoch
    X_hat(:,(j-1)*N+1:j*N) = (signal_hat)';
```

```

    % calculate the MSE for current epoch
    mse(j) = (norm(Eppilepsy_Subject1(:,(j-1)*N+1:j*N) -
(signal_hat)', 'fro')/norm(Eppilepsy_Subject1(:,(j-1)*N+1:j*N), 'fro'))^2;
%   fprintf('Segment %d out of %d: MSE = %f\n',j,segNb, mse(j));

    % Calculate SSIM
    windowLen = 100;
    [mssim, ssim_map] = ssim_1d(Eppilepsy_Subject1(:,(j-1)*N+1:j*N),(signal_hat)',
windowLen);
    ssim(j) = mssim;

%   fprintf('Segment %d out of %d: MSE = %f | SSIM=%f\n',j,segNb, mse(j),ssim(j));
end

%% Figure
fs=250;
time=0:1/fs:5000/fs-1/fs;

% Example Traces
figure;
subplot(211);plot(time,Eppilepsy_Subject1(5,1:5000),'r','linewidth',2);hold
on;plot(time,X_hat(5,1:5000),'b','linewidth',2);
    legend('Original Signal at Channel 5','Reconstructed Signal at Channel 5');
xlabel('Time(s)');

subplot(212);plot(time,Eppilepsy_Subject1(28,1:5000),'r','linewidth',2);hold
on;plot(time,X_hat(28,1:5000),'b','linewidth',2);
    legend('Original Signal at Channel 25','Reconstructed Signal at Channel 25');
    xlabel('Time(s)');

% Calculate Median of results
median(mse)
median(ssim)

/*****

*   Title: SSIM Index
*   Author: Wang, Z
*   Date: 2012
*   Code version: 1.0
*   Availability: https://www.cns.nyu.edu/~lcv/ssim/ssim\_index.m
*****/

%SSIM Index

```

```
function [mssim, ssim_map] = ssim_1d(sig1, sig2, windowLen)
```

```
C1 = 0;
```

```
C2 = 0;
```

```
C3 = 0;
```

```
N = length(sig1);
```

```
for j = 1 : N-windowLen+1
```

```
    mu1 = mean(sig1(j : j+windowLen-1 ));
```

```
    mu2 = mean(sig2(j : j+windowLen-1 ));
```

```
    mu1_sq = mu1^2;
```

```
    mu2_sq = mu2^2;
```

```
    sigma1 = std(sig1(j : j+windowLen-1 ));
```

```
    sigma2 = std(sig2(j : j+windowLen-1 ));
```

```
    sigma1_sq = sigma1^2;
```

```
    sigma2_sq = sigma2^2;
```

```
    sigma_12 = mean((sig1(j : j+windowLen-1 ) - mu1).*(sig2(j : j+windowLen-1 ) - mu2));
```

```
    ssim_map(j) = (2*mu1*mu2+C1)/(mu1_sq + mu2_sq + C1) *  
(2*sigma1*sigma2+C2)/(sigma1_sq+sigma2_sq+C2)...  
    * (sigma_12+C3)/(sigma1*sigma2+C3);
```

```
end
```

```
mssim = mean(ssim_map);
```

```
%% Comparison Traces of Beylkin, DCT and No dictionary for different  
CRs
```

```
% Aggregates EEG
```

```
sum_Reconstruction_Data_Beylk_77=sum(X_hat);
```

```
% Normalized data
```

```
nor_data_blk_77=sum_Reconstruction_Data_Beylk_77/length(sum_Reconstruction_Data_Beylk_77);
```

```
data_blk_77_re=nor_data_blk_77(:,1:5000);
```

```
fs=250; % Sampling Frequency,250 Hz
```

```
time=0:1/fs:5000/fs-1/fs;
```

```
% Figure
```

```
subplot(4,3,1);
```

```
plot(time,data_cr,'b','linewidth',2);hold on;plot(time,data_blk_128_re,'r','linewidth',2);
```

```
title('Beylkin,CR=50% ');
```

```
xlabel('Time(s)');
```

```
subplot(4,3,4);
```

```
plot(time,data_cr,'b','linewidth',2);hold on;plot(time,data_blk_102_re,'r','linewidth',2);
```

```

title('Beylkin,CR=60% ','FontName','Times New Roman','fontsize',14);
xlabel('Time(s)');

subplot(4,3,7);
plot(time,data_cr,'b','linewidth',2);hold on;plot(time,data_blk_77_re,'r','linewidth',2);
title('Beylkin,CR=70% ');
xlabel('Time(s)');

subplot(4,3,10);
plot(time,data_cr,'b','linewidth',2);hold on;plot(time,data_blk_51_re,'r','linewidth',2);
title('Beylkin,CR=80% ');
xlabel('Time(s)');

subplot(4,3,2);
plot(time,data_cr,'b','linewidth',2);hold on;plot(time,data_DCT_128_re,'r','linewidth',2);
title('DCT,CR=50% ');
xlabel('Time(s)');

subplot(4,3,5);
plot(time,data_cr,'b','linewidth',2);hold on;plot(time,data_DCT_102_re,'r','linewidth',2);
title('DCT,CR=60% ');
xlabel('Time(s)');

subplot(4,3,8);
plot(time,data_cr,'b','linewidth',2);hold on;plot(time,data_DCT_77_re,'r','linewidth',2);
title('DCT,CR=70% ');
xlabel('Time(s)');

subplot(4,3,11);
plot(time,data_cr,'b','linewidth',2);hold on;plot(time,data_DCT_51_re,'r','linewidth',2);
title('DCT,CR=80% ');
xlabel('Time(s)');

subplot(4,3,3);
plot(time,data_cr,'b','linewidth',2);hold
on;plot(time,data_NO_DIC_128_re,'r','linewidth',2);
title('No dictionary,CR=50% ');
xlabel('Time(s)');

subplot(4,3,6);
plot(time,data_cr,'b','linewidth',2);hold
on;plot(time,data_NO_DIC_102_re,'r','linewidth',2);
title('Beylkin,CR=60% ');
xlabel('Time(s)');

subplot(4,3,9);
plot(time,data_cr,'b','linewidth',2);hold
on;plot(time,data_NO_DIC_77_re,'r','linewidth',2);
title('No dictionary');
xlabel('Time(s)');

subplot(4,3,12);

```

```

plot(time,data_cr,'b','linewidth',2);hold
on;plot(time,data_NO_DIC_51_re,'r','linewidth',2);
title('No dictionary');
xlabel('Time(s)');

```

%% Box plot of NMSE and SSIM for different CRs

```

% Generate Group Variable to store CRs

```

```

g1 = repmat({'50'},15,1);
g2 = repmat({'60'},15,1);
g3 = repmat({'70'},15,1);
g4 = repmat({'80'},15,1);
g=[g1;g2;g3;g4];

```

```

%Variables to store Belkin's NMSE and SSIM Values

```

```

xb1=[Beylkin128;Beylkin_NMSE_102;Beylkin_NMSE_77;Beylkin_NMSE_51];
xb2=[Beylkin_ssim128;Beylkin_SSIM_102;Beylkin_SSIM_77;Beylkin_SSIM_51];

```

```

%Variables to store DCT's NMSE and SSIM Values

```

```

xd1=[DCT_NMSE_128;DCT_NMSE_102;DCT_NMSE_77;DCT_NMSE_51];
xd2=[DCT_SSIM_128;DCT_SSIM_102;DCT_SSIM_77;DCT_SSIM_51];

```

```

%Variables to store no dictionary's NMSE and SSIM Values

```

```

xn1=[NO_DIC_NMSE_128;NO_DIC_NMSE_102;NO_DIC_NMSE_77;NO_DIC_BN
SE_51];
xn2=[NO_DIC_SSIM_128;NO_DIC_SSIM_102;NO_DIC_SSIM_77;NO_DIC_SSIM_
51];

```

```

% Boxplots

```

```

subplot(2,3,1);
h1=boxplot(xb1,g,'symbol','');
set(h1,'LineWidth',2)
set(h1(7,:),'MarkerSize',10)
set(gca, 'YGrid','on')
title('Beylkin')
xlabel('CR(%));
ylabel('NMSE');

```

```

subplot(2,3,2);
h2=boxplot(xd1,g,'symbol','');
set(h2,'LineWidth',2)
set(h2(7,:),'MarkerSize',10)
set(gca, 'YGrid','on')
title('DCT');
xlabel('CR(%));
ylabel('NMSE');

```

```

subplot(2,3,3);
h3=boxplot(xn1,g,'symbol','');
set(h3,'LineWidth',2)
set(h3(7,:),'MarkerSize',10)

```

```

set(gca, 'YGrid','on')
title('No dictionary');
xlabel('CR(%)');
ylabel('NMSE');

subplot(2,3,4);
h4=boxplot(xb2,g,'symbol','');
set(h4,'LineWidth',2)
set(h4(7,:), 'MarkerSize',10)
set(gca, 'YGrid','on')
title('Beylkin');
xlabel('CR(%)');
ylabel('SSIM');

subplot(2,3,5);
h5=boxplot(xd2,g,'symbol','');
set(h5,'LineWidth',2)
set(h5(7,:), 'MarkerSize',10)
set(gca, 'YGrid','on')
title('DCT');
xlabel('CR(%)');
ylabel('SSIM');

subplot(2,3,6);
h6=boxplot(xn2,g,'symbol','');
set(h6,'LineWidth',2)
set(h6(7,:), 'MarkerSize',10)
set(gca, 'YGrid','on')
title('No dictionary');
xlabel('CR(%)');
ylabel('SSIM');

```

%%Power Consumption Calculation at different Sampling Rate

```

clear; clc;

C1 = 32; % number of channel of 1st dataset
C2 = 29; % number of channel of 2nd dataset
C3 = 23; % number of channel of 3rd dataset

M= 128; % number of compressed samples
N=256; %Total number of samples

P_AMP = 0.9; % Amplifier Power consumption

% Sampling Frequency
fs1 = 0.25;
fs2 = 50;
fs3 = 100;

```

```

%ADC Power consumption at different fs
P_ADC1=0.1;
P_ADC2 = 12;
P_ADC3=25;

j = 5; % Transmitter Power 5 nj/b

R = 12; % ADC Resolution

P_RNG = 2.9;%RNG Power
P_MULT = 352;% Multiplier Power

% Processing power
P_proc = P_RNG + P_MULT;

% Sensing power for 1st Dataset
P_sense11 = C1*(P_AMP + P_ADC1);
P_sense12 = C1*(P_AMP + P_ADC2);
P_sense13 = C1*(P_AMP + P_ADC3);

% Communication power for 1st Dataset
P_comm11 = C1*M/N*J*fs1*R;
P_comm12 = C1*M/N*J*fs2*R;
P_comm13 = C1*M/N*J*fs3*R;

% Systems power for 1st Dataset
P_total1 = P_sense11 + P_proc + P_comm11
P_total2 = P_sense12 + P_proc + P_comm12
P_total3 = P_sense13 + P_proc + P_comm13

% Sensing power for 2nd Dataset
P_sense21 = C2*(P_AMP + P_ADC1);
P_sense22 = C2*(P_AMP + P_ADC2);
P_sense23 = C2*(P_AMP + P_ADC3);

% Communication power for 2nd Dataset
P_comm21 = C2*M/N*J*fs1*R;
P_comm22 = C2*M/N*J*fs2*R;
P_comm23 = C2*M/N*J*fs3*R;

% Total power for 2nd Dataset
P_tota21 = P_sense21 + P_proc + P_comm21
P_tota22 = P_sense22 + P_proc + P_comm22
P_tota23 = P_sense23 + P_proc + P_comm23

% Sensing power for 3rd Dataset
P_sense31 = C3*(P_AMP + P_ADC1);
P_sense32 = C3*(P_AMP + P_ADC2);
P_sense33 = C3*(P_AMP + P_ADC3);

% Communication power for 3rd Dataset
P_comm31 = C3*M/N*J*fs1*R;

```

```

P_comm32 = C3*M/N*J*fs2*R;
P_comm33 = C3*M/N*J*fs3*R;
4
% Total power for 1st Dataset
P_tota31 = P_sense31 + P_proc + P_comm31
P_tota32 = P_sense32 + P_proc + P_comm32
P_tota33 = P_sense33 + P_proc + P_comm33

%Variables to Store Power
X1=[P_tota11,P_tota12,P_tota13];
X2=[P_tota21,P_tota22,P_tota23];
X3=[P_tota31,P_tota32,P_tota33];
%Variable to Store Sampling frequency
Y=[fs1,fs2,fs3];

%Figure
figure
plot(Y,X1,'--',Y,X2,'-', Y,X3,'-', 'LineWidth',2, 'MarkerSize',12);
legend('32 Channel', '29 Channel');
title('Power consumption Vs Sampling Rate');
xlabel('Sampling Rate(kS/s)');
ylabel('Total Power Consumption(uW)');

%% Power Consumption for different resolution and at sampling rate
100kS/s

clear; clc;
C1 = 32; % number of channel of 1st dataset
C2 = 29; % number of channel of 2nd dataset
C3 = 23; % number of channel of 3rd dataset

M= 128; %number of compressed samples
N=256; % Total number of samples

P_AMP = 0.9; %Power consumption at amplifier

P_ADC1=19; %Power consumption at ADC of resolution 8
P_ADC2=23; %Power consumption at ADC of resolution 10
P_ADC3=25; %Power consumption at ADC of resolution 12

j = 5; %Transmitter Power 5 nj/b

fs = 100; %Sampling frequency
R1=8; % Resolution of ADC1
R2 = 10; % Resolution of ADC2
R3=12; % Resolution of ADC3

P_RNG = 2.9; % Power consumption at RNG
P_MULT = 352; % Multiplier power consumption

```

```

% Processing power
P_proc = P_RNG + P_MULT;

% Sensing power for 1st Dataset
P_sense11 = C1*(P_AMP + P_ADC1);
P_sense12 = C1*(P_AMP + P_ADC2);
P_sense13 = C1*(P_AMP + P_ADC3);

% Communication power for 1st dataset
P_comm11 = C1*M/N*J*fs*R1;
P_comm12 = C1*M/N*J*fs*R2;
P_comm13 = C1*M/N*J*fs*R3;

%Total power for 1st dataset
P_tot11 = P_sense11 + P_proc + P_comm11
P_tot12 = P_sense12 + P_proc + P_comm12
P_tot13 = P_sense13 + P_proc + P_comm13

% Sensing power for 2nd Dataset
P_sense21 = C2*(P_AMP + P_ADC1);
P_sense22 = C2*(P_AMP + P_ADC2);
P_sense23 = C2*(P_AMP + P_ADC3);

% Communication power for 2nd dataset
P_comm21 = C2*M/N*J*fs*R1;
P_comm22 = C2*M/N*J*fs*R2;
P_comm23 = C2*M/N*J*fs*R3;

%Total power for 2nd datase
P_tot21 = P_sense21 + P_proc + P_comm21
P_tot22 = P_sense22 + P_proc + P_comm22
P_tot23 = P_sense23 + P_proc + P_comm23

% Sensing power for 3rd Dataset
P_sense31 = C3*(P_AMP + P_ADC1);
P_sense32 = C3*(P_AMP + P_ADC2);
P_sense33 = C3*(P_AMP + P_ADC3);

% Communication power for 3rd dataset
P_comm31 = C3*M/N*J*fs*R1;
P_comm32 = C3*M/N*J*fs*R2;
P_comm33 = C3*M/N*J*fs*R3;

%Total power for 3rd datase
P_tot31 = P_sense31 + P_proc + P_comm31
P_tot32 = P_sense32 + P_proc + P_comm32
P_tot33 = P_sense33 + P_proc + P_comm33

%Variables to Store Power
X1=[P_tot11,P_tot12,P_tot13];
X2=[P_tot21,P_tot22,P_tot23];
X3=[P_tot31,P_tot32,P_tot33];

```

```

%Variables to Resolutions
Y=[R1,R2,R3];

% Figure
figure
plot(Y,X1,'--',Y,X2,':',Y,X3,'-', 'LineWidth',2, 'MarkerSize',12);
legend('32 Channel','29 Channel','23 Channel');
title (' Power Consumption vs Resolution');
xlabel('ADC Resolution(bits)');
ylabel('Total Power Consumption(mW)');

```

%% Power Consumption at different CR

```

clear; clc;

C = 23; % number of channe

%number of compressed samples
M1= 128;
M2=102;
M3=77;
M4=51;

N=256; % Total number of samples

P_AMP = 0.9; %Power consumption at amplifier
P_ADC=0.1; %Power consumption at ADC of

J = 5; % Transmitter Power 5 nj/b
fs1 = .25; %Sampling frequency 0.25 kS/s
R = 12; % Resolution of ADC

P_RNG = 2.9; % Power consumption at RNG
P_MULT = 352; % Multiplier power consumption

% Processing power
P_proc = P_RNG + P_MULT;

% Sensing power
P_sense11 = C*(P_AMP + P_ADC);

% Communication Power
P_comm11 = C*M1/N*J*fs1*R;
P_comm12 = C*M2/N*J*fs1*R;
P_comm13 = C*M3/N*J*fs1*R;
P_comm14 = C*M4/N*J*fs1*R;

%Total power
P_total1 = P_sense11 + P_proc + P_comm11
P_total2 = P_sense11 + P_proc + P_comm12

```

```
P_tot13 = P_sense11 + P_proc + P_comm13
```

```
P_tot14 = P_sense11 + P_proc + P_comm14
```

```
%Variables to Store Power
```

```
X1=[P_tot11,P_tot12,P_tot13,P_tot14];
```

```
%Variables to Store CRs
```

```
Y=[M1,M2,M3,M4];
```

```
%Figure
```

```
figure
```

```
plot(Y,X1,'-');
```

```
title('Power Consumption vs Resolution');
```

```
xlabel('CR%','FontName');
```

```
ylabel('Total Power Consumption(mW)');
```